SIGNAL DESIGN AND PROCESSING TECHNIQUES FOR WSR-88D AMBIGUITY RESOLUTION

Part 7: Phase Coding and Staggered PRT Implementation, data collection, and processing

National Severe Storms Laboratory Report

prepared by: Sebastian Torres, Dusan Zrnic, and Yannick Dubel
with contributions by: Svetlana Bachmann and Christopher Curtis

October 2003

NOAA, National Severe Storms Laboratory
1313 Halley Circle, Norman, Oklahoma 73069

SIGNAL DESIGN AND PROCESSING TECHNIQUES FOR WSR-88D AMBIGUITY RESOLUTION

Part 7: Phase Coding and Staggered PRT Implementation, data collection, and processing

Contents

SIGNAL DESIGN AND PROCESSING TECHNIQUES FOR WSR-88D AMBIGUITY RESOLUTION

Part 7: Phase Coding and Staggered PRT Implementation, data collection, and processing

1. Introduction

The Radar Operations Center (ROC) of the National Weather Service (NWS) has funded the National Severe Storms Laboratory (NSSL) to address the mitigation of range and velocity ambiguities in the WSR-88D. This is the seventh report in the series that deals with range-velocity ambiguity resolution in the WSR-88D. It documents NSSL's accomplishments in FY03. Whereas the pertinent accomplishments are listed, we emphasize that the funding by ROC specifically devoted to the task could not cover these accomplishments. The shortfall was in excess of one man year. Nonetheless, the slack was filled by funding from the NWS Office of Science and Technology.

In previous reports two complimentary techniques have been proposed for mitigating the range and velocity ambiguities. These are the systematic phase coding (SZ type) and staggered PRT. Analysis and simulations indicate that phase coding cannot eliminate the long PRT scan for reflectivity estimation if the estimates must be unambiguous to 460 km. Phase coding is effective on uniform PRT sequences which are conducive to spectral analysis and good ground clutter filtering. Increase in clear range is at least twice the unambiguous range of the inherent uniform PRT, but not all overlaid echoes can be separated. Further, multiple overlaid signals might also cause total loss of information. Staggered PRT can provide clear range and relatively large unambiguous velocity. But for large unambiguous range the errors in spectral moments might be prohibitive. The main disadvantage of staggered PRT is that ground clutter filtering is less effective and that spectral analysis, although possible, is severely impaired by the non uniform spacing of samples. The two methods are complementary and a volume coverage pattern has been suggested to take advantage of the benefits offered by each method; phase coding at two lowest elevations and staggered PRT at higher elevations (Sachidananda et al. 2001).

Until summer of 2002 there were very few data sets of phase encoded returns: one from an Oklahoma squall line and a couple from Florida. Moreover there were no data sets with staggered pulse train. By the end of the summer, NSSL had upgraded its research and development WSR-88D (KOUN) to transmit phase coded data and decode the first trip in real time. Further upgrades followed during the fall of 2002. These engineering developments are documented in section 2 of this report. These were substantial, including unlimited time series recording and reading (in Matlab and native formats), processing of staggered PRT in real time, and expansion of volume coverage patterns to include mix of modes. Further, NSSL collected a very large set of time series data, both in phase coding mode and staggered PRT mode. Brief description of these events is also listed in section 2.

Section 3 describes work on the SZ phase coding. It documents the steps taken to insure that the collected data are correct. Thus, a discussion of phase shifter influence and examination of individual radials of data are contained therein. Then, the description of the SZ-2 algorithm (the one that needs long and short PRT data) is presented. This description is taken from the Interim report (2003 prepared by NSSL and NCAR). A minor addition (one line) has been made to accommodate an omission made in the interim report. Some examples of the velocity and reflectivity fields produced by this algorithm (Matlab implementation) are also in Section 3.

Otherwise, all existing phase coded events have been processed by the algorithm and images are posted on the internet.

Section 4 describes work on the staggered PRT. First is the description of the algorithm as implemented to run on the KOUN in real time. An identical version of the algorithm is implemented in Matlab to process time series data. A relatively simple method to filter ground clutter filter is listed, and censoring is addressed as well. Examples of data fields and comparison with fields from a relatively close WSR-88D complete this section.

Section 5 discusses implications of the results from sections 3 and 4. Compromises and practical considerations are given. Recommendations of VCP are revised and compatibility with dual polarization and whitening techniques is addressed. Also listed are unresolved issues requiring further study.

The report concludes with section 6 and there is an appendix containing the Algorithm Enunciation Language (AEL) of the SZ-2 algorithm.

2. Engineering Development

Modifications on the research and development WSR-88D for implementing phase coding, staggered PRT as well as collecting time series data are briefly listed herein. The changes were built on the proof of concept radar controller and signal processor which were designed and configured at NSSL. Henceforth, we refer to that system as RRDA. The RRDA consists of a single-board host computer (performing real-time monitoring and control functions), a synchronizer (for generation of timing signals and triggers for the transmitter, receiver, and all built-in test and calibration equipment), and a highly scalable digital signal processor (multiprocessor) with its own high-speed interconnect fabric (based on Power PC processors and Mercury Computer Systems' RaceWay interconnect)

2.1. Expanded VCP definitions

One of the first issues considered before the implementation of phase coding and staggered PRT acquisition modes was the suitability of legacy volume coverage pattern (VCP) definitions. Legacy WSR-88D VCPs are specified in Message 7 of the Interface Control Document for the RDA/RPG (document no. 2620002A). A close look at the RPG Message 7 revealed that it provides insufficient capabilities to completely define either phase coding or staggered PRT waveforms. For example, the "Waveform Type and Configuration" parameter can take either a "Constant Phase" or "Random Phase" value; no provision for systematic phase codes is made here. In addition, the definition of a "Staggered Pulse Pair" mode is totally ambiguous (what are the PRTs?, how many pulses of each PRT are executed?) since this mode is not currently supported on the WSR-88D.

To accommodate this and other project's needs the current VCP definition was expanded to allow the specification of high-resolution data, horizontal/vertical raster (sector scans), searchlight, phase coding, and staggered PRT modes. Table 2.1 shows the expanded VCP definition where the new and modified fields are highlighted. A dark shade indicates a new field, and a light shade a modified field. The changes were made such that the resulting VCP definitions are backward compatible with the legacy definitions for all supported modes. For instance, when new fields default to a zero value, they indicate the legacy mode of operation.

Transmission of phase coded signals is specified via the "Waveform Configuration" field, which was expanded to include a "Phase Coding Sequence Number". A zero in this field indicates no phase coding and non-zero entries between 1 and 126 specify one of 126 predefined code sequences (e.g., 1 represents the SZ(8/64) code). A 127 is used to specify user-defined, downloadable phase sequences. A new RPG/RDA message is proposed to define a downloadable phase sequence. This simple message consists of the phase sequence length and the actual phase code sequence, where each phase is specified as multiples of 2π/128. The proposed message structure is given in Table 2.2.

Staggered PRT patterns can be specified using up to three PRTs (or pulse repetition frequency numbers). A pulse count M is specified for each PRT, and an overall pattern count M_p determines how many times the basic pattern is repeated. For example, a standard staggered pattern that alternates PRT #1 and PRT #2 for a total of 64 pulses is specified as:

	#1	#2	#3
PRF #	1	2	0
M	1	1	0
M_p	32		

A more complicated block staggered pattern that alternates blocks of 4 pulses using PRT #4 and blocks 6 pulses using PRT #3 for a total of 50 pulses is specified as:

	#1	#2	#3
PRF #	4	3	0
M	4	6	0
M_p	5		

New VCP definitions allow the specification of evolutionary techniques on a scan-by-scan basis. This is consistent with the VCP proposed for range-velocity ambiguity mitigation by Sachidananda et al. (2002).

MESSAGE 7 - VOLUME COVERAGE PATTERN DATA

Name	Description	Format	Units	Range (or Value)	Accuracy /Precision	Byte Location
Message Size	Number of Halfwords in Message	Short	Halfwords	23-594 (?)	1	1-2
Pattern Type	Constant Elevation Cut Horizontal Raster Scan Vertical Raster Scan Searchlight	Short	N/A	2 4 8 16	N/A	3-4
Pattern Number	Maintenance/Test Constant Elevation Types Horizontal Raster Types Vertical Raster Types Searchlight Types	Short	N/A	>255 1-99 100-149 150-199 200-249	1	5-6
Number of Cuts		Short	N/A	1-25	1	7-8
Clutter Map Group Number		Short	N/A	1-99	1	9-10
Doppler Velocity Resolution	0.5 m/s 1.0 m/s	Char	N/A	2 4	N/A	11
Pulse Width	Short Long	Char	N/A	2 4	N/A	12
Sampling Range Resolution	250 m 50 m	Char	N/A	0 1	N/A	13
Reflectivity Range Resolution	1 km 250 m	Char	N/A	0 1	N/A	14
Velocity and Spectrum Width Range Resolution	250 m 1 km	Char	N/A	0 1	N/A	15
Radial Angular Interval	1.0 deg 0.5 deg	Char	N/A	0 1	N/A	16
Spare						17-22

Table 2.1. Extended Volume Coverage Pattern (VCP) definition. New fields are highlighted in dark gray, modified fields are highlighted in light gray.

For each cut:

Name	Description	Format	Units	Range (or Value)	Accuracy /Precision	Byte Location
Scanning Angle/ Searchlight Elevation Angle	For Constant Elevation Scan, Horizontal Raster Scan, or Searchlight this is the el. angle. For Vertical Raster Scan this is the azimuth angle.	Short	Bams			1-2
Waveform Configuration	Linear Channel Log Channel Phase Coding Sequence No.	Char	N/A	MSB=0 MSB=1 0 no phase coding 1-126 hard-coded sequence 127 downloaded sequence (see Phase Coding Sequence Message)	N/A	3
Waveform Type	Contiguous Surveillance Range Unambiguous Doppler Range Ambiguous Doppler Batch Staggered	Char	N/A	1 2 3 4 5	N/A	4
Surveillance PRF Number	For the Staggered type this is ignored	Short	N/A	1-8	1	5-6
Surveillance PRF Pulse Count	For the Staggered type this is the pattern repetition count	Short	N/A	1-999	1	7-8
Scan Rate/ Searchlight Azimuth Angle	For Constant Elevation and Horizontal Raster Scans this is the azimuth rate. For Vertical Raster Scans this is the elevation rate. For Searchlight this is the azimuth angle.	Short	Bams			9-10
Reflectivity Threshold		Short	dB	-12.0 to 20	1/8 dB	11-12
Velocity Threshold		Short	dB	-12.0 to 20	1/8 dB	13-14
Spectrum Width Threshold		Short	dB	-12.0 to 20	1/8 dB	15-16
SNR Threshold	Thresholds as defined above Do not apply any thresholds	Char	N/A	0 1	N/A	17

Table 2.1 (cont'd). Extended Volume Coverage Pattern (VCP) definition. New fields are highlighted in dark gray, modified fields are highlighted in light gray.

Name	Description	Format	Units	Range (or Value)	Accuracy /Precision	Byte Location
Spare						18
Raster Edge Angle 1/ Searchlight Radial Count	In Horizontal Raster Scans this is the counter-clockwise edge angle. In Vertical Raster Scans this is the lower edge angle. In Searchlight this is the number of radials to complete a cut.	Short	Bams			19-20
Raster Edge Angle 2	In Horizontal Raster Scans this is the clockwise edge angle. In Vertical Raster Scans this is the upper edge angle	Short	Bams			21-22
Edge Angle 1	Sector 1 Beginning Azimuth Angle For the Staggered type this is ignored	Short	Bams			23-24
Doppler PRF Number 1	For the Staggered type this is the PRF number for T1	Short	N/A	1-8	1	25-26
Doppler PRF Pulse Count 1	For the Staggered type this is the pulse count for T1	Short	N/A	1-999	1	27-28
Spare						29-30
Edge Angle 2	Sector 2 Beginning Azimuth Angle For the Staggered type this is ignored	Short	Bams	0 If only one sector is defined		31-32
Doppler PRF Number 2	For the Staggered type this is the PRF number for T2	Short	N/A	0 If only one sector is defined 1-8 Otherwise	1	33-34
Doppler PRF Pulse Count 2	For the Staggered type this is the pulse count for T2	Short	N/A	0 If only one sector is defined 1-999 Otherwise	1	35-36
Spare						37-38

Table 2.1 (cont’d). Extended Volume Coverage Pattern (VCP) definition. New fields are highlighted in dark gray, modified fields are highlighted in light gray.

Name	Description	Format	Units	Range (or Value)	Accuracy /Precision	Byte Location
Edge Angle 3	Sector 3 Beginning Azimuth Angle For the Staggered type this is ignored	Short	Bams	0 If only one sector is defined		39-40
Doppler PRF Number 3	For the Staggered type this is the PRF number for T3	Short	N/A	0 If only one sector is defined or in the Staggered type if only 2 PRFs are defined 1-8 Otherwise	1	41-42
Doppler PRF Pulse Count 3	For the Staggered type this is the pulse count for T3	Short	N/A	0 If only one sector is defined or in the Staggered type if only 2 PRFs are defined 1-999 Otherwise	1	43-44
Spare						45-46

Table 2.1 (cont'd). Extended Volume Coverage Pattern (VCP) definition. New fields are highlighted in dark gray, modified fields are highlighted in light gray.

MESSAGE 19 - PHASE CODING SEQUENCE MESSAGE

Name	Description	Format	Units	Range (or Value)	Accuracy /Precision	Byte Location
Message Size	Number of Halfwords in Message	Short	Halfwords	260 (or we can make it variable in the range 5-260)	1	1-2
Phase Coding Sequence Length	Number of Phases in the Coding Sequence	Short	N/A	1-256	N/A	3-4
Phase Code 1		Char	Scaled radians	0-127/128*2π	2π/128	5
Phase Code 2		Char	Scaled radians	0-127/128*2π	2π/128	6
…						
Phase Code 256		Char	Scaled radians	0-127/128*2π	2π/128	260

Table 2.2. Proposed message for user-defined, downloadable phase coding sequences from the RPG into the RDA.

2.2. Phase coding

The WSR-88D has a built-in, 7-bit phase shifter which is used for calibration of the instantaneous Automatic Gain Control (AGC) circuits. Thus, the phase shifter is accessible to the host computer via the receiver interface on the sequencer board. Software was developed for the sequencer and host computer to pass the desired switching phase code to the phase shifter and subsequently modulate the RF signal on a pulse-by-pulse basis. In addition, real-time software was written to process the returned signals from the first trip only. This was expedient and necessary.

All modifications to produce and process phase coding data could be integrated with relative ease into the existing RRDA code. Although NSSL's version of the signal processor has six PowerPC processors, the RRDA uses only two of those to replicate the full functionality of the legacy signal processor. It became apparent that the full version of phase coding including ground clutter filtering, data censoring, plus other amenities on the RRDA might involve more than two processors, requiring a substantial change in programs. Thus, we settled for processing of first trip echo only in real time knowing well that we would reprocess the recorded time series data several times.

Processing at least the first trip echo in real time was deemed essential for several reasons. First and foremost was to monitor data quality. Whereas it is not possible from images of velocity fields to insure that data are impeccable, obvious errors can easily be noticed. Second, real time displays can guide data collection effort. The extent and severity of ambiguity problems can be seen immediately, and an observed situation can be compared (mentally) to previously collected samples. Because of time constraints and conflicting demands for the radar (by JPOLE participants) it was not possible to continuously collect data and rely on statistical serendipity to obtain a wide variety of range overlaid echoes. Operator interaction with the display and his memory allowed to quickly asses a storm situation and decide to start or stop data collection.

2.3. Staggered PRT

Implementation of staggered PRT required close cooperation between the sequencer, host computer, and signal processor. The functionality of the sequencer was expanded to enable the generation of staggered patterns that match the new VCP specifications. Further, the legacy set of 8 PRTs was expanded so that new PRTs can be defined as multiples of the 9.6 MHz basic clock cycle. This allows generating staggered PRT sequences with any desirable stagger ratio and maximum unambiguous range. Same considerations to avoid blind data collection and have real time quality control prompted us to implement a basic staggered PRT algorithm on the RRDA for real time processing. This algorithm is described in Section 4.

2.4. Data recording and formatting

One of the most important features of the RRDA is its capability to record up to 12 hours of continuous base data and time series data. Base data and AGC-corrected in-phase and quadrature-phase components and the corresponding metadata (or header) are recorded with no interruptions into a 130 GB disk array. Tools were developed to navigate, extract, and convert this data for off-line processing using MATLAB. Data are extracted and grouped into radials and there is one file per radial.

While base data (reflectivity, Doppler velocity, and spectrum width) are recorded using the format specified by Digital Radar Data Message (Message 1) of the RDA/RPG Interface

Control Document, time series data are recorded using a non-standard format. Files of time series data contain the actual time series and the corresponding header. Time series data for one radial are structured as a two-dimensional array of complex numbers: $data(m,n) = I(m,n) + jQ(m,n)$, where m is the pulse number and n the range bin. The header is stored in a data structure and is divided into metadata and control variables. A description of these fields is provided in Table 2.3.

Metadata Variables

Field Name	Value	Description
`function`	unsigned integer, 1 – process surveillance 2 – process range ambiguous Doppler 3 – process range unambiguous Doppler 4 – process batch surveillance 5 – process batch Doppler 6 – process staggered 7 – measure bias and noise 8 – measure balance and gain 9 – collect input data	Digital Signal Processor mode of operation; only functions 1-6 are used in operational modes
`radial_type`	unsigned integer, 1 – base data radial 2 – calibration radial	Operational data is of type 1
`vcp_type`	unsigned integer, 2 – constant elevation 4 – horizontal raster 8 – vertical raster 16 – searchlight	Standard VCPs are of the “constant elevation type”
`channel`	unsigned integer, 0 – linear channel 128 – log channel	Linear channel is used when collecting data
`pulse_width`	unsigned integer, 2 – short pulse 4 – long pulse	Short pulse normally used when collecting data from precipitation events
`samp_rng_resol`	unsigned integer, 0 – 250 m sampling 1 – 50 m sampling	Sampling resolution of A/D converter, all data has been collected with 250 m sampling

Table 2.3. Time series data header description. Metadata variables.

Metadata Variables

Field Name	Value	Description
`ref_threshold`	integer, 1/8 of a dB (i.e. 16 = 2.0 dB, 28 = 3.5 dB)	Reflectivity values with echo power measured above this signal-to-noise threshold are declared to be significant
`vel_threshold`	integer, 1/8 of a dB (i.e. 16 = 2.0 dB, 28 = 3.5 dB)	Velocities with echo power measured above this signal-to-noise threshold are declared to be significant
`wid_threshold`	integer, 1/8 of a dB (i.e. 16 = 2.0 dB, 28 = 3.5 dB)	Spectrum widths with echo power measured above this signal-to-noise threshold are declared to be significant
`vcp_no`	unsigned integer	Number corresponding to a VCP definition
`cut_no`	unsigned integer	Elevation cut number
`sector_no`	unsigned integer	Sector number (elevation cuts can be broken down into sectors; however, this is not a commonly used feature)
`radial_no`	unsigned integer, (0, ~360) for 1 deg. elevation cuts (0, ~720) for 0.5 deg. elevation cuts	Index of the radial in the elevation cut
`pattern_count`	unsigned integer	Number of patterns in the radial, this is 1 for uniform PRT and the number of staggered PRT patterns for staggered PRT
`prt_count`	unsigned integer	Number of PRTs in the pattern, this is 1 for uniform PRT and up to three for staggered PRT patterns
`prt_no`	unsigned integer, array of size MAX_STAG_PRT=3	System PRT number that corresponds to a predefined set of PRTs, there is one value in this array for uniform PRT and up to three values for staggered
`prt`	float, array of size MAX_STAG_PRT=3, microseconds	PRT in microseconds

Table 2.3 (cont'd). Time series data header description. Metadata variables.

Metadata Variables

Field Name	Value	Description
`pulse_count`	unsigned integer, array of size MAX_STAG_PRT=3	Number of pulses for each PRT; this is the number of pulses in the radial for a uniform PRT and the number of pulses in each block of the staggered PRT pattern
`bin_count`	unsigned integer, array of size MAX_STAG_PRT=3	Number of 250 m bins in the PRT for each corresponding PRT
`radial_bin_count`	unsigned integer	Total number of bins in the radial; this is pulse_count times bin_count for a uniform PRT, but is radial_pulse_count (see below) times max(bin_count) for staggered PRT, shorter PRTs are padded with zeros so that the array is not ragged
`radial_pulse_count`	unsigned integer	Total number of pulses in the radial
`last_radial`	integer (Boolean)	Flag; nonzero value indicates last radial in the cut
`last_cut`	integer (Boolean)	Flag; nonzero value indicates last elevation cut in the VCP (only set when last_radial is set)
`idt_count`	unsigned integer	Number of interference detection tags
`blank_status`	integer (Boolean)	Flag; nonzero value indicates blanking, but none of the recorded data should have any blanking
`az`	float, degrees	Antenna azimuth for this radial
`el`	float, degrees	Antenna elevation for this radial
`rate`	float, degrees/second	Rotation rate of the antenna
`ref_resol`	float	Not used, reflectivity data always has a resolution of 0.5 dBZ
`vel_resol`	unsigned integer, 2 – 0.5 m/s 4 – 1 m/s	Resolution of velocity data for output

Table 2.3 (cont'd). Time series data header description. Metadata variables.

Metadata Variables

Field Name	Value	Description
`Syscal`	float, dB	Calibration constant to obtain reflectivity values in dBZ units
`noise`	float, scaled watts	Measured system noise
`time`	unsigned integer, seconds	Number of seconds since 00:00:00, January 1, 1970 (UNIX time)
`phase_code_length`	unsigned integer	Length of the phase coding sequence, 0 for no phase coding
`phase_code`	unsigned char, array of size MAX_PC_SIZE = 256	Actual phase is -2π phase_code[i]/128 in radians

Table 2.3 (cont'd). Time series data header description. Metadata variables.

Control Variables

Field Name	**Value**	**Description**
`gcf_enable`	integer (Boolean)	Flag; enables/disables ground clutter filtering
`gcf_ctrl`	integer (Boolean)	Flag; allows overriding of notch width from the map; the notch width is given by gcf_nw (see below)
`gcf_nw`	float, m/s	Notch width for ground clutter filter; only used if gcf_ctrl is set
`spf_enable`	integer (Boolean)	Flag; enables/disables strong point clutter filtering
`isu_enable`	integer (Boolean)	Flag; enables/disables interference suppression unit
`void_snr_th`	integer (Boolean)	Flag; if set, disregards SNR thresholds ref_threshold, vel_threshold, and wid_threshold and marks all data as significant
`ref_rng_resol`	unsigned integer, 0 – 1 km 1 – 250 m	Resolution of output bins for reflectivity
`vel_wid_rng_resol`	unsigned integer, 0 – 250 m 1 – 1 km	Resolution of output bins for velocity and spectrum width
`rad_ang_interval`	unsigned integer, 0 – 1 deg. 1 – 0.5 deg.	Radial angular interval; azimuthal sampling interval
`invalid_pulses`	integer (Boolean)	Flag; indicates problems with time series data

Table 2.3 (cont’d). Time series data header description. Control variables.

2.5. Data collection

a. Description of VCPs

Both phase-coded and staggered PRT time series data were recorded with the KOUN research radar and processed offline using a MATLAB-based WSR-88D Signal Processing Subsystem simulator. Phase coded data were recorded using VCP 43 and VCP 44[1] whereas staggered PRT data were recorded using VCP 45a, VCP 45b, VCP 46a, VCP 46b, VCP 47b, VCP 48, or VCP 49. Tables 4 through 12 describe the scan strategies associated with each VCP and use the following variables:

- **Elev.**: Elevation angle (deg)
- **AZ rate**: Antenna rotation speed (deg/s)
- **Period**: Period of one 360 deg scan (s)
- **Dwell time:** Period of one radial (ms)
- **WF type**: Waveform type. One of the following:
  - **CS,x**: Contiguous Surveillance, PRT #x
  - **CD,x**: Non Phase Coded Contiguous Doppler, PRT #x
  - **B**: Batch mode
  - **SZ(n/M)**: SZ Phase Coded Contiguous Doppler
  - **ST(r)**: Staggered PRT (with no overlay resolution and r as the stagger ratio)
- **PRT #**: PRT number
- **Short PRT #**: Short PRT number (for staggered PRT and batch modes)
- **Long PRT #**: Long PRT number (for staggered PRT and batch modes)
- **M**: Number of pulses in one radial (for batch mode M(x,y) means x is the surveillance number of pulses and y is the Doppler number of pulses)
- T_u: PRT period (ms)
- T_1: Short PRT period (for staggered PRT and batch modes) (ms)
- T_2: Long PRT period (for staggered PRT and batch modes) (ms)
- r_{ar}: Maximum unambiguous range for the reflectivity field (km)
- r_{av}: Maximum unambiguous range for the velocity field (km)
- v_a: Effective maximum unambiguous velocity (obtained after de-aliasing for the staggered PRT mode) (m/s)

---

[1] Due to a problem with the phase-shifter controller, phase-coded data in VCP 44 are anomalous. That is, of the 128 pulses in each radial, the first 64 are correctly phase coded and the last 64 are not phase coded. Incidentally, these data can be used for side-by-side performance comparisons between phase-coded and non-phase-coded radials. As of September of 2003 this issue has been rectified.

Elev. (deg)	AZ rate (deg/s)	Period (s)	Dwell time (ms)	WF type	PRT #	M	T_u (ms)	r_{ar} (km)	r_{av} (km)	v_a (m/s)
0.48	20.03	17.97	46.6	CS,1	1	15	3.11	466	-	-
0.48	20.03	17.97	49.92	CD,8	8	64	0.78	-	234	35.52
0.48	20.03	17.97	49.92	SZ(8/64)	8	64	0.78	468	468	35.52
0.48	13.39	26.89	74.67	CD,4	4	64	1.17	-	350	23.74
0.48	13.39	26.89	74.67	SZ(8/64)	4	64	1.17	700	700	23.74
1.49	20.03	17.97	46.6	CS,1	1	15	3.11	466	-	-
1.49	20.03	17.97	49.92	CD,8	8	64	0.78	-	234	35.52
1.49	20.03	17.97	49.92	SZ(8/64)	8	64	0.78	468	468	35.52

Table 2.4. VCP 43

Elev. (deg)	AZ rate (deg/s)	Period (s)	Dwell time (ms)	WF type	PRT #	M	T_u (ms)	r_{ar} (km)	r_{av} (km)	v_a (m/s)
0.48	10.01	35.97	99.41	CS,1	1	32	3.11	466	-	-
0.48	10.01	35.97	99.84	CD,8	8	128	0.78	-	234	35.52
0.48	10.01	35.97	99.84	SZ(8/64)	8	128	0.78	468	468	35.52
0.48	6.69	53.81	149.34	CD,4	4	128	1.17	-	350	23.74
0.48	6.69	53.81	149.34	SZ(8/64)	4	128	1.17	700	700	23.74
1.49	10.01	35.97	99.41	CS,1	1	32	3.11	466	-	-
1.49	10.01	35.97	99.84	CD,8	8	128	0.78	-	234	35.52
1.49	10.01	35.97	99.84	SZ(8/64)	8	128	0.78	468	468	35.52

Table 2.5. VCP 44[1]

Elev. (deg)	AZ rate (deg/s)	Period (s)	Dwell time (ms)	WF type	Short PRT #	Long PRT #	M	T_1 (ms)	T_2 (ms)	r_{ar} (km)	r_{av} (km)	v_a (m/s)
0.48	5.83	61.71	171.09	ST(168/233)	2	1	32	2.24	3.11	466	336	26.7
0.48	16.04	22.44	62.29	ST(117/175)	8	4	32	0.78	1.17	175	117	71.2
1.49	5.83	61.71	171.09	ST(168/233)	2	1	32	2.24	3.11	466	336	26.7
1.49	16.04	22.44	62.29	ST(117/175)	8	4	32	0.78	1.17	175	117	71.2

Table 2.6. VCP 45a

Elev. (deg)	AZ rate (deg/s)	Period (s)	Dwell time (ms)	WF type	PRT #	Short PRT #	Long PRT #	M	T_u (ms)	T_1 (ms)	T_2 (ms)	r_{ar} (km)	r_{av} (km)	v_a (m/s)
0.48	10.06	35.77	99.41	CS,1	1	-	-	32	3.11	-	-	466	-	-
0.48	20.03	17.97	49.92	CD,8	8	-	-	64	0.78	-	-	-	234	35.52
0.48	10.2	35.31	98.13	ST(2/3)	-	9	10	32	-	1.23	1.84	276	184	45.1
1.49	10.06	35.77	99.41	CS,1	1	-	-	32	3.11	-	-	466	-	-
1.49	20.03	17.97	49.92	CD,8	8	-	-	64	0.78	-	-	-	234	35.52
1.49	10.2	35.31	98.13	ST(2/3)	-	9	10	32	-	1.23	1.84	276	184	45.1
2.5	10.06	35.77	99.41	CS,1	1	-	-	32	3.11	-	-	466	-	-
2.5	20.03	17.97	49.92	CD,8	8	-	-	64	0.78	-	-	-	234	35.52
2.5	10.2	35.31	98.13	ST(2/3)	-	9	10	32	-	1.23	1.84	276	184	45.1

Table 2.7. VCP 46a

Elev. (deg)	AZ rate (deg/s)	Period (s)	Dwell time (ms)	WF type	PRT #	Short PRT #	Long PRT #	M	T_u (ms)	T_1 (ms)	T_2 (ms)	r_{ar} (km)	r_{av} (km)	v_a (m/s)
0.48	18.67	19.29	52.81	CS,1	1	-	-	17	3.11	-	-	466	-	-
0.48	19.23	18.72	51.31	CD,5	5	-	-	52	0.99	-	-	-	296	28.08
0.48	5.84	61.59	171.09	ST(168/233)	-	2	1	32	-	2.24	3.11	466	336	26.7
0.48	10.2	35.31	98.13	ST(2/3)	-	9	10	32	-	1.23	1.84	276	184	45.1
0.48	7.81	46.09	128	ST(2/3)	-	23	24	32	-	1.6	2.4	360	240	34.6
1.45	19.84	18.14	49.71	CS,1	1	-	-	16	3.11	-	-	466	-	-
1.45	19.23	18.72	51.31	CD,5	5	-	-	52	0.99	-	-	-	296	28.08
1.45	5.84	61.59	171.09	ST(168/233)	-	2	1	32	-	2.24	3.11	466	336	26.7
1.45	10.2	35.31	98.13	ST(2/3)	-	9	10	32	-	1.23	1.84	276	184	45.1
1.45	7.81	46.09	128	ST(2/3)	-	23	24	32	-	1.6	2.4	360	240	34.6
2.42	16.12	22.34	59.09	B	-	5	1	47(6,41)	-	0.99	3.11	466	296	28.08
2.42	5.84	61.59	171.09	ST(168/233)	-	2	1	32	-	2.24	3.11	466	336	26.7
2.42	10.2	35.31	98.13	ST(2/3)	-	9	10	32	-	1.23	1.84	276	184	45.1
2.42	7.81	46.09	128	ST(2/3)	-	23	24	32	-	1.6	2.4	360	240	34.6

Table 2.8. VCP 45b

Elev. (deg)	AZ rate (deg/s)	Period (s)	Dwell time (ms)	WF type	PRT #	Short PRT #	Long PRT #	M	T_u (ms)	T_1 (ms)	T_2 (ms)	r_{ar} (km)	r_{av} (km)	v_a (m/s)
0.48	18.67	19.29	52.81	CS,1	1	-	-	17	3.11	-	-	466	-	-
0.48	19.23	18.72	51.31	CD,5	5	-	-	52	0.99	-	-	-	296	28.08
0.48	18.7	19.25	53.47	ST(168/233)	-	2	1	10	-	2.24	3.11	466	336	26.7
0.48	18.12	19.87	55.2	ST(2/3)	-	9	10	18	-	1.23	1.84	276	184	45.1
0.48	17.86	20.15	56	ST(2/3)	-	23	24	14	-	1.6	2.4	360	240	34.6
1.45	19.84	18.14	49.71	CS,1	1	-	-	16	3.11	-	-	466	-	-
1.45	19.23	18.72	51.31	CD,5	5	-	-	52	0.99	-	-	-	296	28.08
1.45	18.7	19.25	53.47	ST(168/233)	-	2	1	10	-	2.24	3.11	466	336	26.7
1.45	18.12	19.87	55.2	ST(2/3)	-	9	10	18	-	1.23	1.84	276	184	45.1
1.45	17.86	20.15	56	ST(2/3)	-	23	24	14	-	1.6	2.4	360	240	34.6
2.42	16.12	22.34	59.09	B	-	5	1	47(6,41)	-	0.99	3.11	466	296	28.08
2.42	15.59	23.09	64.16	ST(168/233)	-	2	1	12	-	2.24	3.11	466	336	26.7
2.42	16.3	22.08	61.33	ST(2/3)	-	9	10	20	-	1.23	1.84	276	184	45.1
2.42	15.63	23.03	64	ST(2/3)	-	23	24	16	-	1.6	2.4	360	240	34.6

Table 2.9. VCP 46b

Elev. (deg)	AZ rate (deg/s)	Period (s)	Dwell time (ms)	WF type	PRT #	Short PRT #	Long PRT #	M	T_u (ms)	T_1 (ms)	T_2 (ms)	r_{ar} (km)	r_{av} (km)	v_a (m/s)
0.48	10.06	35.77	99.41	CS,1	1	-	-	32	3.11	-	-	466	-	-
0.48	20.03	17.97	49.92	CD,8	8	-	-	64	0.78	-	-	-	234	35.52
0.48	12.5	28.79	80	ST(2/3)	-	23	24	20	-	1.6	2.4	360	240	34.6
1.49	10.06	35.77	99.41	CS,1	1	-	-	32	3.11	-	-	466	-	-
1.49	20.03	17.97	49.92	CD,8	8	-	-	64	0.78	-	-	-	234	35.52
1.49	12.5	28.79	80	ST(2/3)	-	23	24	20	-	1.6	2.4	360	240	34.6
2.5	10.06	35.77	99.41	CS,1	1	-	-	32	3.11	-	-	466	-	-
2.5	20.03	17.97	49.92	CD,8	8	-	-	64	0.78	-	-	-	234	35.52
2.5	12.5	28.79	80	ST(2/3)	-	23	24	20	-	1.6	2.4	360	240	34.6

Table 2.10. VCP 47a

Elev. (deg)	AZ rate (deg/s)	Period (s)	Dwell time (ms)	WF type	PRT #	Short PRT #	Long PRT #	M	T_u (ms)	T_1 (ms)	T_2 (ms)	r_{ar} (km)	r_{av} (km)	v_a (m/s)
0.48	10.06	35.77	99.41	CS,1	1	-	-	32	3.11	-	-	466	-	-
0.48	20.03	17.97	49.92	CD,8	8	-	-	64	0.78	-	-	-	234	35.52
0.48	18.12	19.87	55.2	ST(2/3)	-	9	10	18	-	1.23	1.84	276	184	45.1
1.49	10.06	35.77	99.41	CS,1	1	-	-	32	3.11	-	-	466	-	-
1.49	20.03	17.97	49.92	CD,8	8	-	-	64	0.78	-	-	-	234	35.52
1.49	18.12	19.87	55.2	ST(2/3)	-	9	10	18	-	1.23	1.84	276	184	45.1
2.5	10.06	35.77	99.41	CS,1	1	-	-	32	3.11	-	-	466	-	-
2.5	20.03	17.97	49.92	CD,8	8	-	-	64	0.78	-	-	-	234	35.52
2.5	18.12	19.87	55.2	ST(2/3)	-	9	10	18	-	1.23	1.84	276	184	45.1

Table 2.11. VCP 48

Elev. (deg)	AZ rate (deg/s)	Period (s)	Dwell time (ms)	WF type	PRT #	Short PRT #	Long PRT #	M	T_u (ms)	T_1 (ms)	T_2 (ms)	r_{ar} (km)	r_{av} (km)	v_a (m/s)
0.48	10.06	35.77	99.41	CS,1	1	-	-	32	3.11	-	-	466	-	-
0.48	20.03	17.97	49.92	CD,8	8	-	-	64	0.78	-	-	-	234	35.52
0.48	17.85	20.16	56	ST(2/3)	-	23	24	14	-	1.6	2.4	360	240	34.6
1.49	10.06	35.77	99.41	CS,1	1	-	-	32	3.11	-	-	466	-	-
1.49	20.03	17.97	49.92	CD,8	8	-	-	64	0.78	-	-	-	234	35.52
1.49	17.85	20.16	56	ST(2/3)	-	23	24	14	-	1.6	2.4	360	240	34.6
2.5	10.06	35.77	99.41	CS,1	1	-	-	32	3.11	-	-	466	-	-
2.5	20.03	17.97	49.92	CD,8	8	-	-	64	0.78	-	-	-	234	35.52
2.5	17.85	20.16	56	ST(2/3)	-	23	24	14	-	1.6	2.4	360	240	34.6

Table 2.12. VCP 49

b. Description of collected data

Below we list all the cases where time series data were collected using the KOUN research radar. A snapshot of the reflectivity field (obtained with a long uniform PRT) is provided for each event. Also listed are a brief description of the meteorological event, the types of collected data (SZ-2 and/or Staggered), and the VCPs collected for each case.

For all these cases, fields of reflectivity, velocity, and spectrum width are displayed and described on the NSSL's Mitigation of Range/Velocity Ambiguities web page. This page can be accessed at:

`http://cimms.ou.edu/rvamb/Mitigation_R_V_Ambiguities.htm`

From the main page, links provide access to the phase coded and staggered PRT cases. For both methods, we provide links to each date when data collection experiments were conducted. Thumbnails of all spectral moments obtained for each elevation scan in every collected VCP provide easy access to the fields. Spectral moment thumbnails are linked with their corresponding full-size image. Volume coverage pattern definitions are also linked from the VCP name.

Reflectivity field (uniform long PRT)	**Event description**
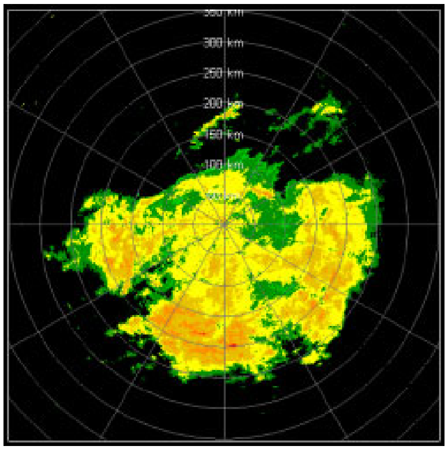	**10/08/02** On 8 October 2002, a large region of stratiform precipitation slowly moved across Oklahoma. Polarimetric signatures indicate a bright band at radial distances far from KOUN. <u>Collected data:</u> SZ-2: VCP 43
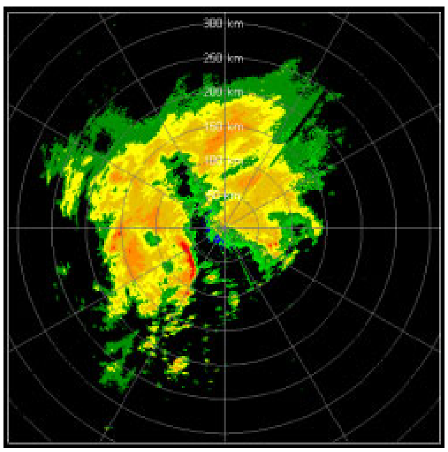	**10/29/02** The asymmetric squall line from 28 Oct completes its track across Oklahoma (00-5:33 GMT). Following this event, an AP bloom with biological scatterers forms around KOUN. <u>Collected data:</u> SZ-2: VCP 43
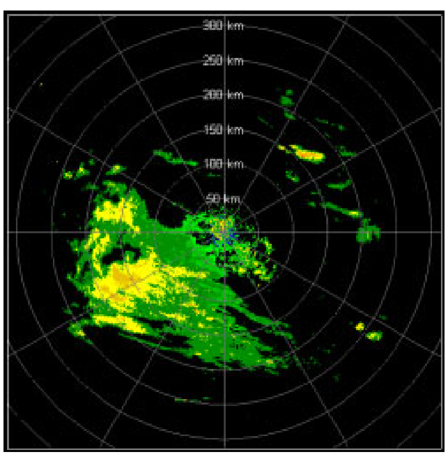	**02/14/03** During the evening of 13 February 2003, a region of stratiform precipitation moved slowly over central Oklahoma. This precipitation was very light, producing drizzle over most of the region. <u>Collected data:</u> SZ-2: VCP 43 Staggered: VCP 45a

Reflectivity field (uniform long PRT)	Event description
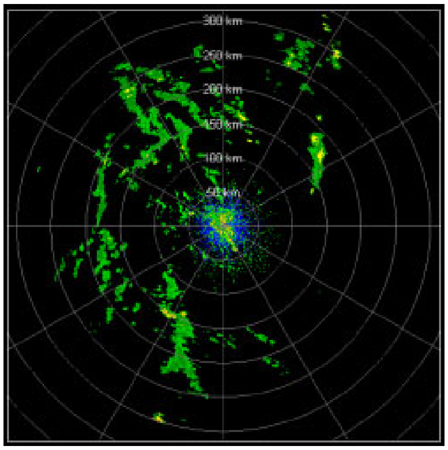	**03/17/03** Several severe storms developed over western Oklahoma during the afternoon of the 17th and tracked slowly eastward during the evening, before dissipating over central portions of Oklahoma. Four tornadoes accompanied this severe weather outbreak, with two of them resulting in F1 damage. <u>Collected data:</u> SZ-2: VCP 43 Staggered: VCP 46a
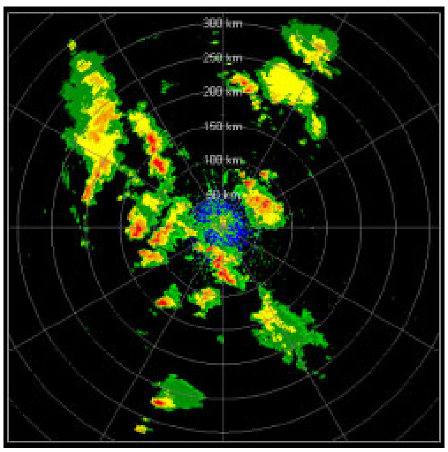	**03/18/03** Several severe storms developed over western Oklahoma during the afternoon of the 17th and tracked slowly eastward during the evening, before dissipating over central portions of Oklahoma. Four tornadoes accompanied this severe weather outbreak, with two of them resulting in F1 damage. <u>Collected data:</u> SZ-2: VCP 43 Staggered: VCP 45a, VCP 46a, VCP 47a, VCP 48, VCP 49
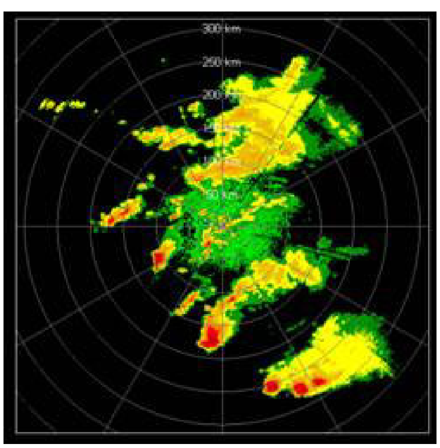	**04/06/03** On this day a scattered collection of severe storms developed in Oklahoma, some of which formed distinct clusters. Several cells had reflectivity in excess of 60 dBZ. Triple overlay occurred for some of the storms to the NE and SE of KOUN. <u>Collected data:</u> SZ-2: VCP 43 Staggered: VCP 46a, VCP 47a, VCP 48, VCP 49

Reflectivity field (uniform long PRT)	**Event description**
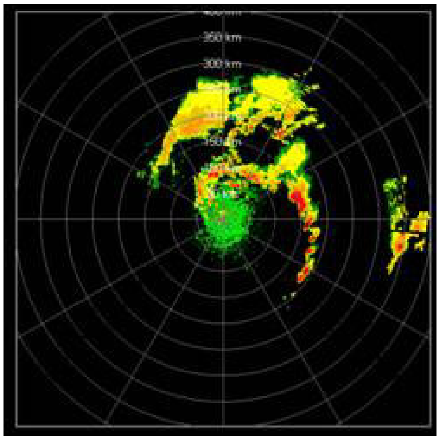	**05/16/03** During the night and early morning hours on 16 May 2003, a Mesoscale Convective System (MCS) moved across central Oklahoma, producing heavy rainfall in some areas. Polarimetric signatures indicate there were biological scatters around KOUN prior to this evening. Later that afternoon, convective cells formed around KOUN in association with a upper-level low. Most storms produced locally heavy showers only. However, a few cells developed supercellular characteristics, with the best observed storm producing sited tornadoes over Haskell Co. (~20-21 GMT). No hail was reported in association with these storms. <u>Collected data:</u> SZ-2: VCP 43 Staggered: VCP 46a, VCP 47a, VCP 48, VCP 49
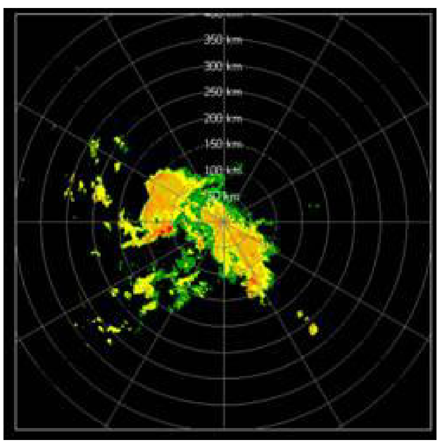	**06/04/03** This event was a Mesoscale Convective System (MCS) that developed early in the morning in North Texas and Southwestern Oklahoma. It is typical for that time of year. It propagated to the NE and was over the KOUN radar in mid morning. By that time, the system developed a mesoscale convective vortex in its NW part which caused formation of three intense cells. <u>Collected data:</u> SZ-2: VCP 43 Staggered: VCP 45b, VCP 46b
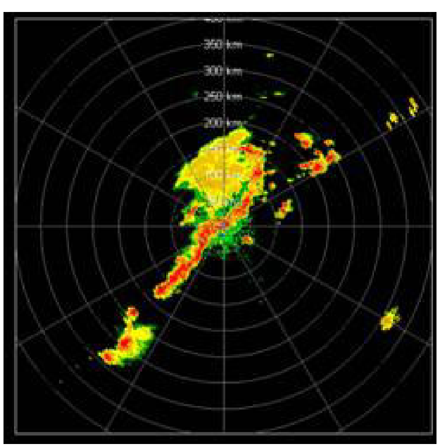	**06/11/03** On 10-11 June 2003, a squall line developed west of KOUN and moved across central Oklahoma, dumping heavy rainfall and flooding streets in Norman, OK. Hail was produced by cells located near Corn and Hinton. AP occurred behind the line between 2:45 and 7 GMT. <u>Collected data:</u> SZ-2: VCP 43 Staggered: VCP 45b, VCP 46b

Reflectivity field (uniform long PRT)	Event description
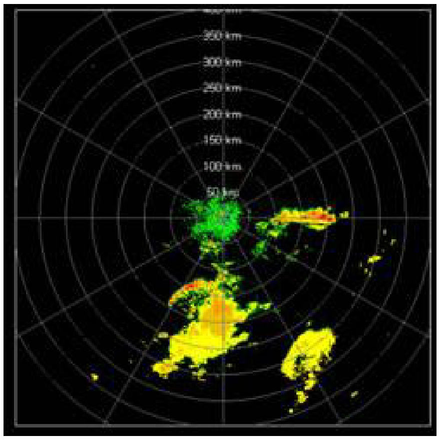	**06/13/03** On 13 June 2003, AP occurred around KOUN between 03:15 - 08:55 GMT. By 8:41 GMT, convective cells had developed over southwest Oklahoma, and proceeded toward central Oklahoma by 13 GMT. <u>Collected data:</u> SZ-2: VCP 43 Staggered: VCP 45b, VCP 46b
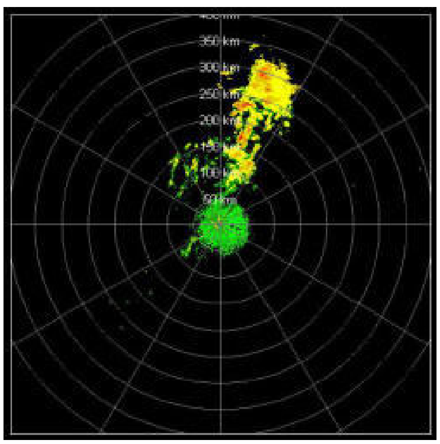	**06/25/03** On 25 June, two convective lines began to develop over north-central and southwest Oklahoma. The more northern line evolved into a squall line, producing locally heavy amounts of rainfall. These lines moved southeastward across Oklahoma between 20 GMT 25 June and 13 GMT 26 June. A new region of convective cells developed over southwest Oklahoma during the later morning hours of 26 June, producing light rainfall. <u>Collected data:</u> SZ-2: VCP 43
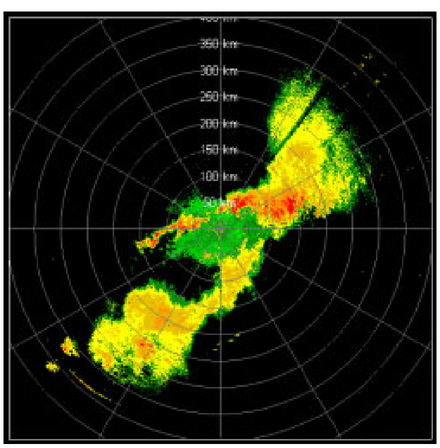	**06/26/03** On 25 June, two convective lines began to develop over north-central and southwest Oklahoma. The more northern line evolved into a squall line, producing locally heavy amounts of rainfall. These lines moved southeastward across Oklahoma between 20 GMT 25 June and 13 GMT 26 June. A new region of convective cells developed over southwest Oklahoma during the later morning hours of 26 June, producing light rainfall. <u>Collected data:</u> SZ-2: VCP 44 Staggered: VCP 45b

3. Phase coding

This section describes work on the SZ phase coding. It documents the steps taken to insure that the collected data are correct. First, we discuss the performance of the WSR-88D phase shifter and examine the performance on individual radials of data. Then, the description of the SZ-2 algorithm is presented. This description is taken from the NCAR-NSSL Interim Report (2003). Finally, we show some examples of the velocity and reflectivity fields produced by this algorithm.

3.1. Phase shifter analysis

In the report by Frush (1997) it was established that the phase shifter rms noise is less than 0.2° which is sufficient for good performance of the SZ coding scheme. A previous report hints that the achieved phase is stable but differs from the commanded phase. That is, there is a systematic bias. In the RVP8 processor the phase of each transmitted pulse can be measured to eliminate the bias. But in the time series data collected with the KOUN radar the phases of the phase shifter differ from the exact SZ phases. Hence, the following two issues concerning the phase shifter are pertinent for the SZ phase coding scheme.

- What phases to use for decoding time series?
- How to determine these exact phases in the operational system - from pulse to pulse measurement or periodic calibration?

We performed closed loop measurement to determine the exact phases for decoding the phase coded data. Antenna was stationary; phase-coded and not-phase-coded time series data of a tower were recorded. Two such sets are discussed herein. One was obtained on Feb 10, 2003

(02/10) and the other on April 2, 2003 (04/02) with the antenna pointed at azimuth 305.8°, and elevation 0.3°. A sweep of time series data consists of 468 consecutive (in range-time) *I*, *Q* samples and one radial contains 64 sweeps of such data. The powers of the return signal (in logarithmic units) for one radial of the first and second sets are in Fig. 3.1 and Fig. 3.2, respectively. The test set for the estimation of the phase change consists of 100 radials.

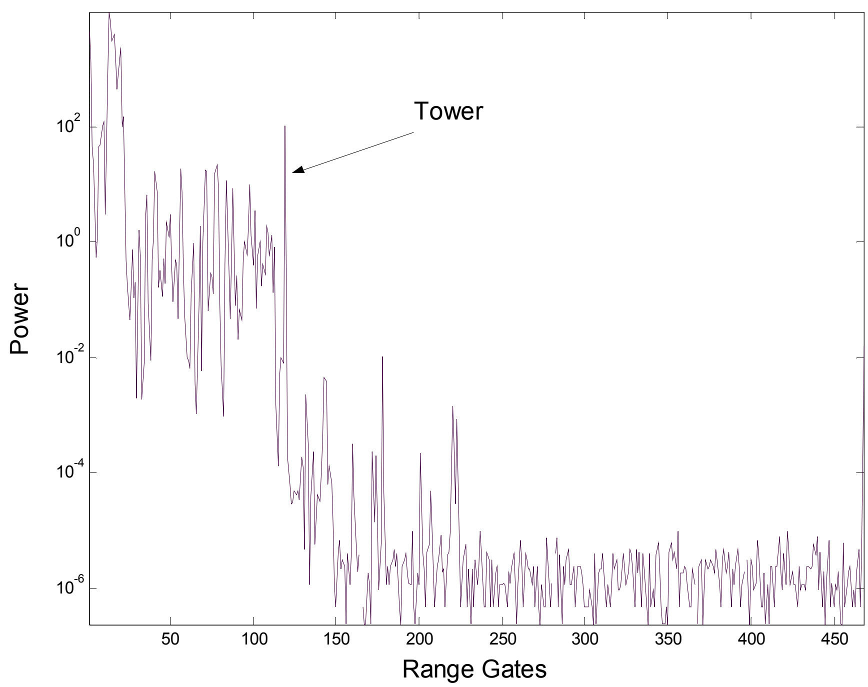

Fig. 3.1: Power (not calibrated) of the return signal for one radial (Date 02/10).

There were changes made to the system and a failure in transmitter between the two data collections; hence, the absolute powers in the two figures differ. Winds were calm on 02/10 but were 22 mph gusting to 31mph on 04/02; this might have caused the difference in the signals. However, strong signal from the tower (119th range gate) is evident (SNR of about 60 dB) and has a stable shape. This signal (at 29.125 km from the antenna) was chosen for estimating the stability and repeatability of the phase sequence generated by the phase shifter.

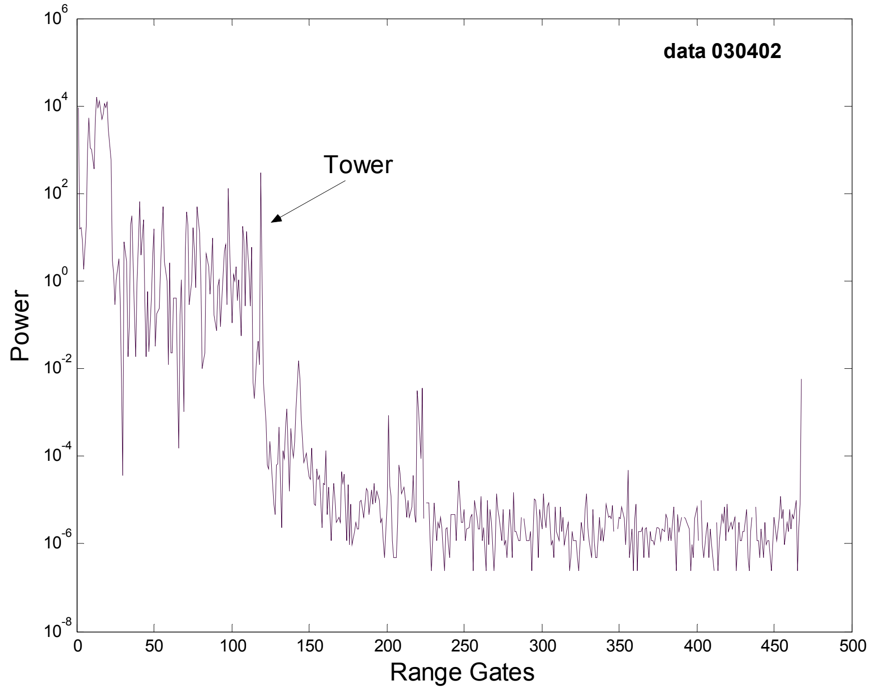

Fig. 3.2: Power (not calibrated) of the return signal for one radial (Date 04/02).

Commanded phases used for phase-coding are given in degrees in the second column of Tables 3.1 and 3.2. All phases are in the range -180° to 180°. The measured phase is estimated from the average of 100 sample phases as follows

$$\hat{\Psi}(k) = \frac{1}{100}\sum_{r=1}^{100} \arg\left[V_r(1)V_r^*(k)\right], \tag{3.1}$$

where $V_r(k)$ is the complex received signal from the r-th radial and k-th sweep (k =1, 2, ..., 64). Note that the k-th sweep is encoded with the k-th phase of the switching code. The estimated phase $\hat{\Psi}(k)$ is in the third column of Tables 3.1 and 3.2. The phase bias, which is given by the differences $\Delta(k) = \Psi(k) - \hat{\Psi}(k)$ between the commanded and estimated sequences of phases, is quite small. These differences are shown in the fourth column of Tables 3.1 and 3.2.

k	Commanded Phase	Estimated Phase	Difference [3]-[2]	Standard Deviation
1	0	0	0	0
2	-22.5	-21.5447	0.9553	0.9715
3	-112.5	-112.4008	0.0992	0.2268
4	45.0	45.0811	0.0811	0.2231
5	45.0	45.0203	0.0203	0.2124
6	-157.5	-158.4123	-0.9123	0.9307
7	112.5	111.9415	-0.5585	0.6130
8	90.0	89.8464	-0.1536	0.3178
9	90.0	89.8114	-0.1886	0.3143
10	67.5	67.9936	0.4936	0.5508
11	-22.5	-21.4976	1.0024	1.0250
12	135.0	134.4742	-0.5258	0.5919
13	135.0	134.4190	-0.5810	0.6464
14	-67.5	-66.5753	0.9247	0.9724
15	-157.5	-158.4108	-0.9108	0.9536
16	180.0	178.9186	-1.0814	1.1069
17	180.0	178.8632	-1.1368	1.1770
18	157.5	156.8656	-0.6344	0.7031
19	67.5	68.0014	0.5014	0.5848
20	-135.0	-135.3065	-0.3065	0.4071
21	-135.0	-135.3887	-0.3887	0.4643
22	22.5	22.5191	0.0191	0.2909
23	-67.5	-66.5941	0.9059	0.9549
24	-90.0	-88.9298	1.0702	1.1082
25	-90.0	-88.9571	1.0429	1.0714
26	-112.5	-112.4027	0.0973	0.2450
27	157.5	156.9293	-0.5707	0.6324
28	-45.0	-44.0539	0.9461	0.9916
29	-45.0	-44.0982	0.9018	0.9469
30	112.5	112.0190	-0.4810	0.5570
31	22.5	22.5154	0.0154	0.2738
32	0	0.0237	0.0237	0.3144
33	0	0.0226	0.0226	0.3281
34	-22.5	-21.5263	0.9737	1.0189
35	-112.5	-112.4115	0.0885	0.3150
36	45.0	45.0769	0.0769	0.2941
37	45.0	45.0144	0.0144	0.3234
38	-157.5	-158.4388	-0.9388	1.0009
39	112.5	111.9217	-0.5783	0.6772
40	90.0	89.8152	-0.1848	0.3973
41	90.0	89.8135	-0.1865	0.3930
42	67.5	67.9805	0.4805	0.6320
43	-22.5	-21.4864	1.0136	1.0925
44	135.0	134.4600	-0.5400	0.6614
45	135.0	134.4071	-0.5929	0.6957
46	-67.5	-66.5765	0.9235	0.9878
47	-157.5	-158.3987	-0.8987	0.9699
48	180.0	178.9430	-1.0570	1.1221
49	180.0	178.8859	-1.1141	1.1809
50	157.5	156.9017	-0.5983	0.7130
51	67.5	68.0369	0.5369	0.6566
52	-135.0	-135.2968	-0.2968	0.5187
53	-135.0	-135.3857	-0.3857	0.5786
54	22.5	22.5291	0.0291	0.4014
55	-67.5	-66.5886	0.9114	0.9872
56	-90.0	-88.9195	1.0805	1.1516
57	-90.0	-88.9111	1.0889	1.1587
58	-112.5	-112.3874	0.1126	0.4264
59	157.5	156.9397	-0.5603	0.6939
60	-45.0	-44.0765	0.9235	1.0064
61	-45.0	-44.1269	0.8731	0.9581
62	112.5	111.9904	-0.5096	0.6679
63	22.5	22.4851	-0.0149	0.4469
64	0	0.0042	0.0042	0.4309
		rms	0.67	0.74

Table 3.1. Commanded phase, estimated phase, phase difference, and standard deviation of estimated phase (02/10). Phases are in degrees.

k	Commanded Phase	Estimated Phase	Difference [3]-[2]	Standard Deviation
1	0	0	0	0
2	-22.5	-21.6502	0.8498	1.0168
3	-112.5	-112.5322	-0.0322	0.8747
4	45.0	44.9247	-0.0753	0.9080
5	45.0	44.8409	-0.1591	1.0216
6	-157.5	-158.3160	-0.8160	1.1928
7	112.5	111.8618	-0.6382	0.8921
8	90.0	89.6101	-0.3899	0.7225
9	90.0	89.5985	-0.4015	0.9218
10	67.5	67.9115	0.4115	1.0932
11	-22.5	-21.5697	0.9303	1.3523
12	135.0	134.6499	-0.3501	1.0598
13	135.0	134.6559	-0.3441	0.8732
14	-67.5	-66.6952	0.8048	0.9891
15	-157.5	-158.2264	-0.7264	1.0485
16	180.0	179.4035	-0.5965	1.1815
17	180.0	179.3872	-0.6128	1.2441
18	157.5	157.5204	0.0204	1.0694
19	67.5	67.9358	0.4358	1.0265
20	-135.0	-135.3983	-0.3983	0.8502
21	-135.0	-135.5324	-0.5324	0.7974
22	22.5	22.4569	-0.0431	0.8598
23	-67.5	-66.7793	0.7207	1.3241
24	-90.0	-88.9767	1.0233	1.4689
25	-90.0	-89.0676	0.9324	1.4246
26	-112.5	-112.4897	0.0103	0.7895
27	157.5	157.5255	0.0255	0.6232
28	-45.0	-44.1145	0.8855	1.0925
29	-45.0	-44.1513	0.8487	1.2340
30	112.5	111.9338	-0.5662	1.1560
31	22.5	22.4896	-0.0104	1.0692
32	0	0.0712	0.0712	1.0482
33	0	0.0720	0.0720	0.8603
34	-22.5	-21.6160	0.8840	1.0813
35	-112.5	-112.4401	0.0599	0.7932
36	45.0	44.9536	-0.0464	0.9936
37	45.0	44.9263	-0.0737	1.0499
38	-157.5	-158.3122	-0.8122	1.3720
39	112.5	111.8961	-0.6039	1.1900
40	90.0	89.6116	-0.3884	0.8695
41	90.0	89.5824	-0.4176	0.7221
42	67.5	67.9500	0.4500	0.9156
43	-22.5	-21.5791	0.9209	1.3501
44	135.0	134.6690	-0.3310	1.1045
45	135.0	134.5944	-0.4056	1.1461
46	-67.5	-66.7499	0.7501	1.1810
47	-157.5	-158.3387	-0.8387	1.1453
48	180.0	179.3656	-0.6344	0.9764
49	180.0	179.3462	-0.6538	1.1105
50	157.5	157.5235	0.0235	0.9635
51	67.5	67.9379	0.4379	1.1017
52	-135.0	-135.4104	-0.4104	0.9962
53	-135.0	-135.4908	-0.4908	0.9109
54	22.5	22.4261	-0.0739	0.5446
55	-67.5	-66.7692	0.7308	1.0182
56	-90.0	-89.0160	0.9840	1.3502
57	-90.0	-89.0271	0.9729	1.4073
58	-112.5	-112.5126	-0.0126	1.0583
59	157.5	157.5697	0.0697	0.9504
60	-45.0	-44.1322	0.8678	1.2019
61	-45.0	-44.1961	0.8039	1.1101
62	112.5	111.8796	-0.6204	1.1339
63	22.5	22.4296	-0.0704	1.0875
64	0	0.0624	0.0624	1.0493
		Rms	0.57	1.06

Table 3.2: Commanded, estimated phase, phase difference, and standard deviation of estimated phase (04/02). Phases are in degrees.

k	Commanded Phase	Estimated Phase 02/10	Estimated Phase 04/02	Difference [3]-[4]
1	0	0	0	0
2	-22.5	-21.5447	-21.6502	0.1055
3	-112.5	-112.4008	-112.5322	0.1313
4	45.0	45.0811	44.9247	0.1564
5	45.0	45.0203	44.8409	0.1794
6	-157.5	-158.4123	-158.3160	-0.0963
7	112.5	111.9415	111.8618	0.0797
8	90.0	89.8464	89.6101	0.2362
9	90.0	89.8114	89.5985	0.2129
10	67.5	67.9936	67.9115	0.0821
11	-22.5	-21.4976	-21.5697	0.0721
12	135.0	134.4742	134.6499	-0.1757
13	135.0	134.4190	134.6559	-0.2368
14	-67.5	-66.5753	-66.6952	0.1199
15	-157.5	-158.4108	-158.2264	-0.1844
16	180.0	178.9186	179.4035	-0.4849
17	180.0	178.8632	179.3872	-0.5240
18	157.5	156.8656	157.5204	-0.6548
19	67.5	68.0014	67.9358	0.0656
20	-135.0	-135.3065	-135.3983	0.0918
21	-135.0	-135.3887	-135.5324	0.1436
22	22.5	22.5191	22.4569	0.0621
23	-67.5	-66.5941	-66.7793	0.1852
24	-90.0	-88.9298	-88.9767	0.0469
25	-90.0	-88.9571	-89.0676	0.1105
26	-112.5	-112.4027	-112.4897	0.0871
27	157.5	156.9293	157.5255	-0.5962
28	-45.0	-44.0539	-44.1145	0.0606
29	-45.0	-44.0982	-44.1513	0.0532
30	112.5	112.0190	111.9338	0.0852
31	22.5	22.5154	22.4896	0.0258
32	0	0.0237	0.0712	-0.0475
33	0	0.0226	0.0720	-0.0494
34	-22.5	-21.5263	-21.6160	0.0897
35	-112.5	-112.4115	-112.4401	0.0285
36	45.0	45.0769	44.9536	0.1233
37	45.0	45.0144	44.9263	0.0880
38	-157.5	-158.4388	-158.3122	-0.1266
39	112.5	111.9217	111.8961	0.0256
40	90.0	89.8152	89.6116	0.2036
41	90.0	89.8135	89.5824	0.2311
42	67.5	67.9805	67.9500	0.0305
43	-22.5	-21.4864	-21.5791	0.0928
44	135.0	134.4600	134.6690	-0.2090
45	135.0	134.4071	134.5944	-0.1873
46	-67.5	-66.5765	-66.7499	0.1733
47	-157.5	-158.3987	-158.3387	-0.0600
48	180.0	178.9430	179.3656	-0.4226
49	180.0	178.8859	179.3462	-0.4603
50	157.5	156.9017	157.5235	-0.6217
51	67.5	68.0369	67.9379	0.0990
52	-135.0	-135.2968	-135.4104	0.1136
53	-135.0	-135.3857	-135.4908	0.1052
54	22.5	22.5291	22.4261	0.1030
55	-67.5	-66.5886	-66.7692	0.1806
56	-90.0	-88.9195	-89.0160	0.0965
57	-90.0	-88.9111	-89.0271	0.1160
58	-112.5	-112.3874	-112.5126	0.1251
59	157.5	156.9397	157.5697	-0.6300
60	-45.0	-44.0765	-44.1322	0.0557
61	-45.0	-44.1269	-44.1961	0.0692
62	112.5	111.9904	111.8796	0.1108
63	22.5	22.4851	22.4296	0.0555
64	0	0.0042	0.0624	-0.0582
			rms	0.23

Table 3.3: Comparison of 0210 and 0402 data sets. Phases are in degrees.

The magnitude of the maximum difference $|\Delta(k)|$ (from the fourth column of Tables 3.1 and 3.2) is 1.14° for data acquired on 02/10 and it is 1.02° for data from 04/02; the root mean square Δ_{rms} of the differences is 0.67° and 0.57°, respectively. Standard deviations of estimated phases are shown in the fifth column of Tables 3.1 and 3.2 for each designated phase of the code. The rms of standard deviations is 0.74° and 1.06°, respectively. Average bias (i.e., the average of all values in the fourth column) is 0.02° for 02/10 data and 0.039° for 04/02 data. Also of interest are the differences between the mean values of the two days (see Table 3.3); the largest difference is 0.63° and the rms of differences between mean values for the two days is 0.23°. Clearly, the mean values of the phases are very stable and a good part of the difference between the two days might be due to propagation effects.

Coded data is decoded for the first trip echo according to

$$V_d(k) = V(k)\exp\left[j\frac{2\pi\Psi(k)}{360}\right], \tag{3.2}$$

where $\Psi(k)$ is the phase code in degrees, and could be either the commanded or the estimated code. A mismatch between the commanded and estimated phase sequences may lead to an error in the decoding of time-series and therefore to performance degradation. To quantify the effects of this error on the spectrum, the data was decoded by using commanded and estimated phase sequences.

Let $F(m)$ = DFT$\{V_d(k)\}$ be discrete Fourier transform of decoded time series. The average power spectrum (over 100 radials) is then found as

$$S(n) = \frac{1}{100}\sum_{r=1}^{100}\left|F_r(n)\right|^2. \tag{3.3}$$

Power spectra for the two days are plotted in Figs. 3.3 and 3.4. "No coding" refers to time series that were not phase coded, and the corresponding spectral floor is composed of receiver noise, system artifacts, and propagation effects. Deviations from that floor are attributed to the effects of coding/decoding.

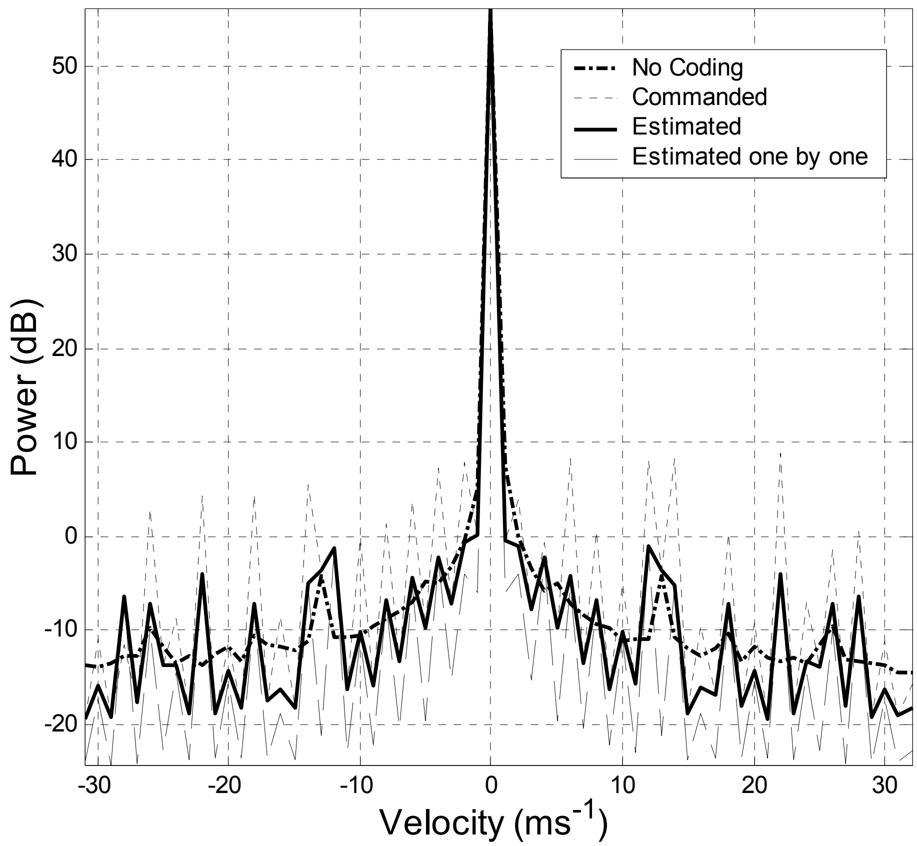

Fig. 3.3 Power spectra (02/10) of sequences decoded using various phase estimates.

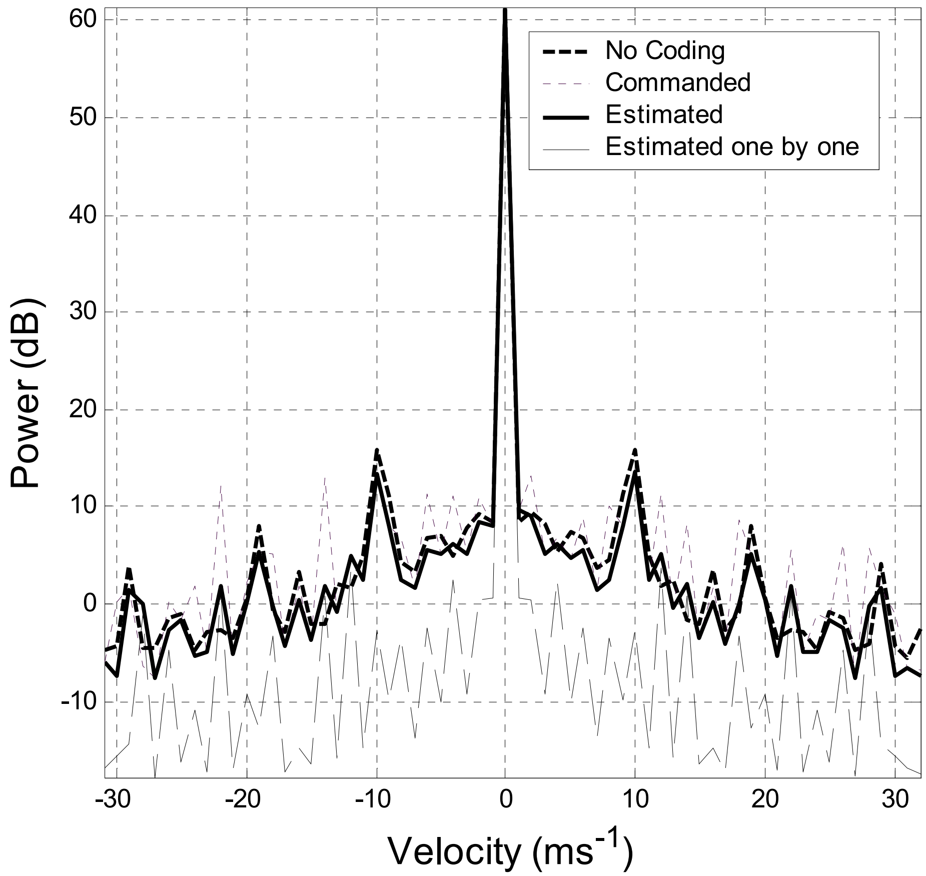

Fig. 3.4 Power spectra (0402) of sequences decoded using various phase estimates.

As expected, on both days the commanded phases produce the largest spectral sidelobes, about 45 dB below the peak. Further, decoding the time series with its own phases (labeled "Estimated one by one" in the figures) produces the lowest sidelobes. The signal to total spectral noise ratio SNR can be conveniently defined as

$$SNR = \frac{S(0)}{\sum_{n=1}^{63} S(n)}, \tag{3.4}$$

and its values for the various methods are listed in Table 3.4. Use of the commanded phases consistently results in the lowest SNR, which are comparable for the two days. Also comparable are the SNRs if the measured phase sequence of each radial is applied to decode the radial. This is expected as such individual correction may compensate for some propagation effects. Improvements in the SNR with respect to lowest values (obtained with commanded phases) for the two days are also listed.

	02/10 SNR (dB)	02/10 Improv. (dB)	04/02 SNR (dB)	04/02 Improv. (dB)
One by one per radial	47.24	9.49	47.01	10.54
Average of estimates	45.07	7.32	38.94	2.47
No phase coding	43.85	6.1	37.61	1.14
Commanded SZ(64/8) phases	37.75	0	36.47	0

Table 3.4: SNR from spectra of decoded signals

The reasons for significant difference in the SNRs between the two days and for the cases where there was no phase coding and when average of estimates was used are not know. The fact that individually measured phases (over the radial with 64 sweeps) gives the best SNR suggests that instantaneous sampling of phase as done in the RVP8 processor might be the best solution. Nonetheless, this should be confirmed by measurements similar to the ones made herein. Meanwhile, the estimated phases (from either Table 3.1 or 3.2) should be used in processing the time series data recorded with the KOUN in the Fall of 2002 and Spring of 2003.

3.2. Analysis of data along a radial

On Aug 25, 2002 we collected the first data set with the SZ(64/8) code. These data were recorded in an experimental format which is no longer used. Matlab files were generated and the analysis herein was meant to check the system quality and gain further experience with the phase coding technique. Recall that up until this time there was one data set of this kind from a WSR-88D, and it was over a limited range and azimuth extent.

We have chosen a radial to the southeast which had ground clutter, some clear air, anomalous propagation, and precipitation. The reflectivity PPI obtained with a long PRT is depicted in Fig. 3.5.

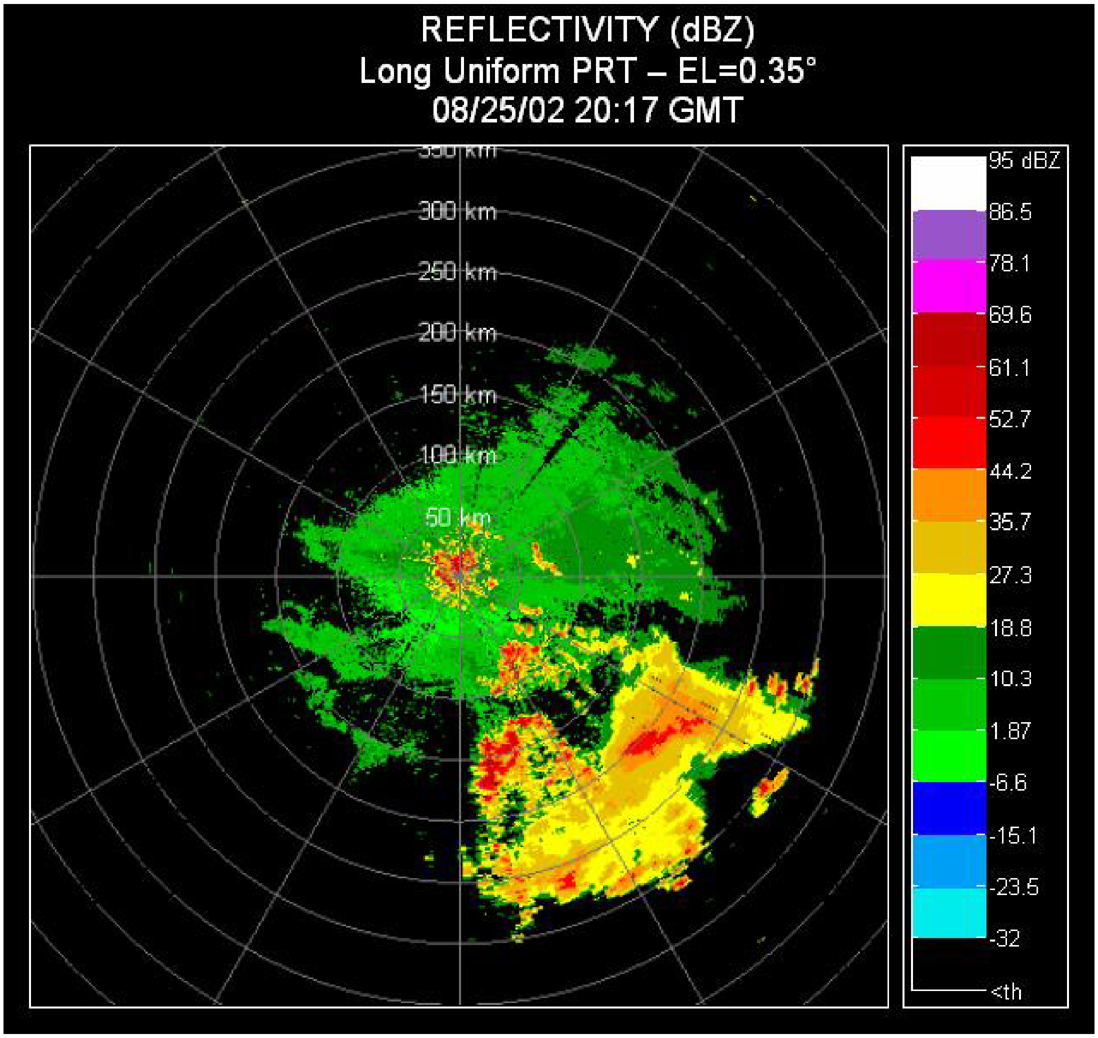

Fig. 3.5. PPI Reflectivity field corresponding to the first phase-coded data set collected on the KOUN research radar in Norman, OK on Aug 25, 2002. Ground clutter echoes due to anomalous propagation are evident south east of the radar.

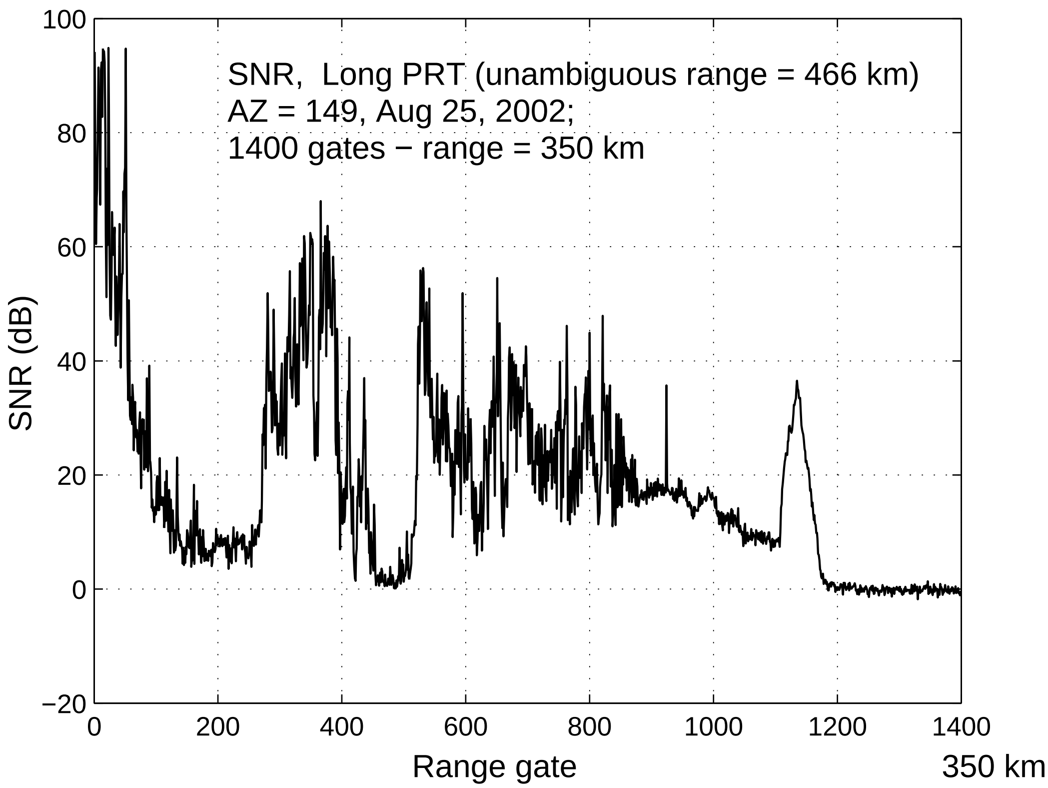

Fig. 3.6. Signal-to-noise ratio as a function of range gate. The gates are spaced 250 m so that the last gate displayed corresponds to 350 km. Because the longest PRT is used, the unambiguous range is 466 km.

The signal to noise ratio SNR is obtained from the data (average from range gates 1250 to the last gate) rather than calibration. At close range (less than 100 gates), strong ground clutter is evident; from gates 300 to 400 anomalous propagation (AP) with some precipitation seems to be present. Then again from about 500 to 900 there is AP and beyond precipitation extends close to gate 1200, it is then followed by receiver noise.

The weather echo was sampled at this same location with phased coded waveform and two PRTs. One PRT corresponds to an unambiguous range of 175 km (or 700 gates). This is about a maximum short PRT that can be used; it has an unambiguous velocity of 21.2 m s^{-1}. The other PRT produces an unambiguous range of 117 km (468 gates) and unambiguous velocity of 31.7 m s^{-1}.

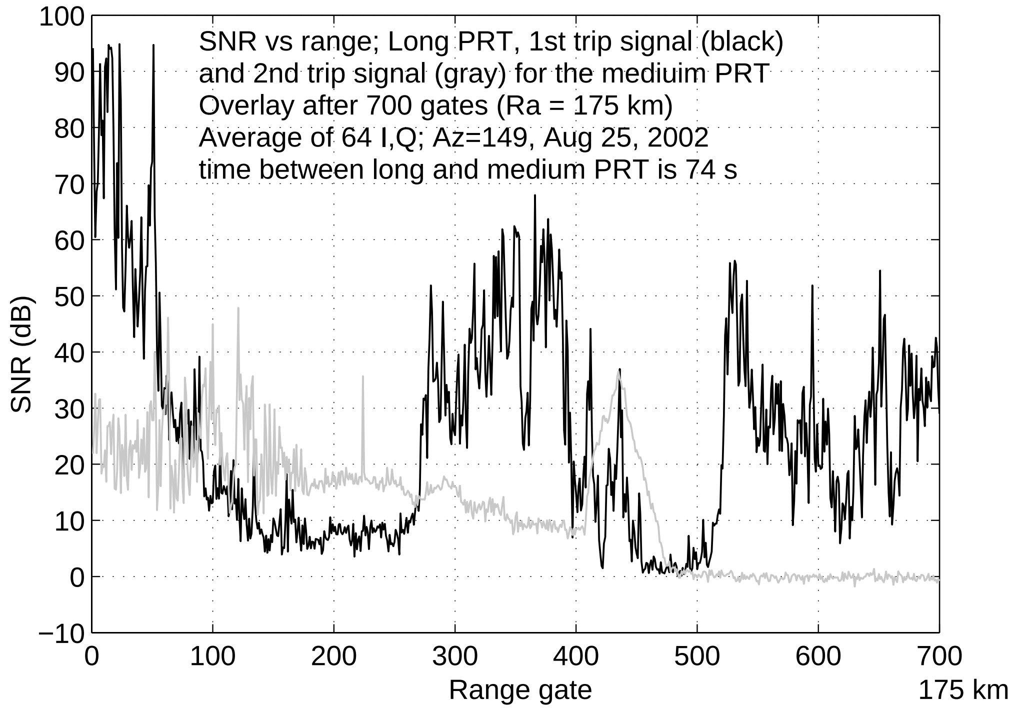

Fig. 3.7. SNR of the 1st and 2nd trip echo (for medium PRT) obtained from long PRT.

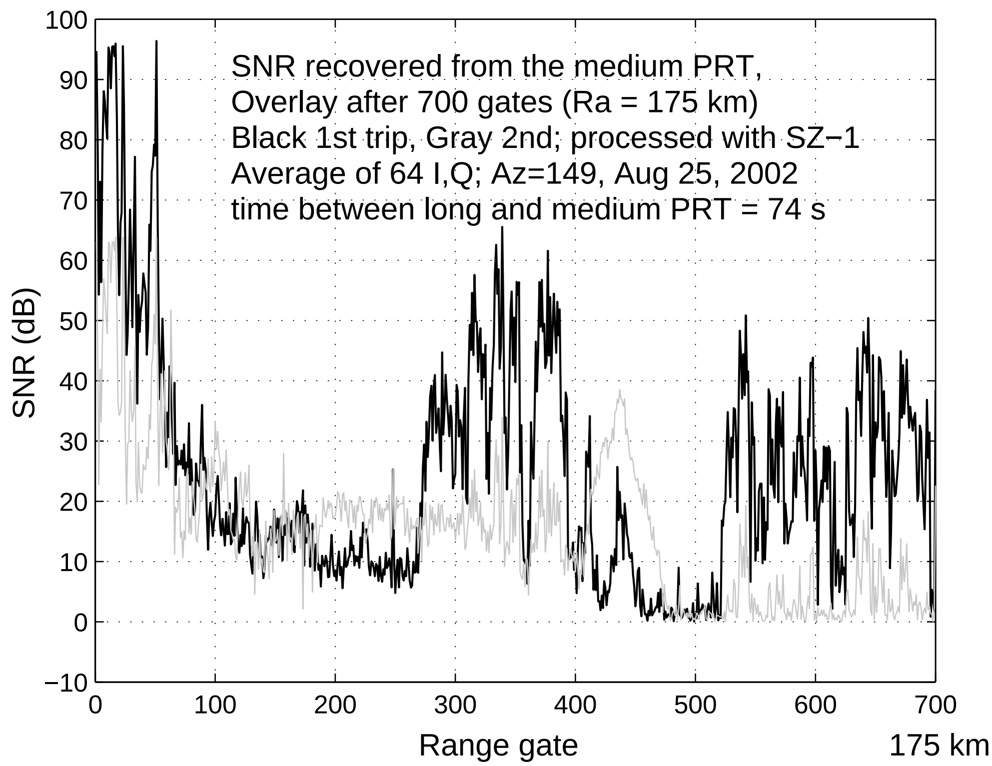

Fig. 3.8. 1st and 2nd trip SNR obtained by applying SZ-1 algorithm to medium PRT data.

Echoes within the first 700 gates in the long PRT contribute to the first trip SNRs of the medium PRT and echoes between the 700th gate and 1400th gate of the long PRT contribute the SNR of the second trip in the medium PRT. These are plotted in Fig. 3.7.

The SZ-1 algorithm has been applied to the time series from the medium PRT to retrieve the first- and second-trip echoes (Fig. 3.8). Comparison of Fig. 3.7 and 3.8 indicate that the first-trip ground clutter is well retrieved (no ground clutter filter is applied). The first-trip AP clutter (between 275 and 450) also looks reasonable and differences might be due to statistical uncertainty and slight spatial displacement (beams are not indexed in the WSR-88D); moreover there was a 74 s time lapse between the two data sets. It stands out that the leakage from the first-trip strong ground clutter to the second-trip signal is about 30 dB and that the retrieved second trip signal from gate 175 to 400 (Fig. 3.8) fluctuates much more than the actual signal (Fig. 3.7). The storm core, between range gates 400 and 475, is well retrieved. Then, at the end there is evidence of coupling of the strong signal to the noise; this can be avoided if a separate long PRT precedes the short PRT; that is the SZ-2 algorithm is used.

Differences in powers (dB scale) between the 1st and 2nd trip obtained from the long PRT (i.e., black curve minus the gray curve in Fig. 3.7) are plotted in Fig. 3.9. We expect that 1st and 2nd trip signals differing less than 30 dB could be separated provided their spectra are relatively narrow. This is borne out by the result in Fig. 3.8 and by superposition of the “true” SNR profile (black curve) and retrieved SNR in Fig. 3.10.

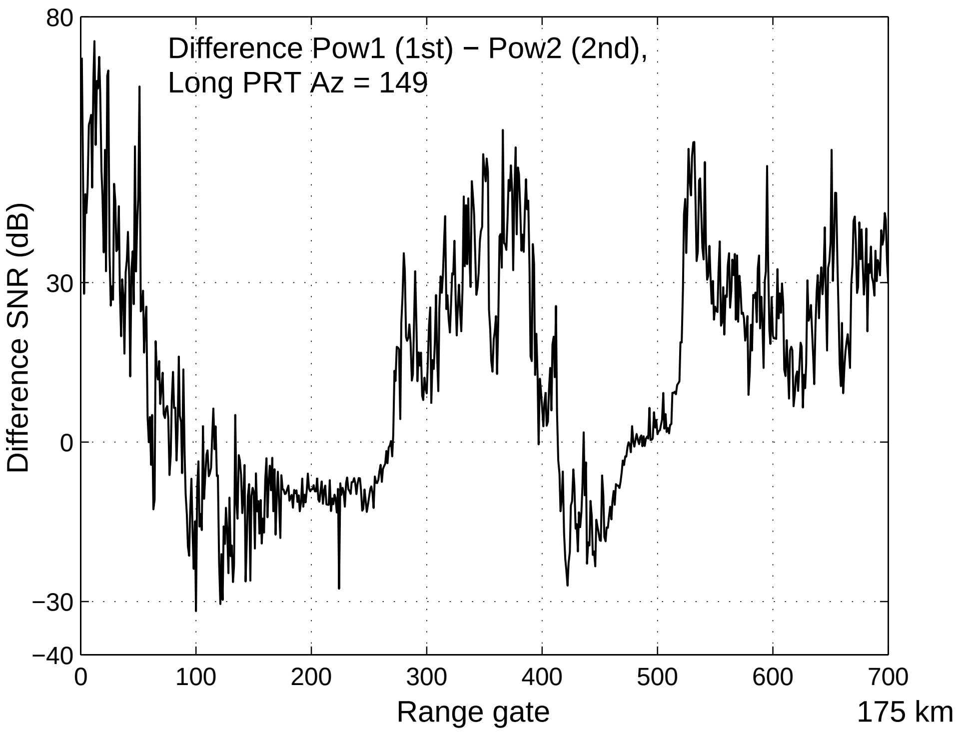

Fig. 3.9. Power difference in dB expressed as difference in SNR between the first-trip echo and second-trip echo. Long PRT data (Fig. 3.6) has been used.
About 20 % of differences exceed 30 dB.

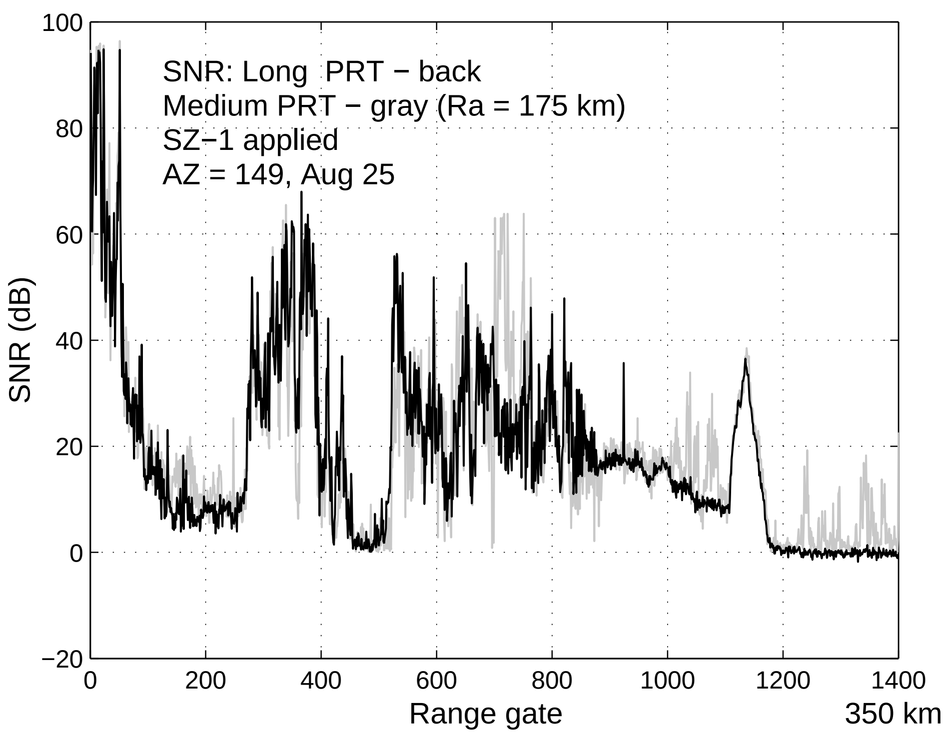

Fig. 3.10. SNR from the long PRT and recovered using the SZ-1 algorithm on medium PRT data.

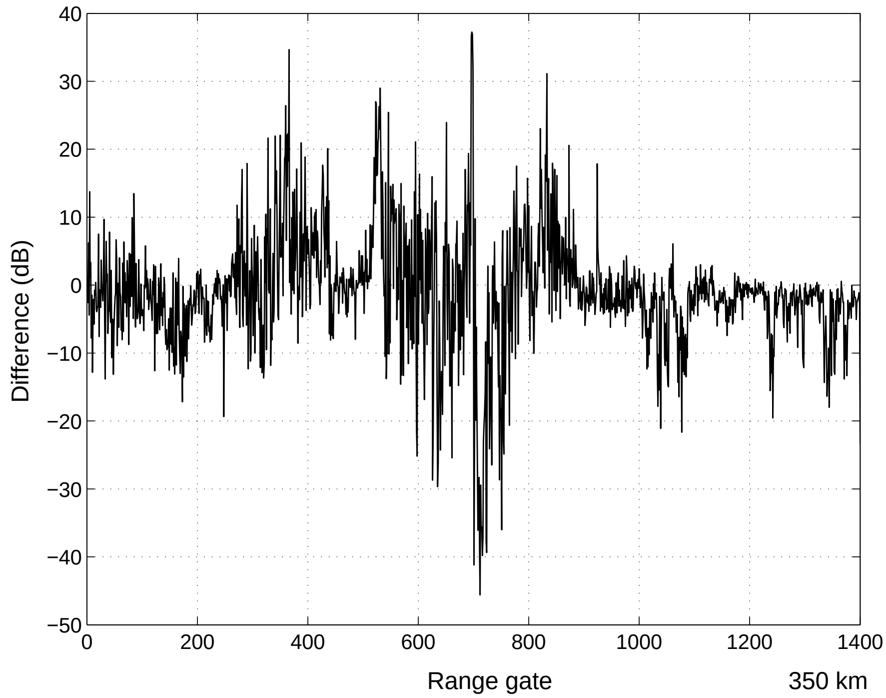

Fig. 3.11. Difference between powers obtained from the long PRT and retrieved using SZ-1 algorithm and the medium PRT (unambiguous range 175 km).

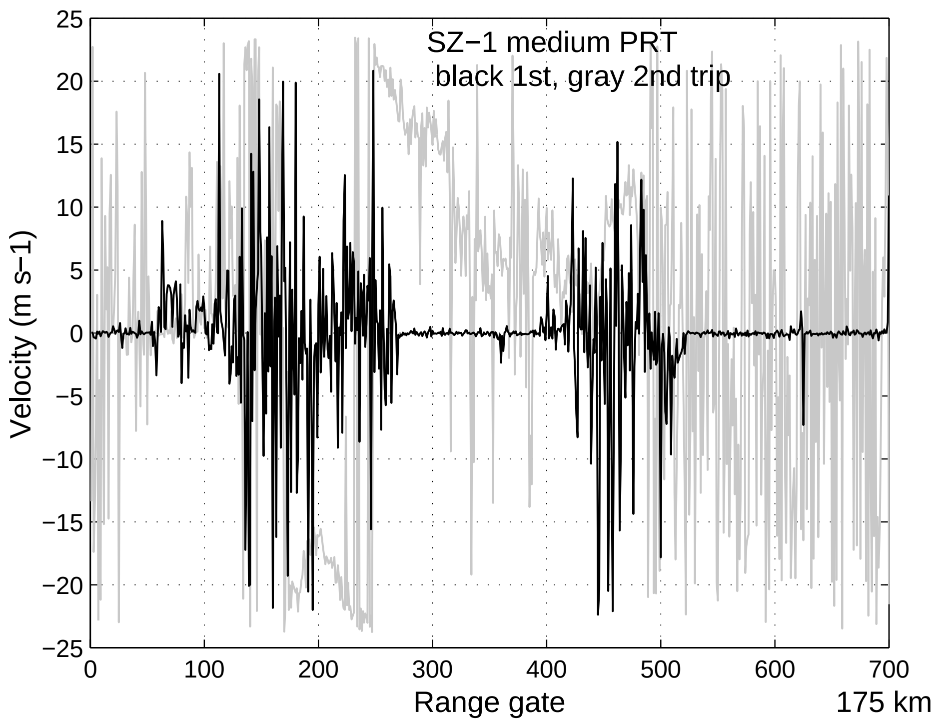

Fig. 3.12. Velocities retrieved with using SZ-1.
The medium PRT has unambiguous range of 175 km.

The mean Doppler velocities in the two trip echoes for the medium PRT are superposed in Fig. 3.12. The SZ-1 algorithm is used. Fluctuations in region of receiver noise can be eliminated if the long PRT data is included as done with the SZ-2 algorithm. Zero velocities in the first-trip signal between gates 0 and 50 are caused by ground clutter, whereas between gates 250 and about 400, and from 525 to the end the velocities are due to anomalous propagation.

Comparison between velocities from the long PRT and those retrieved from overlaid echoes is in Fig. 3.13. Agreement in regions of clutter is good, and there is a match also for range gates between 860 and 1025. The long PRT data have been manually dealiased but no dealiasing has been done on the medium PRT data. Fluctuations are larger in velocities obtained from the medium PRT data.

Spectrum widths can be obtained from either long or short PRT time series. A pair of autocovariances, at lag 0 and 1 (equivalent to equation 6.27 in Doviak and Zrnic, 1993), or at lag 1 and 2 (equation 6.32 in Doviak and Zrnic, 1993), has been used to generate Fig. 3.14. Somewhat larger values are noted in the data obtained from the ratio of autocovariances at lag 0 to lag 1 (R0/R1 in the figure). This is likely caused by white noise which has not been subtracted from the autocovariance. Computations were done in the spectral domain using sinusoidal weighting on the spectra so that unbiased autocovariances were obtained.

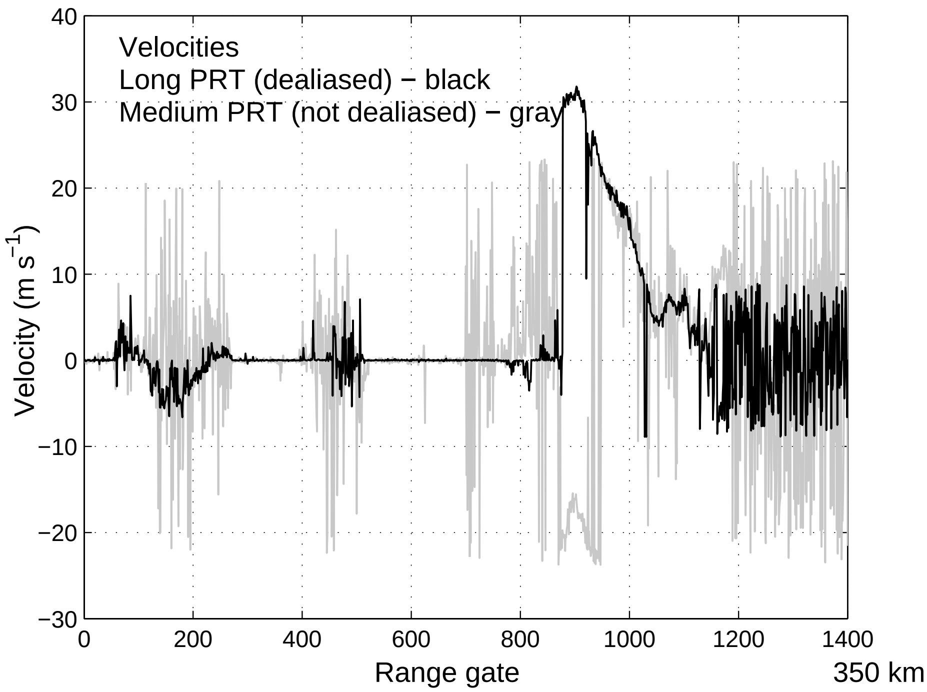

Fig. 3.13. Velocities obtain with from the long-PRT time series (black graph); continuity is used to dealias these velocities. Gray graph represents velocities obtained from the medium-PRT time series; no dealiasing is employed.

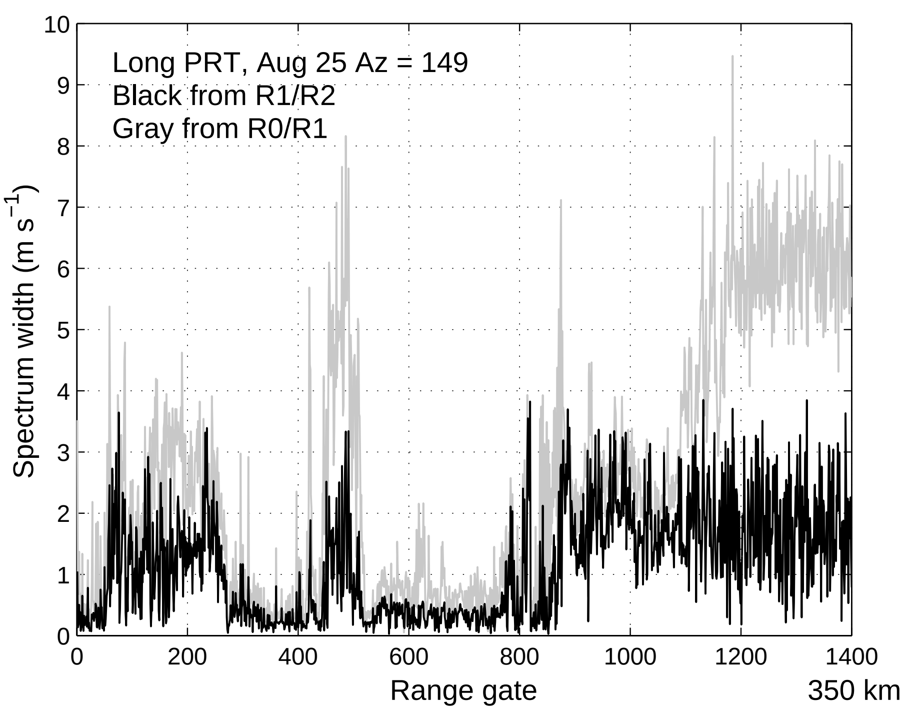

Fig. 3.14. Spectrum widths obtained from autocovariance ratios. Long PRT.

Retrieved spectrum widths from in the two trips at medium PRT are in Fig. 3.15. Large values in second trip data are situated in regions where ground clutter from first trip is overlaid. Comparison of spectrum widths (Fig. 3.16) indicates best agreement in regions of clutter and anomalous propagation. This gives a false sense of accomplishment as data from such regions is censored. In precipitation there is general agreement, but discrepancies abound.

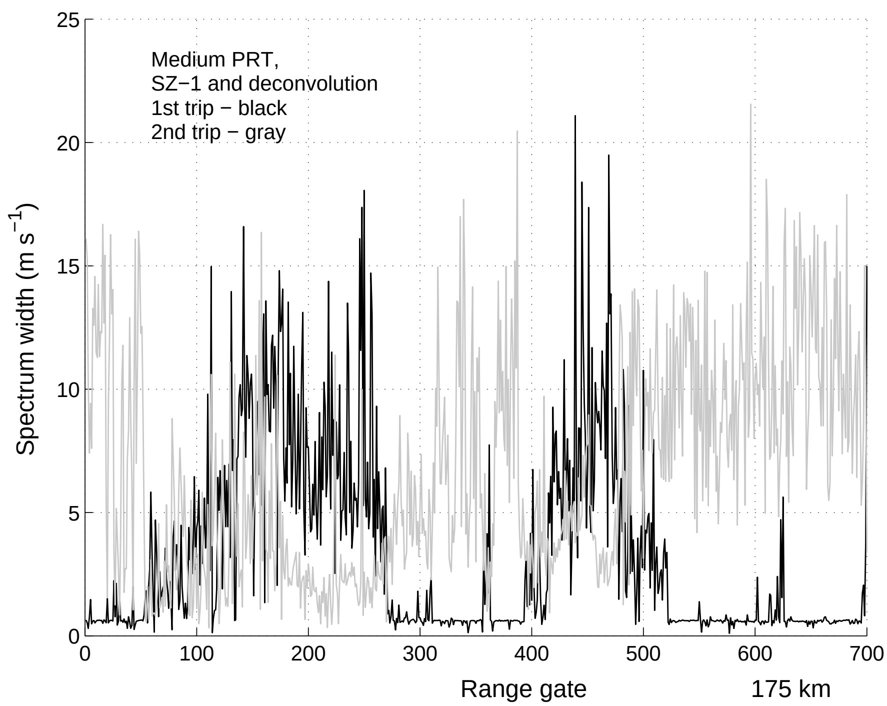

Fig. 3.15. Spectrum widths for the 1st and 2nd trips retrieved using the SZ-1 algorithm and deconvolution.

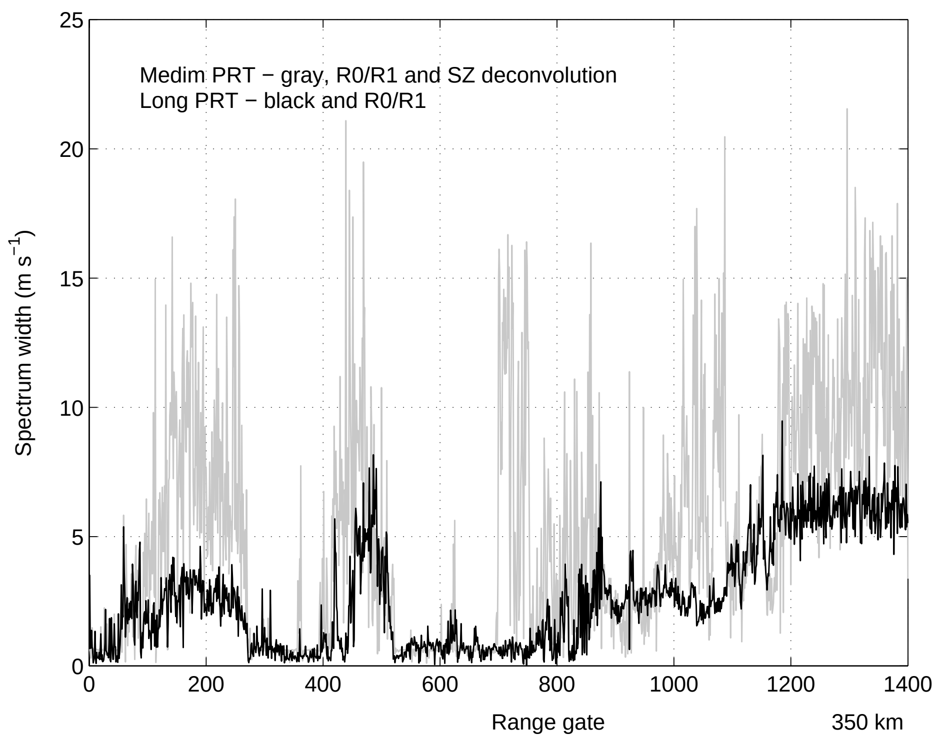

Fig. 3.16. Spectrum widths from long and medium PRTs.

3.3. Implementation and testing of the SZ-2 Algorithm

The SZ-2 algorithm was written and tested on time series data and incorporated into a processing scheme patterned after the current WSR-88D. NCAR contributed to the censoring part of the SZ-2 algorithm. The NSSL tested clutter filter was the legacy 5-pole elliptic IIR implementation and a spectral filter. More evaluation is needed but it has been shown by NCAR that IIR clutter filters will bias velocity estimates for the weaker trip echoes and thus it is not recommended. However, since the long PRT scan is not phase coded, the legacy IIR clutter filters could be used for the long PRT scans. Censoring the SZ-2 moments is accomplished using power, spectrum width, and SNR calculated from the accompanying long PRT data. Censoring of recovered moments have been tested but on a small number of cases due to lack of appropriate data and time. More verification needs to be done. The SZ-2 algorithm is the current choice for the lowest two elevations whereby the scans are the same as on the WSR-88D except the short PRTs are phase coded.

a. Algorithm Description

The SZ-2 algorithm was first introduced by Sachidananda et al. (1998) as part of his studies of range-velocity ambiguity resolution algorithms that use systematic phase coding. Unlike the stand-alone SZ-1 algorithm, SZ-2 relies on power and spectrum width estimates obtained using a long pulse repetition time (PRT). The SZ-2 algorithm is computationally simpler than its stand-alone counterpart as it only tries to recover the Doppler velocities associated with a strong and weak trip signals. Analogously to the legacy "split cut", the volume coverage pattern (VCP) is designed such that a scan with phase-coded signals using a short PRT (~ 780 μs) is immediately preceded by a non-phase-coded scan (at the same elevation angle) using a long PRT (~ 3.1 ms). Hence, the determination of the number and location of overlaid trips can be done by examining the overlaid-free long-PRT powers. The following is a description of the SZ-2 algorithm as tailored for insertion into the signal processing pipeline of the WSR-88D. Note that this is the same description as the one in the NCAR-NSSL Interim Report (2003) with a minor correction in step 13.b of the algorithm.

b. List of variables

ATMOS	Atmospheric attenuation (dB)
B	Ground clutter filter bypass map
C_T, C_S, C_I	Censoring parameters
CSR	Clutter-to-signal ratio
CSR_{th}	Clutter-to-signal ratio threshold for clutter presence
ECHO	Averaged weather echo signal power (dB)
h	Von Hann window
K_s	Signal-to-noise ratio threshold for recovery of strong trip signals
K_w	Signal-to-noise ratio threshold for recovery of weak trip signals

K_r	Power ratio threshold for recovery of weak trip signals
k_a, k_b	Processing notch filter cut off frequencies (spectral coefficients)
k_o	Processing notch filter center (spectral coefficient)
M	Number of sweeps in a radial
N	Number of range cells in a sweep
N_L	Number of range cells in a sweep of the long-PRT data
$NOISE$	Receiver noise power
NW	Processing notch filter notch width (number of spectral coefficients)
P	Range-unfolded power
P_f	Filtered power
P_L	Power from the long-PRT scan
P_S	Strong-trip power
P_{SW}	Strong-trip power corrected for window losses
P_{th}	Power threshold for significant returns
P_u	Unfiltered power
$\tilde{P}_W$	Weak-trip power
P_W	Weak-trip power corrected for window and notch filter losses
P_{WW}	Weak-trip power corrected for window losses
r	Range (m)
R_A	Lag-one autocorrelation of V_A
R_B	Lag-one autocorrelation of V_B
R_S	Lag-one autocorrelation of V_S
R_W	Lag-one autocorrelation of V_W
S_1	Spectrum of the time-series data cohered for the 1^{st} trip
S_{1F}	Ground clutter filtered spectrum of the time-series data cohered for the 1^{st} trip
S_S	Spectrum of the windowed strong-trip cohered time series
$SYSCAL$	System calibration constant (dB)
t_A	Trip number of the signal with strongest power
t_B	Trip number of the signal with second strongest power
T_s	Pulse repetition time (PRT)
t_S	Trip number of the strong trip signal
t_W	Trip number of the weak trip signal
type	Return type (noise, signal, or overlaid)
$\tilde{v}$	Range-unfolded Doppler velocity
v	Scaled Doppler velocity
V	Time series data
V_1	Time-series data cohered for the 1^{st} trip after ground clutter filtering
$\tilde{V}_1$	Unfiltered time-series data cohered for the 1^{st} trip
V_{1F}	Filtered time-series data cohered for the 1^{st} trip
V_{1W}	Windowed time-series data cohered for the 1^{st} trip
v_a	Maximum unambiguous velocity
V_A	Time series data cohered for the trip t_A
V_B	Time series data cohered for the trip t_B
v_c	Clipped Doppler velocity
v_{PNF}	Processing notch filter center (m s^{-1})
v_S	Strong-trip Doppler velocity

V_S	Strong-trip-cohered time series
V_{SN}	Notched strong-trip-cohered time series
V_{SW}	Windowed strong-trip-cohered time series
v_W	Weak-trip Doppler velocity
V_W	Weak-trip-cohered time series
w	Scaled spectrum width
$\tilde{w}_c$	Clipped spectrum width
WCF	Window correction factor
$\tilde{w}_L$	Spectrum width from the long-PRT scan
$\tilde{Z}$	Reflectivity (dBZ)
Z	Scaled reflectivity
$\tilde{Z}_c$	Clipped reflectivity
Δt	Range-time sampling period
λ	Radar wavelength
ϕ	Modulation code
ψ	Switching code

c. Assumptions

1) The phases of the transmitted pulses are modulated with the SZ(8/64) switching code.

2) The number of pulses transmitted in the dwell time is M = 64. Several options exist to handle fewer pulses within the dwell time and to supply the required 64 pulses to the SZ-2 algorithm, but these are not be discussed here because they have not been tested.

3) The number of range cells is $N = T_s/\Delta t$, where T_s is the pulse repetition time (short PRT) and Δt is the range-time sampling period (Δt = 1.57 μs).

4) A long-PRT surveillance scan precedes the phase-coded scan. Powers and spectrum widths from the surveillance scan are stored and used later by the SZ-2 algorithm.

5) Ground clutter, if present, always occurs in the 1^{st}-trip range interval.

6) The algorithm operates on one radial (M range sweeps) of time-series data at a time.

d. Inputs

1) One radial of phase-coded time series data (and associated metadata):

   $V(n,m) = I(n,m) + jQ(n,m)$, for $0 \le n < N$ and $0 \le m < M$,

   where n indexes the range cells and m the sweeps (or pulses). At least N, M, and the antenna position are included in the associated metadata.

2) Ground-clutter-filtered powers and spectrum widths from the long-PRT surveillance scan:

   $P_L(n)$ and $\tilde{w}_L(n)$, for $0 \le n < N_L$,

   where N_L is the number of range cells in the long-PRT surveillance scan. These data correspond to the surveillance-scan radial that is the closest in azimuth to the phase-coded radial in (1).

3) Measured SZ(8/64) switching code:

   $\psi(m)$, for $0 \le m < M$.

4) Censoring thresholds:

   P_{th}: power threshold for determination of significant returns,

   $K_r(\sigma_{v1},\sigma_{v2})$: maximum strong-to-weak power ratios (p_1/p_2) for recovery of the weaker trip for different values of strong and weak trip spectrum widths (σ_{v1} and σ_{v2}, respectively),

   K_s: signal-to-noise ratio (SNR) threshold for determination of recovery of strong trip,

   K_w: signal-to-noise ratio (SNR) threshold for determination of recovery of weak trip,

   CSR_{th}: clutter-to-signal ratio (CSR) threshold for determination of clutter presence.

e. Outputs

1) Scaled reflectivities, Doppler velocities, and spectrum widths:

   $Z(n)$, $v(n)$, and $w(n)$, for $0 \le n < N_L$.

f. Algorithm

1) Censoring and overlaid trip determination (Inputs: P_L, $\tilde{w}_L$. Outputs: t_A, t_B)

The powers from trips 1 to 4, i.e., $P_L(n)$, $P_L(n+N)$, $P_L(n+2N)$, and $P_L(n+3N)$, are used to determine $t_A(n)$ and $t_B(n)$, the recoverable trips, according to the following algorithm:

For $N_L \le n < 4N$
    $P_L(n) = 0$
End
For $0 \le n < N$
    Sort $\{P_L(n), P_L(n+N), P_L(n+2N), P_L(n+3N)\}$ in descending order to get P_1, P_2, P_3, and P_4, and their corresponding trip numbers t_1, t_2, t_3, and t_4.

    $t_A(n) = 0$
    $t_B(n) = 0$
    If $P_1 > P_{th}$ and $P_1 > (P_2 + P_3 + P_4 + NOISE)K_s$
    (The strongest trip signal has a significant return and its power is above K_s-times the sum of the powers of the other trip signals)
        $t_A(n) = t_1$
        (The strongest trip signal is recoverable)

        If $P_2 > P_{th}$ and $P_2 > (P_3 + P_4 + NOISE)K_w$
        and $P_1/P_2 < K_r\{\tilde{w}_L[n+(t_1-1)N], \tilde{w}_L[n+(t_2-1)N]\}$
        (The second strongest trip signal has a significant return, its power is above K_w-times the sum of the powers of the two weakest trip signals, and the strong-weak power ratio is within the recovery region for the weak trip)
            $t_B(n) = t_2$
            (The second strongest trip signal is recoverable)
        Else
        (Weak-trip recovery conditions are not met)
            $t_B(n) = 0$
            (The second strongest trip signal is not recoverable)
        End
    Else
    (Strong-trip recovery conditions are not met)
        $t_A(n) = 0$
        (The strongest trip signal is not recoverable)
    End
End

In the above algorithm, P_{th} is the power threshold to determine significant returns for velocity estimates (same as in the legacy system). K_s and K_w are the minimum SNRs needed for recovery of the strong and weak trips, respectively. Here, the noise consists of the whitened out-of-trip powers plus the system noise. K_r is the maximum p_1/p_2 ratio for recovery of the weaker trip. K_r is defined as

$$K_r(w_1, w_2) = \begin{cases} C_T(w_2), & w_1 < C_I(w_2) \\ C_S(w_2)[w_1 - C_I(w_2)] + C_T(w_2), & w_1 \geq C_I(w_2) \end{cases},$$

where C_T is the threshold, C_S is the slope and C_I is the intercept all of which depend on w_2 (see next section for more details). A zero in t_B indicates that only one trip is recoverable. Zeros in both t_A and t_B indicate that none of the trips are recoverable.

2) First trip cohering (Inputs: V, ψ. Output: $\tilde{V}_1$)

Time series data are cohered for the 1st trip to filter ground clutter.

$$\tilde{V}_1(n,m) = V(n,m)\exp[-j\psi(m)], \qquad \text{for } 0 \leq n < N \text{ and } 0 \leq m < M.$$

where ψ is the SZ(8/64) switching code.

3) Ground clutter filtering (Input: $\tilde{V}_1$. Output: V_1)

a- Filtering

Case I: Time series data $\tilde{V}_1$ are filtered using the map-based 5-pole elliptic ground clutter filter as in the legacy RDA to get V_{1F}. For details of this process refer to Sirmans (1992). In application to the SZ-2 algorithm, this filter can cause biases in weak-trip mean-velocity estimates (NCAR-NSSL Interim Report, Appendix 6, 2003).

Case II: Time series data $\tilde{V}_1$ are filtered using a frequency domain ground clutter filter (similar to the procedure in Passareli et al. 1981) to get V_{1F} as follows:

1. Windowing

$$V_{1W}(n,m) = \tilde{V}_1(n,m)h(m), \qquad \text{for } 0 \leq n < N \text{ and } 0 \leq m < M,$$

where $h(m) = \frac{1}{2}\left[1 - \cos\left(2\pi\frac{m+1}{M+1}\right)\right]$ is the Von Hann window.

2. Discrete Fourier Transform

$$S_1(n,k) = \sum_{m=0}^{M-1} V_{1W}(n,m)e^{-j\frac{2\pi mk}{M}}, \qquad \text{for } 0 \leq n < N \text{ and } 0 \leq k < M.$$

3. Ground Clutter Filtering

The ground clutter signal is assumed to occupy $2p+1$ spectral components around zero Doppler velocity (i.e., parameter p determines the filter notch width). An ideal notch filter would zero out these components to achieve maximum suppression. However, this process biases the power and velocity estimates of the weather signal. In an attempt to minimize the bias due to clutter filtering, an interpolation is performed across the discarded components (i.e., those spectral components within the notch). The new spectral components are obtained through a linear interpolation on the complex spectral coefficients, where the line ends are computed by averaging 2 components at either side of the notch.

$$S_{1F}(n,k) = \begin{cases} S_1(n,k), & p < k < M-p \\ S_a(n) + \dfrac{S_b(n) - S_a(n)}{2p}(k+p), & 0 \le k \le p \\ S_a(n) + \dfrac{S_b(n) - S_a(n)}{2p}(k-M+p), & M-p \le k < M \end{cases},$$

for $0 \le n < N$ and $0 \le k < M$, where

$$S_a(n) = \frac{S_1(n, M-p-1) + S_1(n, M-p-2)}{2},$$

$$S_b(n) = \frac{S_1(n, p+1) + S_1(n, p+2)}{2}, \qquad \text{for } 0 \le n < N.$$

4. Inverse Discrete Fourier Transform

$$V_{1F}(n,m) = \frac{1}{M} \sum_{k=0}^{M-1} S_{1F}(n,k) e^{j\frac{2\pi mk}{M}}, \qquad \text{for } 0 \le n < N \text{ and } 0 \le m < M.$$

Note: Variations on these or other types of ground clutter filters (e.g., regressive filters) could also be used here.

b- Bypass map

$$V_1(n,m) = \begin{cases} \tilde{V}_1(n,m), & B(n) = 1 \\ V_{1F}(n,m), & B(n) = 0 \end{cases}, \qquad \text{for } 0 \le n < N \text{ and } 0 \le m < M,$$

where B is the range-dependent bypass map corresponding to the input radial (a one indicates to bypass the ground clutter filter and use unfiltered data).

4) Filtered and unfiltered power computation (Inputs: V_1, $\tilde{V}_1$. Outputs: P_u, P_f)

$$P_u(n) = \tfrac{1}{M}\sum_{m=0}^{M-1}\left|\tilde{V}_1(n,m)\right|^2 \text{, and}$$

$$P_f(n) = \tfrac{1}{M}\sum_{m=0}^{M-1}\left|V_1(n,m)\right|^2, \qquad \text{for } 0 \le n < N.$$

5) Trip A and trip B cohering (Inputs: V_1, t_A, t_B, ψ. Outputs: V_A, V_B)

The ground-clutter-filtered signal (cohered for the 1st trip) is now cohered for trip A and trip B using the proper modulation code. If the trip to cohere for is zero (unrecoverable trip) the outputs are set to zero (these will be later ignored by the algorithm).

For $0 \le n < N$
  If $t_A(n) = 0$
    (Unrecoverable trip)
    $V_A(n,m) = 0$, for $0 \le m < M$.
  Else
    (Cohere for trip A)
    $V_A(n,m) = V_1(n,m)\exp[-j\phi_{t_A(n)}(m)]$, for $0 \le m < M$.
  End
  If $t_B(n) = 0$
    (Unrecoverable trip)
    $V_B(n,m) = 0$, for $0 \le m < M$.
  Else
    (Cohere for trip B)
    $V_B(n,m) = V_1(n,m)\exp[-j\phi_{t_B(n)}(m)]$, for $0 \le m < M$.
  End
End

In the previous algorithm ϕ_k is the modulation code for the k-th trip with respect to the 1st trip, obtained from the switching code ψ. In general,

$$\phi_k(m) = \psi[((m-k+1))_M] - \psi(m), \qquad \text{for } 0 \le m < M.$$

In the previous equation $((x))_M$ indicates "x modulo M".

6) Computation of lag-one correlations for trip A and trip B (Input: V_A, V_B. Outputs: R_A, R_B)

$$R_A(n) = \tfrac{1}{M-1}\sum_{m=0}^{M-2} V_A^*(n,m)V_A(n,m+1), \qquad \text{for } 0 \le n < N.$$

$$R_B(n) = \tfrac{1}{M-1} \sum_{m=0}^{M-2} V_B^*(n,m) V_B(n,m+1) \,, \qquad \text{for } 0 \le n < N.$$

7) Strong-Weak trip determination (Inputs: V_A, V_B, R_A, R_B, t_A, t_B. Outputs: V_S, R_S, t_S, t_W)

The final strong/weak trip determination is done using the magnitude of the lag-one autocorrelation estimates (equivalent to using the spectrum widths) from the actual phase-coded data.

For $0 \le n < N$
  If $t_A(n) = 0$
    (No trips can be recovered)
    $t_S(n) = 0$
    $t_W(n) = 0$
    $R_S(n) = 0$
    $V_S(n, m) = 0$, for $0 \le m < M$
  ElseIf $t_B(n) = 0$
    (Only strong trip – trip A – can be recovered)
    $t_S(n) = t_A(n)$
    $t_W(n) = 0$
    $R_S(n) = R_A(n)$
    $V_S(n, m) = V_A(n, m)$, for $0 \le m < M$
  Else
    (Two trips can be recovered)
    If $|R_A(n)| > |R_B(n)|$
      (Trip A is strong, trip B is weak)
      $t_S(n) = t_A(n)$
      $t_W(n) = t_B(n)$
      $R_S(n) = R_A(n)$
      $V_S(n, m) = V_A(n, m)$, for $0 \le m < M$
    Else
      (Trip B is strong, trip A is weak)
      $t_S(n) = t_B(n)$
      $t_W(n) = t_A(n)$
      $R_S(n) = R_B(n)$
      $V_S(n, m) = V_B(n, m)$, for $0 \le m < M$
    End
  End
End

8) Clutter-to-signal ratio (CSR) computation (Inputs: P_u, P_f. Output: CSR)

$$CSR(n) = \frac{P_u(n) - P_f(n)}{P_f(n)} \,, \qquad \text{for } 0 \le n < N.$$

9) Strong trip velocity computation (Input: R_S. Output: v_S)

$$v_S(n) = -\frac{v_a}{\pi}\arg\left[R_S(n)\right], \qquad \text{for } 0 \le n < N,$$

where v_a is the maximum unambiguous velocity corresponding to the current PRT ($v_a = \lambda/4T_s$, where λ is the radar wavelength).

10) Processing notch filter (PNF) center velocity computation (Inputs: v_S, t_S, CSR. Output: v_{PNF})

The PNF's purpose is to remove most of the strong-trip signals. If ground clutter is not present, this is achieved by centering the PNF exactly at the Doppler velocity of the strong-trip signal. Nevertheless, if the strong-trip signal is in the 1st trip, the presence of ground clutter may lead to a different PNF placement. If the CSR is large enough, the ground clutter filter (step 3) leaves residuals that cannot be neglected. In this case, the PNF has to be positioned at a Doppler velocity between the ground-clutter velocity (~ 0 m s^{-1}) and the weather-signal velocity.

Note: The current algorithm uses the middle point between the two Doppler velocities; i.e., $(v_{clutter} + v_{weather})/2 \approx v_{weather}/2$. *However, more complex schemes (e.g., using the CSR in some kind of weighted average) might result in better PNF placement.*

$$v_{PNF}(n) = \begin{cases} v_S(n)/2 & \text{if } CSR(n) > CSR_{th} \text{ and } t_S(n) = 1 \\ v_S(n) & \textit{otherwise} \end{cases}, \qquad \text{for } 0 \le n < N,$$

where CSR_{th} is the CSR below which the clutter signal can be ignored.

11) Windowing (Input: V_S. Output: V_{SW})

Perform this step only if a time-domain ground clutter filter was applied in (3).

$$V_{SW}(n,m) = V_S(n,m)h(m), \qquad \text{for } 0 \le n < N \text{ and } 0 \le m < M,$$

where $h(m) = \frac{1}{2}\left[1 - \cos\left(2\pi\frac{m+1}{M+1}\right)\right]$ is the Von Hann window with no zeros at either end.

12) Discrete Fourier Transform (DFT) (Input: V_{SW}. Output: S_S)

$$S_S(n,k) = \sum_{m=0}^{M-1} V_{SW}(n,m)e^{-j\frac{2\pi mk}{M}}, \qquad \text{for } 0 \le n < N \text{ and } 0 \le k < M.$$

13) Notch filtering (Inputs: S_S, v_{PNF}, t_S, t_W. Output: S_{SN}, NW)

The PNF is an ideal bandstop filter in the frequency domain; i.e., it zeroes out the spectral components within the filter's cutoff frequencies (stopband) and retains those components outside the stopband (passband). With the PNF center (v_{PNF}) in m s^{-1} units, the first step consists of mapping the center velocity into a spectral coefficient number. Next, the stopband is defined by moving half the notch width above and below the central spectral coefficient (these are wrapped around to the fundamental Nyquist interval). However, the notch width depends on the strong- and weak-trip numbers. For strong and weak trips that are one trip away from each other, the modulation code is the one derived from the SZ(8/64) switching code. On the other hand, for strong and weak trips that are two trips away from each other, the modulation code is the one derived from the SZ(16/64) switching code. While the processing with a SZ(8/64) code requires a notch width of 3/4 of the Nyquist interval, the SZ(16/64) is limited to a notch width of half the Nyquist interval.

a. Central spectral coefficient computation:

$$k_o(n) = \begin{cases} \left[\!\left[-v_{PNF}(n)\frac{M}{2v_a} \right]\!\right] & \text{if } v_{PNF}(n) \le 0 \\ \left[\!\left[M - v_{PNF}(n)\frac{M}{2v_a} \right]\!\right] & \text{if } v_{PNF}(n) > 0 \end{cases}, \qquad \text{for } 0 \le n < N.$$

b. Notch width determination: (*Note: This step has been corrected in this version*)

For $0 \le n < N$
  If [$t_S(n) = 1$ and $t_W(n) = 3$] or [$t_S(n) = 2$ and $t_W(n) = 4$] or
   [$t_S(n) = 3$ and $t_W(n) = 1$] or [$t_S(n) = 4$ and $t_W(n) = 2$]
  (Trips are such that modulation code corresponds to SZ(16/64) switching code)
    $NW = M/2$
  Else
  (Trips are such that modulation code corresponds to SZ(8/64) switching code)
    $NW = 3M/4$
  End
End

c. Cutoff frequency computation:

$$k_a(n) = \begin{cases} k_o(n) - \left\lfloor \frac{NW-1}{2} \right\rfloor & \text{if } k_o(n) - \left\lfloor \frac{NW-1}{2} \right\rfloor \ge 0 \\ k_o(n) + M - \left\lfloor \frac{NW-1}{2} \right\rfloor & \text{if } k_o(n) - \left\lfloor \frac{NW-1}{2} \right\rfloor < 0 \end{cases}, \qquad \text{for } 0 \le n < N,$$

$$k_b(n) = \begin{cases} k_o(n) + \left\lceil \frac{NW-1}{2} \right\rceil & \text{if } k_o(n) + \left\lceil \frac{NW-1}{2} \right\rceil < M \\ k_o(n) - M + \left\lceil \frac{NW-1}{2} \right\rceil & \text{if } k_o(n) + \left\lceil \frac{NW-1}{2} \right\rceil \ge M \end{cases}, \qquad \text{for } 0 \le n < N.$$

d. Notch filtering:

$$S_{SN}(n,k)=\begin{cases} S_S(n,k) & \begin{array}{l}\text{if } k_b(n)<k<k_a(n) \text{ for } k_b(n)<k_a(n) \text{ or}\\ \text{if } 0\le k<k_a(n) \text{ or } k_b(n)<k<M \text{ for } k_a(n)<k_b(n)\end{array} \\ 0 & \quad\quad\quad\quad\quad\quad \textit{otherwise} \end{cases}$$

for $0 \leq n < N$ and $0 \leq k < M$, where k_a and k_b are computed in (c).

In the previous equations $[\![x]\!]$ is the nearest integer to x, $\lfloor x \rfloor$ is the nearest integer to x that is smaller than x, and $\lceil x \rceil$ is the nearest integer to x that is larger than x, k_o, k_a, and k_b are zero-based indexes.

Note: The PNF notch width can be adaptive depending on the spectrum width of the strong trip echo to notch the minimum possible and allow better re-cohering of the weak trip echo (e.g., see Cho 2003).

14) Inverse DFT (Input: S_{SN}. Output: V_{SN})

$$V_{SN}(n,m)=\frac{1}{M}\sum_{k=0}^{M-1} S_{SN}(n,k)e^{j\frac{2\pi mk}{M}}, \qquad \text{for } 0 \leq n < N \text{ and } 0 \leq m < M.$$

15) Weak trip cohering (Inputs: V_{SN}, t_S, t_W, ψ. Output: V_W)

$$V_W(n,m)=V_{SN}(n,m)\exp\left[-j\phi_{t_W(n),t_S(n)}(m)\right], \qquad \text{for } 0 \leq n < N \text{ and } 0 \leq m < M,$$

where ϕ_{k_1,k_2} is the modulation code for the k_1-th trip with respect to the k_2-th trip, obtained from the switching code ψ. In general,

$$\phi_{k_1,k_2}(m)=\psi[((m-k_1+1))_M]-\psi[((m-k_2+1))_M], \qquad \text{for } 0 \leq m < M.$$

16) Weak trip power sum computation (after notching) (Input: V_W. Output: $\tilde{P}_W$)

$$\tilde{P}_W(n)=\tfrac{1}{M}\sum_{m=0}^{M-1}\left|V_W(n,m)\right|^2, \qquad \text{for } 0 \leq n < N.$$

17) Power Adjustments (Inputs: P_f, $\tilde{P}_W$, NW. Outputs: P_S, P_W)

a. Window adjustment:

$$P_{SW}(n) = P_f(n)\ WCF, \qquad \text{for } 0 \leq n < N,$$

$P_{WW}(n) = \tilde{P}_W(n)\ WCF,$ for $0 \le n < N$,

where WCF is the window correction factor. For the Von Hann window used in (11) WCF is 2.6257 (or 4.1924 dB).

b. PNF notch width adjustment:

$P_W(n) = (1 - NW/M)^{-1}\ P_{WW}(n),$ for $0 \le n < N$.

c. Strong trip power adjustment:

$$P_S(n) = \begin{cases} P_{SW}(n) - P_W(n), & P_{SW}(n) - P_W(n) > 0 \\ 0 & otherwise \end{cases}, \qquad \text{for } 0 \le n < N.$$

Note: The powers P_S and P_W could be used instead of the powers from the long PRT; herein these are used for censoring.

18) Weak trip correlation sum computation (after notching) (Input: V_W. Output: R_W)

$$R_W(n) = \tfrac{1}{M-1} \sum_{m=0}^{M-2} V_W^*(n,m) V_W(n,m+1), \qquad \text{for } 0 \le n < N.$$

19) Weak trip velocity computation (Input: R_W. Output: v_W)

$$v_W(n) = -\frac{v_a}{\pi} \arg\left[R_W(n)\right], \qquad \text{for } 0 \le n < N.$$

20) Assignment of correct range (Inputs: P_S, P_W, v_S, v_W, t_S, t_W. Outputs: $\tilde{P}$, $\tilde{v}$)

First, initialize unfolded power and velocity vectors. Then, according to the strong and weak trip numbers, powers and Doppler velocity estimates are assigned to their correct trip location.

For $0 \le n < N_L$
    $\tilde{P}(n) = 0$
    $\tilde{v}(n) = 0$
End

For $0 \le n < N$

If $t_S(n) \neq 0$

(Assign power and velocity to the strong trip range location)

$\tilde{P}\{n + [t_S(n) - 1]N\} = P_S(n)$

$\tilde{v}\{n + [t_S(n) - 1]N\} = v_S(n)$

End

If $t_W(n) \neq 0$

(Assign power and velocity to the weak trip range location)

$\tilde{P}\{n + [t_W(n) - 1]N\} = P_W(n)$

$\tilde{v}\{n + [t_W(n) - 1]N\} = v_W(n)$

End

End

21) Censoring and thresholding (Inputs: P_L, $\tilde{P}$, t_S, t_W. Output: *type*)

For $0 \le n < N_L$

If $P_L(n) < P_{th}$ or ($\tilde{P}(n) < P_{th}$ and $\tilde{P}(n) > 0$)

(Either the long- or the short-PRT power is below the SNR threshold.
Not a significant return. Tag as noise)

type(n) = *NOISE LIKE*

Else

(Powers are significant - including the case where $\tilde{P}(n) = 0$. *Temporarily tag as overlaid until the strong and weak trip numbers are examined)*

type(n) = *OVRLD LIKE*

End

End

For $0 \le n < N$

If $t_S(n) \neq 0$ and $type\{n + [t_S(n) - 1]N\} \neq$ *NOISE LIKE*

(Power is significant and strong trip is recoverable. Tag strong trip as signal)

$type\{n + [t_S(n) - 1]N\}$ = *SIGNAL LIKE*

End

If $t_W(n) \neq 0$ and $type\{n + [t_W(n) - 1]N\} \neq$ *NOISE LIKE*

(Power is significant and weak trip is recoverable. Tag weak trip as signal)

$type\{n + [t_W(n) - 1]N\}$ = *SIGNAL LIKE*

End

End

P_{th} is a power threshold to determine significant return.

Note: Sachidananda et al. (2000) suggested the use of CSR to censor v_S.

22) Reflectivity computation (Input: $\tilde{P}$. Output: $\tilde{Z}$)

$\tilde{Z}(n) = ECHO(n) + 20\log_{10}\left[r(n)\right] + SYSCAL + r(n)ATMOS$, for $0 \le n < N_L/4$,

where

$$ECHO(n) = 10\log_{10}\left[\tfrac{1}{4}\sum_{i=0}^{3}\tilde{P}(4n+i) - NOISE\right], \qquad \text{for } 0 \le n < N_L/4.$$

In the previous equations *NOISE* is the receiver noise power, *r* is the range (distance away from the radar), *SYSCAL* is the system calibration constant, and *ATMOS* is the atmospheric attenuation.

23) Clipping and scaling (Inputs: $\tilde{Z}, \tilde{v}, \tilde{w}_L$, *type*. Output: *Z*, *v*, *w*)

The clipping and scaling complies with the current RDA/RPG ICD.

a. Reflectivity (*Z*):

$$\tilde{Z}_c(n) = \begin{cases} -32, & \tilde{Z}(n) < -32 \\ 94.5, & \tilde{Z}(n) > 94.5 \\ \tilde{Z}(n), & otherwise \end{cases}, \qquad \text{for } 0 \le n < N_L/4,$$

$$Z(n) = \begin{cases} [\![2\tilde{Z}_c(n) + 66]\!], & type(n) = SIGNAL\ LIKE \\ 1, & type(n) = OVRLD\ LIKE \\ 0, & type(n) = NOISE\ LIKE \end{cases}, \qquad \text{for } 0 \le n < N_L/4.$$

b. Doppler velocity (*v*):

$$\tilde{v}_c(n) = \begin{cases} -63.5, & \tilde{v}(n) < -63.5 \\ 63, & \tilde{Z}(n) > 63 \\ \tilde{v}(n), & otherwise \end{cases}, \qquad \text{for } 0 \le n < N_L,$$

$$v(n) = \begin{cases} [\![2\tilde{v}_c(n) + 129]\!], & type(n) = SIGNAL\ LIKE \\ 1, & type(n) = OVRLD\ LIKE \\ 0, & type(n) = NOISE\ LIKE \end{cases}, \qquad \text{for } 0 \le n < N_L.$$

c. Spectrum width (w):

We ignore the overlaid type ($OVRLD$) because spectrum width estimates come from the long-PRT scan.

$$\tilde{w}_c(n) = \begin{cases} 0, & \tilde{w}_L(n) \le 0 \\ \frac{v_{aL}}{\sqrt{3}}, & \tilde{w}_L(n) > \frac{v_{aL}}{\sqrt{3}}, \\ \tilde{w}_L(n), & otherwise \end{cases} \qquad \text{for } 0 \le n < N_L,$$

$$w(n) = \begin{cases} [\![2\tilde{w}_c(n) + 129]\!], & type(n) = SIGNAL\ LIKE \\ & \text{or } type(n) = OVRLD\ LIKE \\ 0 & type(n) = NOISE\ LIKE \end{cases}, \qquad \text{for } 0 \le n < N_L,$$

where v_{aL} is the maximum unambiguous velocity corresponding to the long PRT.

g. Recommended Censoring Method

Currently the recommended SZ-2 censoring has two steps. The first step censors based on the signal to noise ratio (SNR) in each trip (as measured by the long PRT scan). The second step thresholds on boundaries designed to exclude the areas of contaminated weak trip radial velocity. These boundaries are obtained from plots of standard deviation of velocity as a function of power ratio and strong and weak trip spectrum widths (w_1 and w_2, see Sachidananda et al. 1998). In steps 1 and 2 we assume that it has been determined which the strong and weak trips are, and that the power ratio, w_1 and w_2 have been computed from the long PRT scan. A preliminary recommendation for the set of censoring parameters was given by NCAR and NSSL (2003); however, additional tests are needed to optimize these parameters before a final recommendation can be made.

h. Block Diagram

Figure 3.17 depicts a block diagram (or signal flow diagram) of the SZ-2 algorithm. The lines represent data flow (scalars, vectors, or matrices) and the boxes refer to specific processing steps. The numbers in the boxes correspond to the steps of the algorithm in the previous section.

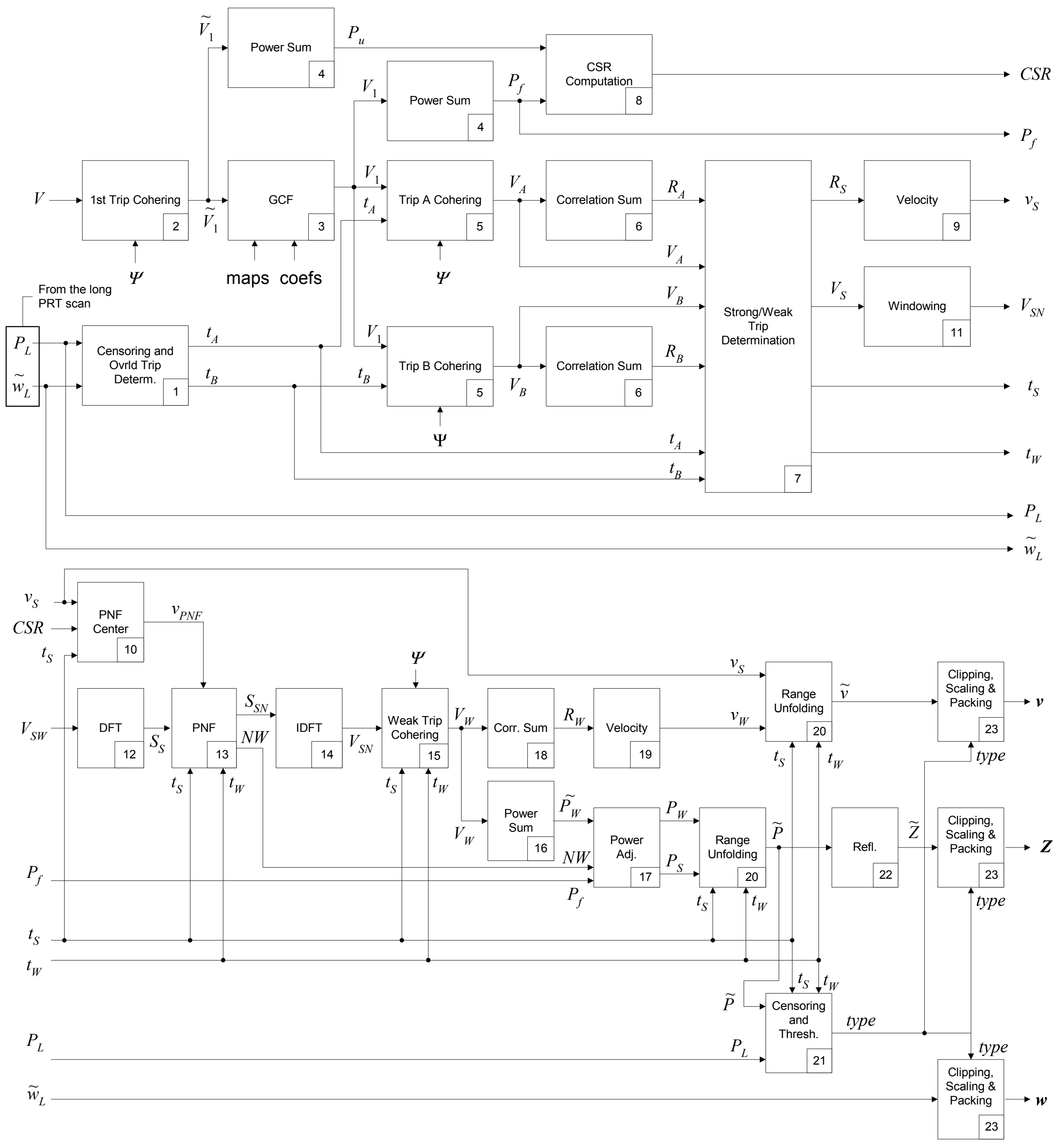

Fig. 3.17. SZ-2 algorithm block diagram.

3.4. Performance of the SZ-2 Algorithm

The performance of the SZ-2 algorithm was evaluated on real weather data. Two examples are shown. The time series data were recorded with the KOUN research radar and processed offline using MATLAB. The code reproduces exactly the algorithm described in the previous section.

a. Case 1: June 4, 2003

This event was a Mesoscale Convective System (MCS) that developed early in the morning in North Texas and Southwestern Oklahoma. It is typical for that time of year. It propagated to the NE and was over the KOUN radar in mid morning. By that time, the system developed a mesoscale convective vortex in its NW part which caused formation of three intense cells. Parameters used for data acquisition are given in the tables below.

PRTs	Period (μs)	Unambiguous range r_a (km)	Unambiguous velocity v_a (m s^{-1})
PRT #1 (long)	3106.7	466	8.92
PRT #4 (medium)	1166.7	175	23.74
PRT #8 (short)	780.0	117	35.52

	Surveillance scan	SZ Doppler scan
Number of pulses per radial	15	64

Data was processed using the following set of thresholds:

K_s	-10 dB
K_w	-10 dB
K_r	30 dB

The fields of reflectivity, velocity, and spectrum width are displayed next. The labels on top of the figures indicate the variable displayed, the PRT (long, medium, or short), the transmitted signal (“PC” for Phase Coded signals and “Non PC” for non phase coded signals), the elevation angle (EL), the date, and the approximate time.

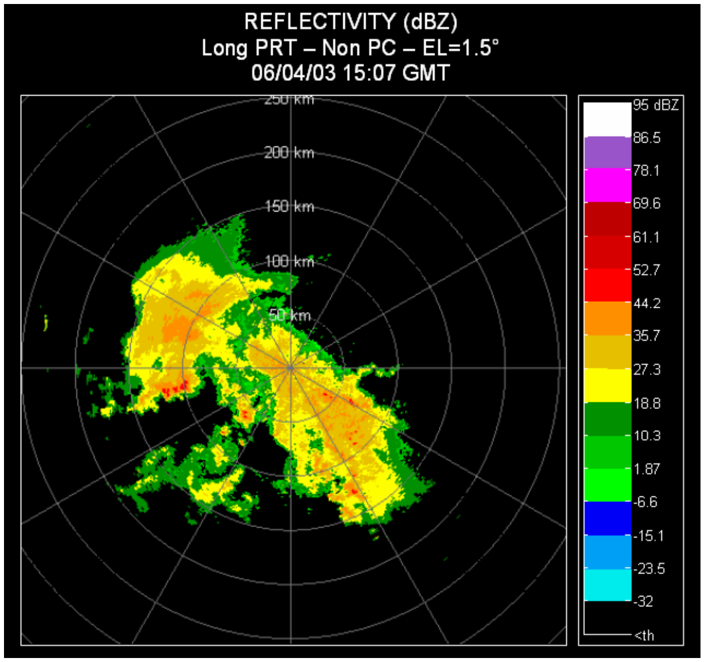

Fig. 3.18. Case 1 (06/04/03). Reflectivity field, long-PRT.

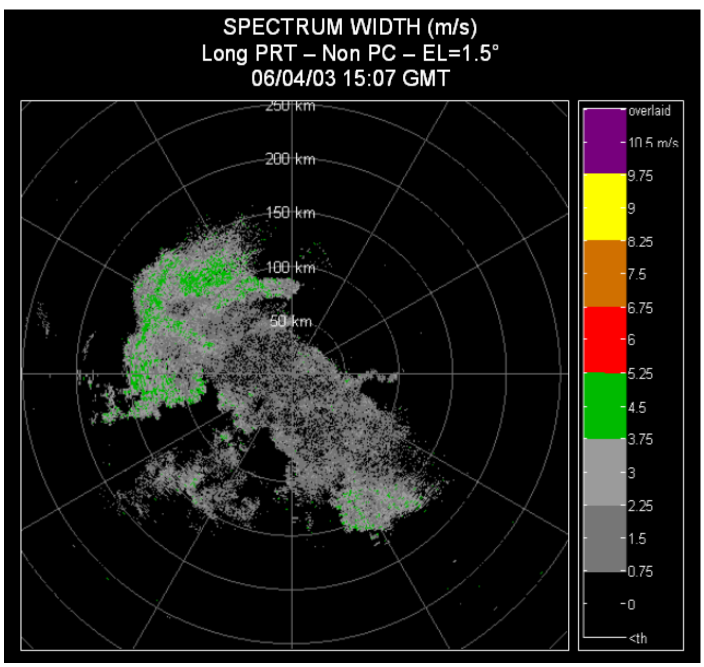

Fig. 3.19. Case 1 (06/04/03). Spectrum width field, long-PRT.

Figures 3.18 and 3.19 were obtained using the long PRT. Because the maximum range of this MCS is smaller than the unambiguous range, the whole phenomenon is contained within the first trip.

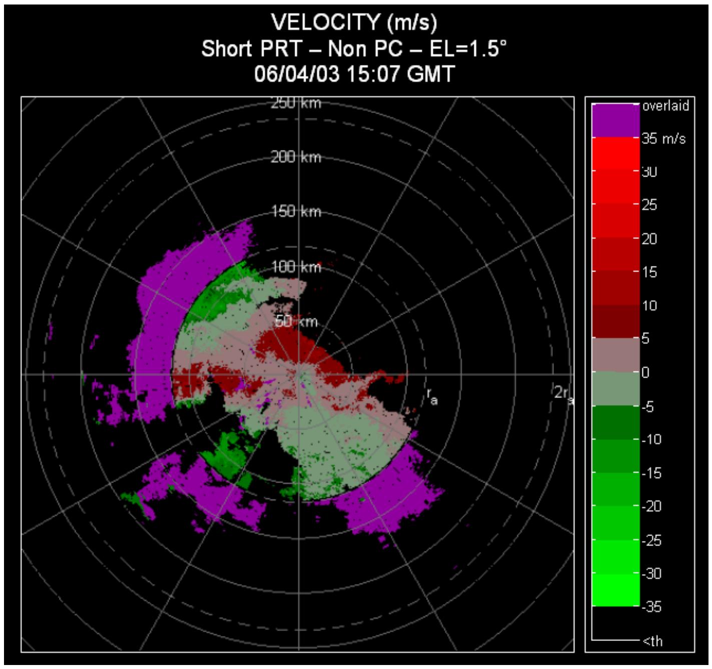

Fig. 3.20. Case 1 (06/04/03). Doppler velocity field. Short-PRT, non-phase-coded.

Figure 3.20 shows the velocity field obtained with the short PRT. The MCS spreads over two trips. Because the transmitted signals are not phase coded, the velocities for the weaker trip are not recoverable. The velocity field is obscured by range-overlay censoring (known as "purple haze" syndrome). Note that there is purple haze almost everywhere beyond the unambiguous range (in this case the second trip is almost weaker than the first trip everywhere).

The transmitted signals are now phase coded, and the recovery of the weak trip is possible, as shown in Fig. 3.21. However, the setting of the threshold K_r prevents the recovery of the weak trip in some areas where the strong trip is very intense (especially in the first range cells of the second trip).

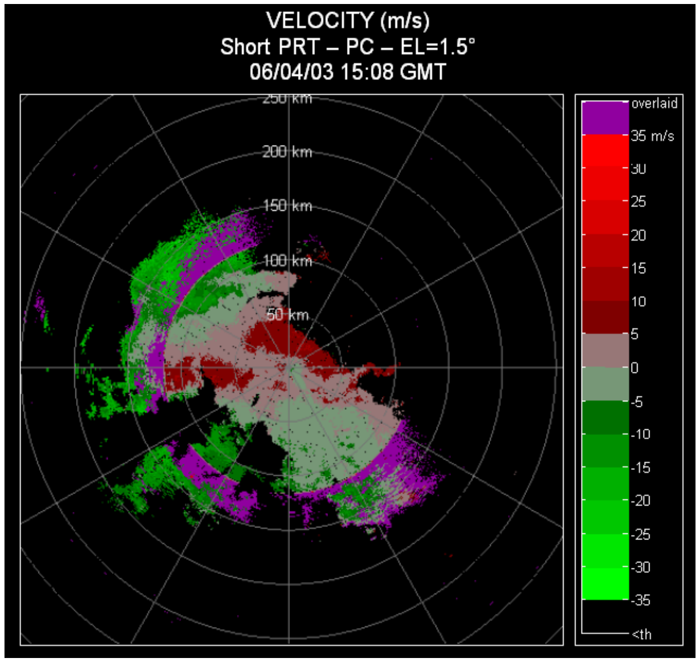

Fig. 3.21. Case 1 (06/04/03). Doppler velocity field Short-PRT, non-phase-coded.

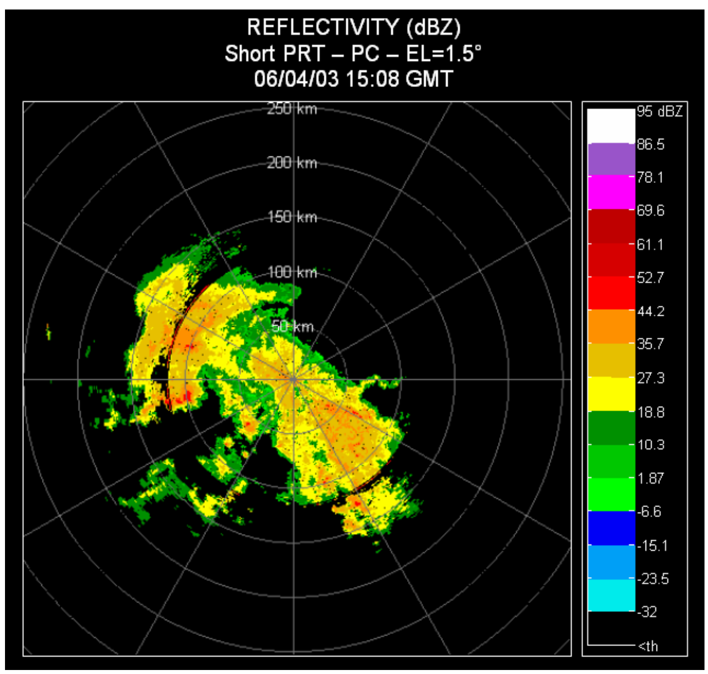

Fig. 3.22. Case 1 (06/04/03). Reflectivity field. Short-PRT, phase-coded.

Figure 3.22 shows the reflectivity field obtained with phase coded transmitted signals. There is a very good agreement with Fig. 3.18, except for the first range cells of the second trip. This is due to the value of the threshold K_r, which causes the censoring of the data at these places. That is, even after ground clutter filtering the residue power of the first trip is much larger than the second trip signal power which therefore can not be recovered.

b. Case 2: April 6, 2003

On this day a scattered collection of severe storms developed in Oklahoma, some of which formed distinct clusters. Several cells had reflectivity in excess of 60 dBZ. Triple overlay occurred for some of the storms to the NE and SE of KOUN. Parameters used for data acquisition are the same as for case 1. Data was processed using the following set of thresholds:

K_s	-10 dB
K_w	-10 dB
K_r	30 dB

The fields of reflectivity, velocity, and spectrum width are displayed next. As before, the labels on the figures indicate the variable displayed, the PRT, the transmitted signal, the elevation angle, the date, and the approximate time.

Figures 3.23 and 3.24 were obtained using the long PRT. Similarly to case 1, the maximum range of this collection of storms is smaller than the unambiguous range, and the whole phenomenon is recovered as a single trip.

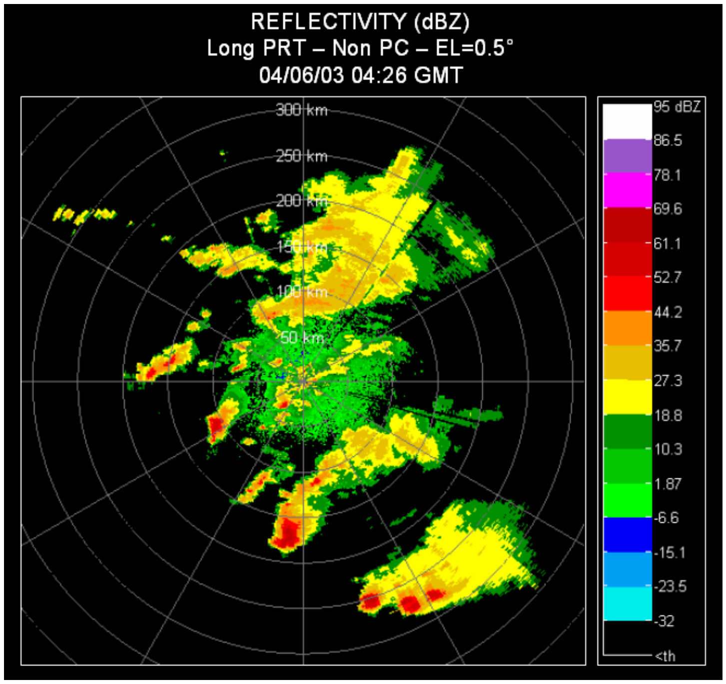

Fig. 3.23. Case 2 (04/06/03). Reflectivity field, long-PRT.

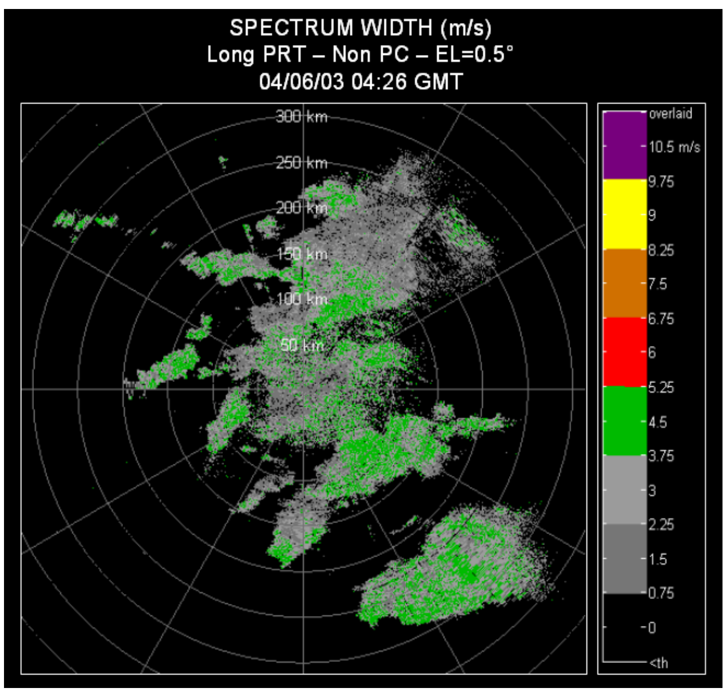

Fig. 3.24. Case 2 (04/06/03). Spectrum width field, long-PRT.

Figure 3.25 shows the velocity field obtained with the short PRT. The collection of storms spreads over three trips. Because the transmitted signals are not phase coded, the velocities for the weaker trips are not recoverable. Almost half of the event has the "purple haze" syndrome, and the third trip is not recovered at all.

After phase coding, the recovery of the two strongest trips is possible. Parts of the third trip are therefore recovered, as shown in Fig. 3.26 for azimuths between 120° and 150° (SE of KOUN). However, the setting of the threshold K_r prevents the recovery of the weak trip in some areas where the strong trip is very intense (especially in the first range cells of the second and third trips).

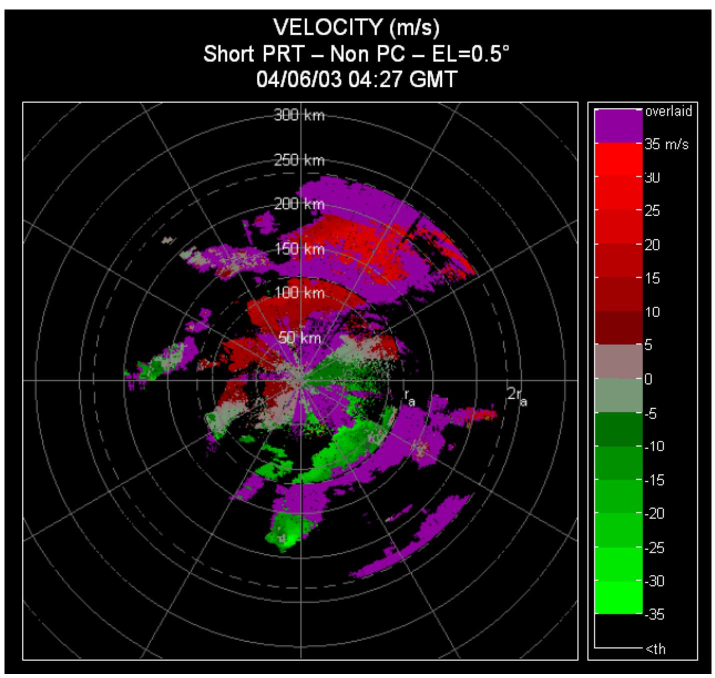

Fig. 3.25. Case 2 (04/06/03). Doppler velocity field. Short-PRT, non-phase-coded.

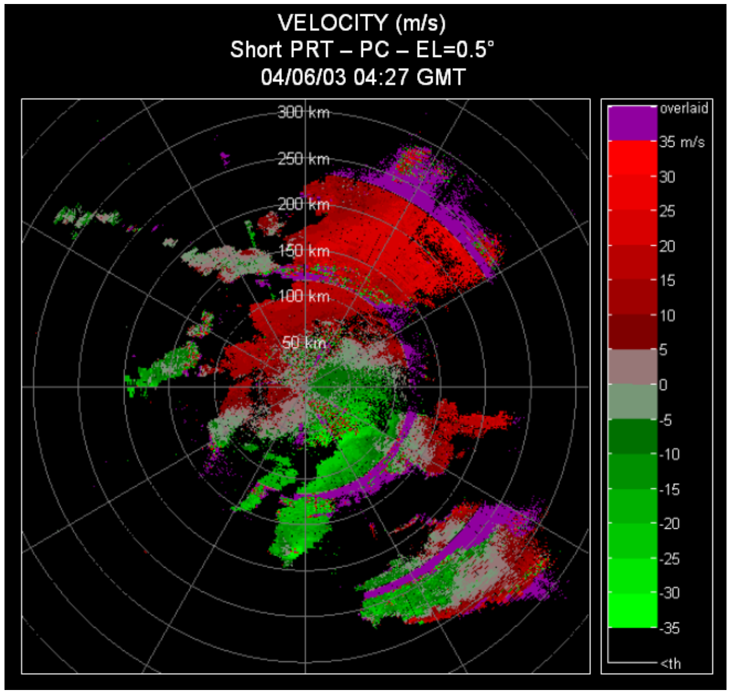

Fig. 3.26. Case 2 (04/06/03). Doppler velocity field. Short-PRT, phase-coded.

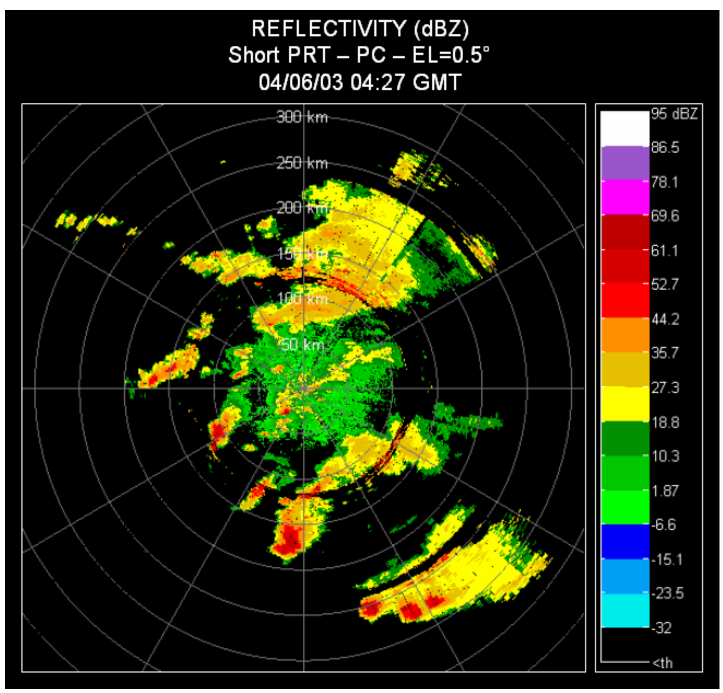

Fig. 3.27. Case 2 (04/06/03). Reflectivity field. Short-PRT, phase-coded.

Figure 3.27 shows the reflectivity field obtained with phase coded transmitted signals. Most of the time, the threshold K_r causes the censoring of the powers at the first range cells of the second and third trips. If not censored, high powers appear at these range cells due to ground clutter contamination.

Figure 3.28 shows the velocity field obtained with the medium PRT. The collection of storms spreads now over two trips. Because the transmitted signals are not phase coded, the velocities for the weaker trip are not recoverable.

For phase coded transmitted signals the recovery of the two trips is possible, as shown in Fig. 3.29. The value of threshold K_r prevents the recovery of the weak trip in some areas where the strong trip is very intense (especially in the first range cells of the second trip). Moreover, some regions like the NE of KOUN around 225 km or the SE of KOUN at about 50 km exhibit a velocity dealiasing problem because the velocities in these areas exceed the maximum unambiguous value.

Figure 3.30 shows the reflectivity field obtained with phase coded transmitted signals. The threshold K_r causes most of the time the censoring of the powers at the first range cells of the second trip. If not censored, high powers appear at these range cells due to ground clutter contamination.

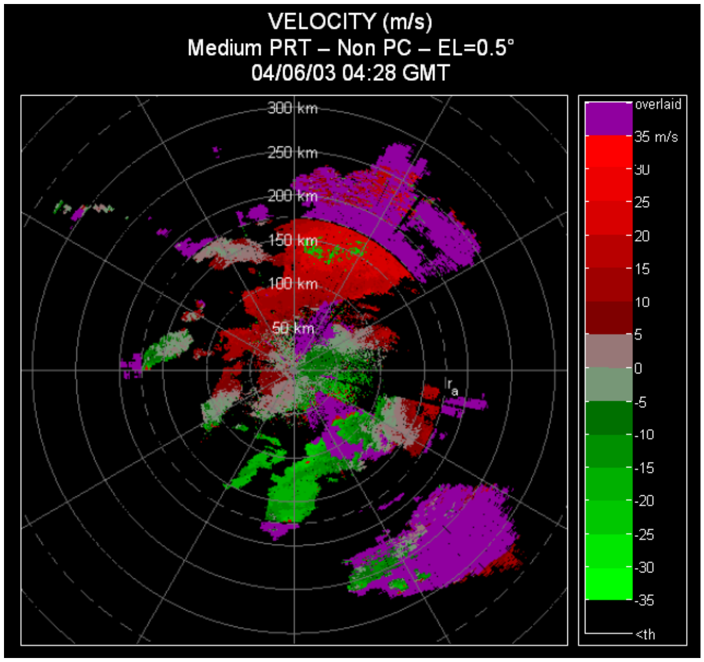

Fig. 3.28. Case 2 (04/06/03). Doppler velocity field. Medium-PRT, non-phase-coded.

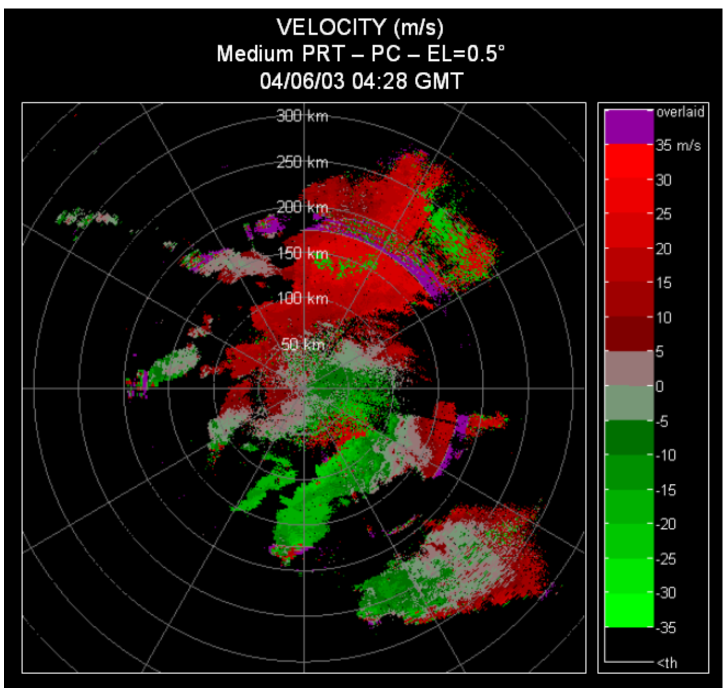

Fig. 3.29. Case 2 (04/06/03). Doppler velocity field. Medium-PRT, phase-coded.

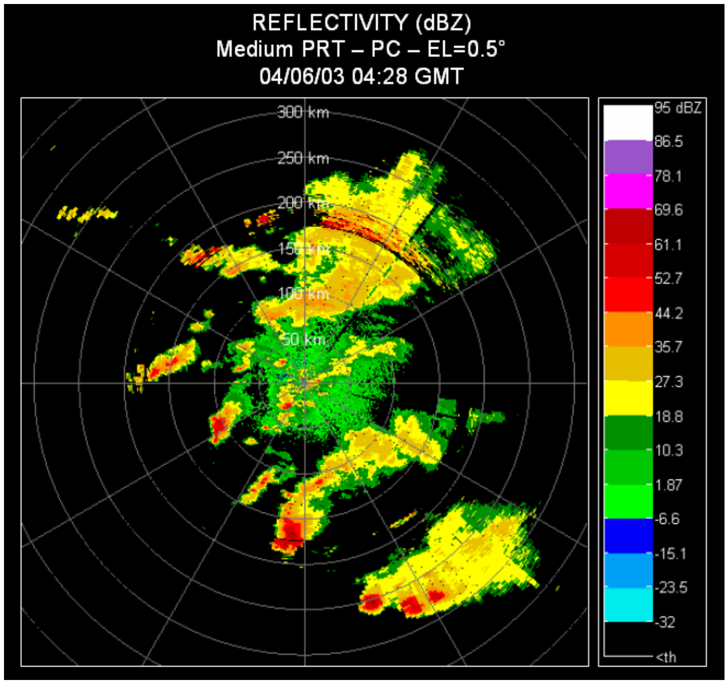

Fig. 3.30. Case 2 (04/06/03). Reflectivity field. Medium-PRT, phase-coded.

4. Staggered PRT

Over the last decade, the staggered PRT (pulse repetition time) technique has emerged as a viable candidate to address the mitigation of range and velocity ambiguities in the WSR-88D (Zrnic and Cook 2002). Its greatest potential is at intermediate elevations where ground clutter is not a major concern. The staggered PRT technique has been thoroughly analyzed through theoretical and simulation studies but had not been implemented on any WSR-88D until recently. Herein we describe a real-time implementation of the staggered PRT sampling and processing on NSSL's WSR-88D research radar.

The staggered PRT technique was first proposed in the context of weather surveillance radars by Sirmans et al. (1976). With this technique, transmitter pulses are spaced at alternating PRTs T_1 and T_2, and pulse-pair autocorrelation estimates are made independently for each PRT. These estimates are suitably combined so that the effective maximum unambiguous velocity becomes $v_a = \lambda/[4(T_2 - T_1)]$ (Zrnic and Mahapatra, 1985). In addition, the unambiguous range is $r_a = cT_1/2$, corresponding to the shorter PRT. This implies that the staggered PRT is equivalent to a uniform PRT of $T_2 - T_1$ for the unambiguous velocity and a uniform PRT of T_1 for the unambiguous range, and each can be independently selected (Sachidananda and Zrnic 2002).

The implementation of the staggered PRT technique on weather radars has been disqualified mainly due to the difficulties in designing efficient ground clutter filters. In addition, due to the non-uniform spacing between pulses, spectral processing of time series is a challenge. Moreover, because the pulse pair autocorrelation is obtained from independent pairs (as opposed to contiguous pairs as in the case of uniform PRT), slightly larger standard errors of estimates are expected. Despite these disadvantages, the staggered PRT technique has emerged as a complement to systematic phase coding in the quest to reduce the effects of velocity and range ambiguities on the WSR-88D.

A real-time implementation of the staggered PRT technique was completed on NSSL's KOUN research RDA (RRDA). The staggered PRT algorithm was tailored to allow a seamless insertion into the current signal processing pipeline (Torres and Zahrai 2002). The implementation incorporates new functionality (e.g., clutter filtering, velocity dealiasing, data censoring) but matches the legacy WSR-88D functionality when appropriate (e.g., interference suppression, strong point clutter censoring). In this first implementation, we assume that there are no storms beyond $r_{a2} = cT_2/2$. That is, echoes from the short PRT can overlay part of the ones from the long PRT, but not vice versa. A technique to resolve more complex overlay situations is given by Sachidananda and Zrnic (2003). Operational tests show that the computational complexity of this method is well within the expected capabilities of the next generation ORDA (Open Radar Data Acquisition). Preliminary results included in this work demonstrate that the staggered PRT technique is a feasible candidate for mitigating range and velocity ambiguities in future enhancements of the national network of weather surveillance radars.

4.1. Algorithm Description

a. Assumptions

1) The transmission sequence alternates two pulse repetition times (PRT) as: T_1, T_2, T_1, T_2, … for a total of M pulses using the short pulse.
2) The PRT ratio is larger than 1/3.
3) $N_1 = T_1/T_s$ and $N_2 = T_2/T_s$, where T_s is the sampling period.

4) There are no echoes beyond max(r_{a1}, r_{a2}), where r_{ai} is the maximum unambiguous range corresponding to T_i

5) We do *not* assume that M is even or that $T_1 < T_2$.

b. Inputs

1) AGC (Automatic Gain Control) corrected data without interference:

   $V(n,m) = I(n,m) + jQ(n,m)$, for even m $0 \le n < N_1$, for odd m $0 \le n < N_2$, and $0 \le m < M$.

   n indexes the range cells and m the sweeps (or pulses).

2) Associated metadata

3) Ground clutter filter maps

4) Adaptation parameters

c. Outputs

1) Scaled reflectivities, Doppler velocities, and spectrum widths:

   $Z(n)$ for $0 \le n < \max(N_1,N_2)$,

   $v(n)$ and $w(n)$ for $0 \le n < \min(N_1,N_2)$.

d. Algorithm:

1) Power and correlation computations for each PRT

$$P_1(n) = \frac{1}{K_s^{(1)}} \sum_{m=0}^{K_s^{(1)}-1} \left|V(n,2m)\right|^2, \qquad \text{for } 0 \le n < N_1,$$

$$P_2(n) = \frac{1}{K_s^{(2)}} \sum_{m=0}^{K_s^{(2)}-1} \left|V(n,2m+1)\right|^2, \qquad \text{for } 0 \le n < N_2,$$

$$R_1(n) = \frac{1}{K_p^{(1)}} \sum_{m=0}^{K_p^{(1)}-1} V(n,2m)V^*(n,2m+1), \qquad \text{for } 0 \le n < \min(N_1, N_2),$$

$$R_2(n) = \frac{1}{K_p^{(2)}} \sum_{m=0}^{K_p^{(2)}-1} V(n,2m+1)V^*(n,2m+2), \qquad \text{for } 0 \le n < \min(N_1, N_2).$$

K_s is the number of sweeps used in the power computations, and K_p is the number of pairs used in the correlation computations. These constants depend on the total number of sweeps M, and they may differ for short and long PRT estimates depending on the parity of M as

$$K_s^{(1)} = \begin{cases} \frac{M}{2}, & M \text{ even} \\ \frac{M+1}{2}, & M \text{ odd} \end{cases},$$

$$K_s^{(2)} = \begin{cases} \frac{M}{2}, & M \text{ even} \\ \frac{M-1}{2}, & M \text{ odd} \end{cases},$$

$$K_p^{(1)} = \begin{cases} \frac{M}{2}, & M \text{ even} \\ \frac{M-1}{2}, & M \text{ odd} \end{cases}, \text{ and}$$

$$K_p^{(2)} = \begin{cases} \frac{M-2}{2}, & M \text{ even} \\ \frac{M-1}{2}, & M \text{ odd} \end{cases}.$$

2) Clutter filtering

The clutter filtering algorithm removes the magnitude squared of the I and Q mean (or DC) component in those locations where the site-dependent clutter filter bypass map indicates the need for clutter filtering. Filtered powers and correlations are computed as

$$\tilde{P}_1(n) = P_1(n) - \left|\bar{V}(n)\right|^2 \left[1 - B(n)\right], \qquad \text{for } 0 \le n < N_1,$$

$$\tilde{P}_2(n) = P_2(n) - \left|\bar{V}(n)\right|^2 \left[1 - B(n)\right], \qquad \text{for } 0 \le n < N_2,$$

$$\tilde{R}_1(n) = R_1(n) - \left|\bar{V}(n)\right|^2 \left[1 - B(n)\right], \qquad \text{for } 0 \le n < \min(N_1, N_2),$$

$$\tilde{R}_2(n) = R_2(n) - \left|\bar{V}(n)\right|^2 \left[1 - B(n)\right], \qquad \text{for } 0 \le n < \min(N_1, N_2).$$

$\bar{V}(n)$ is the mean of V computed using all sweeps, where available, and only long-PRT sweeps beyond the short PRT as

$$\bar{V}(n) = M^{-1} \sum_{m=0}^{M-1} V(n,m), \qquad \text{for } 0 \le n < \min(N_1, N_2), \text{ and}$$

$$\bar{V}(n) = 2M^{-1} \begin{cases} \sum_{m=0}^{M/2-1} V(n,2m), & N_1 > N_2 \\ \sum_{m=1}^{M/2-1} V(n,2m+1), & N_2 > N_1 \end{cases}, \qquad \text{for } \min(N_1, N_2) \le n < \max(N_1, N_2).$$

$B(n)$ is the clutter filter bypass map for the corresponding antenna azimuth and elevation positions [$B(n)$ is set to one to indicate that clutter filters are to be bypassed].

3) Vector exchange

If $T_2 < T_1$, swap $\tilde{P}_1$, $\tilde{P}_2$ and $\tilde{R}_1$, $\tilde{R}_2$ so that $\tilde{P}_1$ and $\tilde{R}_1$ correspond to the short PRT, and $\tilde{P}_2$ and $\tilde{R}_2$ correspond to the long PRT.

4) Strong point clutter canceling

Processing is as in the legacy system. Strong-point clutter canceling is applied to $\tilde{P}_1$, $\tilde{P}_2$, $\tilde{R}_1$, and $\tilde{R}_2$ based on $\tilde{P}_2$ powers.

5) Velocity computation

a. Computation of Doppler velocities for each PRT using the corresponding correlation estimates:

$$v_1(n) = -\frac{\lambda}{4\pi T_1} \arg\left\{\tilde{R}_1(n)\right\}, \qquad \text{for } 0 \le n < N_1,$$
$$v_2(n) = -\frac{\lambda}{4\pi T_2} \arg\left\{\tilde{R}_2(n)\right\}, \qquad \text{for } 0 \le n < N_1.$$

b. Computation of errors for each possible aliasing case:

$$\left.\begin{aligned} \alpha_1(n) &= v_1(n) - v_2(n), \\ \alpha_2(n) &= v_1(n) - v_2(n) - 2v_{a2}, \\ \alpha_3(n) &= v_1(n) - v_2(n) + 2v_{a2}, \\ \alpha_4(n) &= v_1(n) - v_2(n) + 2v_{a1} - 2v_{a2}, \\ \alpha_5(n) &= v_1(n) - v_2(n) - 2v_{a1} + 2v_{a2}, \end{aligned}\right\} \qquad \text{for } 0 \le n < N_1.$$

c. Identification of most-likely aliasing case:

$$\beta(n) = \arg\min_i \left|\alpha_i(n)\right|, \qquad \text{for } 1 \le i \le 5 \text{ and } 0 \le n < N_1.$$

d. Velocity dealiasing based on v_1 and aliasing case:

$$v(n) = \begin{cases} v_1(n), & \beta(n) = 1,2,3 \\ v_1(n) + 2v_{a1}, & \beta(n) = 4 \\ v_1(n) - 2v_{a1}, & \beta(n) = 5 \end{cases}, \qquad \text{for } 0 \leq n < N_1.$$

6) Spectrum width computation

The spectrum width computation method corresponds to the algorithm implemented in the legacy WSR-88D signal processor. This method exhibits fewer errors if powers and correlation estimates from the long PRT are used. An alternative method that is unbiased (Doviak and Zrnic 1993) is computationally more complex because it requires computations of lag-2 correlations.

$$w(n) = \frac{\lambda}{4\pi T_2}\left\{ \ln\left[\frac{\left(\tilde{P}_2(n) - N\right)^2}{\left|\tilde{R}_2(n)\right|^2} \right] \right\}^{1/2}, \qquad \text{for } 0 \leq n < N_1.$$

7) Combined echo power computation

To compute the reflectivity, data are extracted from the two power arrays P_1 and P_2 with different rules for each of the three segments depicted in Figure 4.1. For segment I, data are extracted only from P_1, since P_2 may be contaminated on those range bins with overlaid powers. An average of P_1 and P_2 is extracted for segment II, given that both power vectors are "clean" there. Finally, segment III data are obtained from P_2.

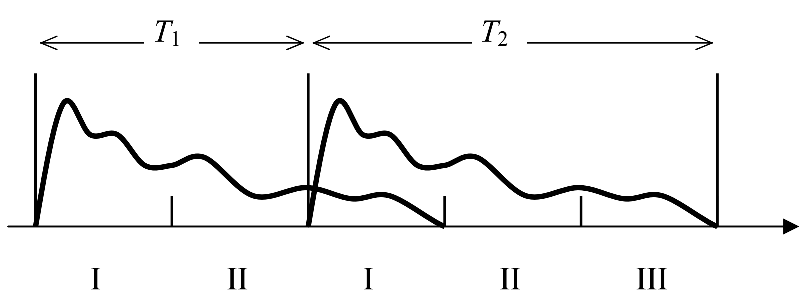

Fig. 4.1. Signal powers in the staggered PRT algorithm. Roman numerals indicate segment numbers used in the reflectivity computation and censoring algorithms.

Finally, the combined echo power computation is performed as:

$$ECHO(n) = 10\log_{10}\left[\frac{1}{4}\sum_{k=0}^{3} P(4n+k) - NOISE\right], \qquad \text{for } 0 \le n < N_2/4,$$

where

$$P(n) = \begin{cases} \tilde{P}_1(n), & 0 \le n < N_2 - N_1 \\ \frac{1}{2}[\tilde{P}_1(n) + \tilde{P}_2(n)], & N_2 - N_1 \le n < N_1 \\ \tilde{P}_2(n), & N_1 \le n < N_2 \end{cases},$$

and *NOISE* is the noise power.

8) Determination of significant returns for reflectivity using reflectivity threshold

$$SR_Z(n) = \begin{cases} 0, & n = 0 \text{ or } ECHO(n) < T_Z + NOISE \\ 1, & ECHO(n) \ge T_Z + NOISE \end{cases}, \qquad \text{for } 0 \le n < N_2/4,$$

where T_Z is the reflectivity threshold and *NOISE* the noise power, both in dB.

9) Reflectivity computation

$$Z(n) = ECHO(n) + SYSCAL + n\,ATMOS + 20\log_{10}(n), \quad \text{for } 0 \le n < N_2/4,$$

where *SYSCAL* is the system calibration constant, and *ATMOS* is the atmospheric attenuation depending on the antenna elevation angle.

10) Reflectivity clipping and scaling

As a final step, reflectivity estimates are thresholded based on the SNR, and data are scaled and formatted to be received, displayed, and processed by the RPG (Radar Product Generation) unit.

$$\tilde{Z}(n) = \begin{cases} 94.5 \text{ dBZ}, & Z(n) > 94.5 \text{ dBZ} \\ Z(n), & -32 \text{ dBZ} \le Z(n) \le 94.5 \text{ dBZ} \\ -32 \text{ dBZ}, & Z(n) < -32 \text{ dBZ} \end{cases}, \qquad \text{for } 0 \le n < N_2/4,$$

$$Z_s(n) = \begin{cases} 0, & SR_Z(n) = 0 \\ [\![2\tilde{Z}(n) + 66]\!], & SR_Z(n) = 1 \end{cases}, \qquad \text{for } 0 \le n < N_2/4.$$

11) Individual echo power computations

$$ECHO_i(n) = 10\log_{10}\left[\tfrac{1}{4}\sum_{k=0}^{3}\tilde{P}_i(4n+k) - NOISE\right], \qquad \text{for } 0 \le n < N_i/4 \text{ and } i = 1, 2,$$

where *NOISE* is the noise power

12) Determination of return type

Censoring of velocity and spectrum width data is only necessary in segment I. This is done by analyzing P_1 in segment I and P_2 in segment III (see Fig. 4.1). The idea is to determine whether second trip signals mask first trip signals in segment I of P_2. While such overlaid echoes appear in every other pulse and do not bias velocity estimates at those range locations, overlaid powers act as noise. Therefore, when second trip powers in segment I of P_2 are above a preset fraction of their first trip counterparts, the corresponding velocity and spectrum width estimates exhibit very large errors and must be censored.

For $n = 0$
    (Initialize all cells as having noise)
    $RT(n)$ = *NOISE LIKE*
End

(Range gates that may have overlaid echoes)
For $1 \le n < N_2/4 - N_1/4$
    if ($ECHO_1(n) > T_M$)
        (Powers from the short PRT are significant)
        if ($ECHO_1(n) > ECHO_2(n + N_1/4) + T_O$) or ($ECHO_2(n + N_1/4) < T_M$)
        (Powers from the short PRT are larger than the corresponding powers from the long PRT by a threshold, or the powers from the long PRT are insignificant)
            $RT(n)$ = *SIGNAL LIKE*
        else
        (Powers from the short PRT overlay powers from the long PRT)
            $RT(n)$ = *OVERLAID LIKE*
        end
    else
    (Powers from the short PRT are not significant)
        $RT(n)$ = *NOISE LIKE*
    end
end

(Range gates that cannot have overlaid echoes)
For $N_2/4 - N_1/4 \leq n < N_1/4$
    if ($ECHO_2(n) > T_M$)
    (Powers from the long PRT are significant)
        $RT(n) = SIGNAL\ LIKE$
    else
    (Powers from the long PRT are significant)
        $RT(n) = NOISE\ LIKE$
    end
end

(Range gates that will have overlaid echoes)
For $N_1/4 \leq n < N_2/4$
    $RT(n) = NOISE\ LIKE$
end

where $T_M = \min(T_Z, T_v, T_w)$. T_Z, T_v, and T_w are the reflectivity, velocity, and width thresholds, respectively, and T_O is the overlaid threshold, all in dB.

To show the purple haze for $r > r_{a1}$ in the velocity and spectrum width displays, replace the last for loop with the following one:

(Range gates that will have overlaid echoes)
For $N_1/4 \leq n < N_2/4$
    if ($ECHO_2(n) > T_M$
        $RT(n) = OVERLAID\ LIKE$
    else
        $RT(n) = NOISE\ LIKE$
    end
end

13) Determination of significant returns for velocity using velocity threshold

As a final step, velocity estimates are thresholded based on the SNR, and data are scaled and formatted to be received, displayed, and processed by the RPG (Radar Product Generation) unit.

$$SR_v(n) = \begin{cases} 0, & n = 0 \text{ or } ECHO_1(n) < T_v + NOISE \\ 1, & ECHO_1(n) \geq T_v + NOISE \end{cases}, \qquad \text{for } 0 \leq n < N_1/4,$$

where T_v is the velocity threshold and $NOISE$ the noise power, both in dB.

14) Velocity clipping and scaling

$$\tilde{v}(n) = \begin{cases} -63.5 \text{ m s}^{-1}, & v(n) < -63.5 \text{ m s}^{-1} \\ v(n), & -63.5 \text{ m s}^{-1} \le v(n) \le 63 \text{ m s}^{-1} \\ 63 \text{ m s}^{-1}, & v(n) > 63 \text{ m s}^{-1} \end{cases}, \qquad \text{for } 0 \le n < N_2,$$

$$v_s(n) = \begin{cases} 0, & SR_v(\llbracket \mathrm{mod}(n, N_1)/4 \rrbracket) = 0 \text{ or } RT(\llbracket n/4 \rrbracket) = \mathit{NOISE\ LIKE} \\ 1, & SR_v(\llbracket \mathrm{mod}(n, N_1)/4 \rrbracket) = 1 \text{ and } RT(\llbracket n/4 \rrbracket) = \mathit{OVERLAID\ LIKE} \\ \llbracket 2\tilde{v}(n) + 129 \rrbracket, & SR_v(\llbracket \mathrm{mod}(n, N_1)/4 \rrbracket) = 1 \text{ and } RT(\llbracket n/4 \rrbracket) = \mathit{SIGNAL\ LIKE} \end{cases},$$

for $0 \le n < N_2$,

where $\llbracket x \rrbracket$ is the integer part of x, and mod(x, N) is the remainder after dividing x by N.

15) Determination of significant returns for width using width threshold

As a final step, spectrum width estimates are thresholded based on the SNR, and data are scaled and formatted to be received, displayed, and processed by the RPG (Radar Product Generation) unit.

$$SR_w(n) = \begin{cases} 0 & \text{if } n = 0 \text{ or } ECHO_1(n) < T_w + NOISE \\ 1 & \text{if } ECHO_1(n) \ge T_w + NOISE \end{cases}, \qquad \text{for } 0 \le n < N_1/4,$$

where T_w is the width threshold and *NOISE* the noise power, both in dB.

16) Width clipping and scaling

$$\tilde{w}(n) = \begin{cases} -63.5 \text{ m s}^{-1}, & w(n) < -63.5 \text{ m s}^{-1} \\ w(n), & -63.5 \text{ m s}^{-1} \le w(n) \le 63 \text{ m s}^{-1} \\ 63 \text{ m s}^{-1}, & w(n) > 63 \text{ m s}^{-1} \end{cases}, \qquad \text{for } 0 \le n < N_2,$$

$$w_s(n) = \begin{cases} 0 & \text{if } SR_w(\llbracket \mathrm{mod}(n, N_1)/4 \rrbracket) = 0 \text{ or } RT(\llbracket n/4 \rrbracket) = \mathit{NOISE} \\ 1 & \text{if } SR_w(\llbracket \mathrm{mod}(n, N_1)/4 \rrbracket) = 1 \text{ and } RT(\llbracket n/4 \rrbracket) = \mathit{OVERLAID} \\ \llbracket 2\tilde{w}(n) + 129 \rrbracket & \text{if } SR_w(\llbracket \mathrm{mod}(n, N_1)/4 \rrbracket) = 1 \text{ and } RT(\llbracket n/4 \rrbracket) = \mathit{SIGNAL} \end{cases},$$

for $0 \le n < N_2$,

where $\llbracket x \rrbracket$ is the integer part of x, and mod(x, N) is the remainder after dividing x by N.

4.2. Performance of the Staggered PRT Algorithm

Staggered PRT data was collected and processed in real time using NSSL's KOUN radar. The case under analysis was obtained on April 06, 2003 at 04:39 UCT. KOUN ran a scan at 1.5 deg using two staggered PRT modes. In the first mode the PRTs are short; $T_1 = 1.227$ ms ($r_{a1} = 184$ km) and $T_2 = 1.84$ ms ($r_{a2} = 276$ km) with $M = 64$ pulses. In the second mode the PRTs are long; $T_1 = 1.6$ ms ($r_{a1} = 240$ km) and $T_2 = 2.4$ ms ($r_{a2} = 360$ km) also with $M = 64$ pulses. Note that in both cases $T_1/T_2 = 0.666\ldots$, but the resulting composite maximum unambiguous velocity is $v_a = 45.17$ m s^{-1} for the short PRTs and $v_a = 34.63$ m s^{-1} for the long PRTs. For comparison, we also show reflectivity and Doppler velocity displays for the same event as observed by the KTLX radar in Twin Lakes, OK (located about 20 km to the north of KOUN). The time is 04:37 UCT and the elevation angle is 1.5 deg. Note that the reflectivity display corresponds to the first half of a "split cut" in the WSR-88D, and the Doppler velocity display corresponds to its second half. KTLX ran a scan with a uniform long PRT of 3.107 ms followed by a scan with a uniform short PRT of 0.987 ms. The maximum unambiguous velocity is $v_a = 26.1$ m s^{-1}.

Figs. 4.2 and 4.3 show KOUN's and KTLX's reflectivity fields, respectively. Differences in the reflectivity fields are attributed mainly to KOUN's reduced transmitter power (as it is configured for transmission of dual polarized signals). Other contributions to the mismatches are the different location of radars, different acquisition times, and different calibration constants. Doppler velocity displays of KOUN data are in Figs. 4.4 and 4.5 for the short and long PRTs, respectively. Fig. 4.6 shows the velocity display as obtained with the KTLX radar. As expected, KTLX's velocity display is significantly obscured by the "purple haze" which indicates the presence of unresolvable overlaid echoes. An additional limitation is that KTLX, like all

NEXRAD radars, only displays velocities up to 230 km. KOUN displays velocities without obscuration up to a maximum range of $cT_1/2$ (184 km for the short and 240 km for the long PRT in this case). Whereas velocity estimates agree fairly well in places where both radars show valid data, estimates obtained with the staggered PRT algorithm can alias in regions of low SNR. The choice of PRTs (for a fixed PRT ratio) is dictated by the trade-off between maximum unambiguous velocity and range coverage. Shorter PRT sets provide a larger effective unambiguous velocity but smaller range coverage without overlaid echoes than do longer PRTs.

Finally, the performance of the simple ground clutter filter implemented in this version of the staggered PRT algorithm is inferior compared to the recursive ground clutter filter used in the WSR-88D with uniform PRT sequences. Evidence of this is the velocity bias towards zero observed at ranges close to the radar when comparing KOUN with KTLX velocities.

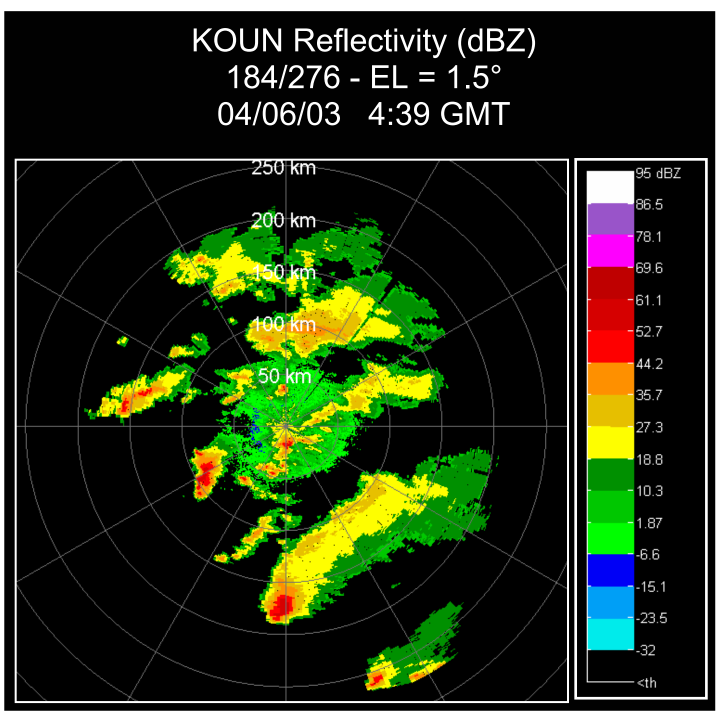

Fig. 4.2. KOUN reflectivity field obtained using the staggered PRT method.

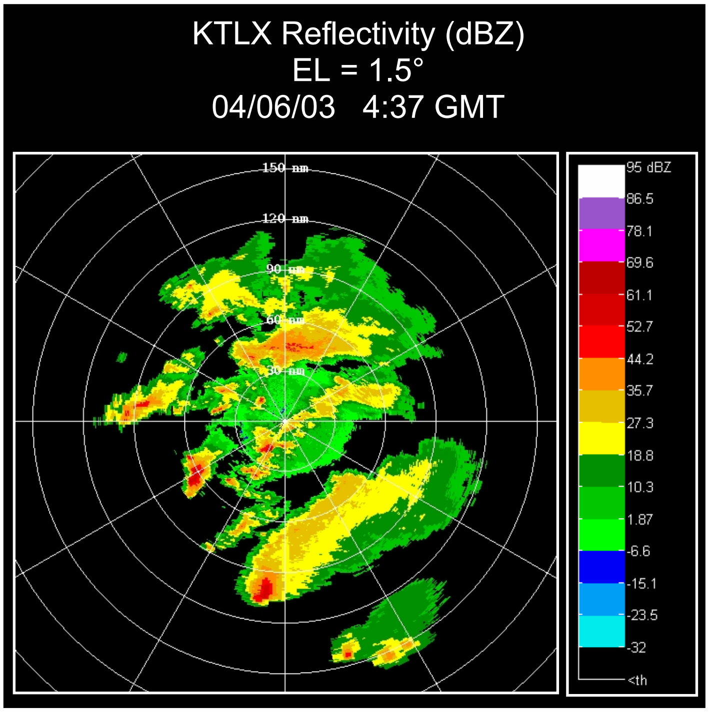

Fig. 4.3. KTLX reflectivity field obtained from legacy VCP 11.

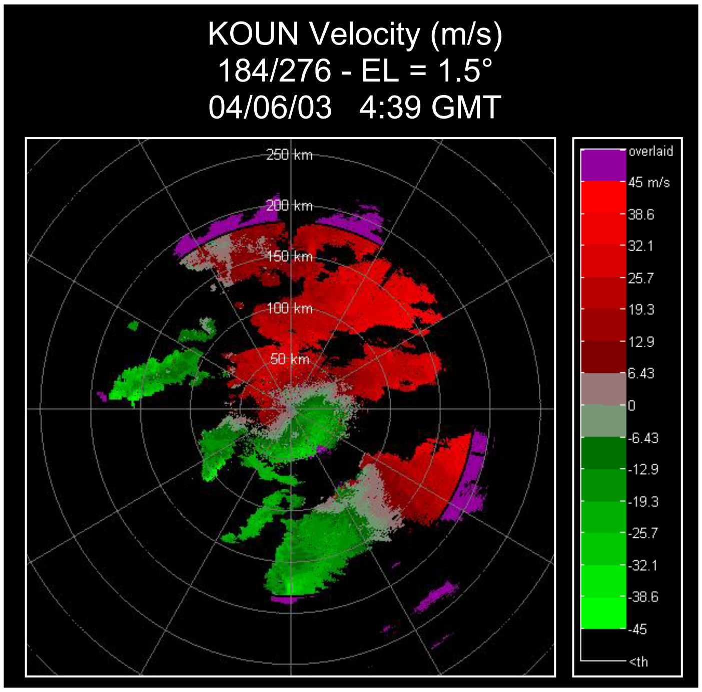

Fig. 4.4. KOUN Doppler velocity field obtained using the staggered PRT method. The set of PRTs for this scan is referred to as “short PRTs” and these correspond to $T_1 = 1.227$ ms ($r_{a1} = 184$ km) and $T_2 = 1.84$ ms ($r_{a2} = 276$ km).

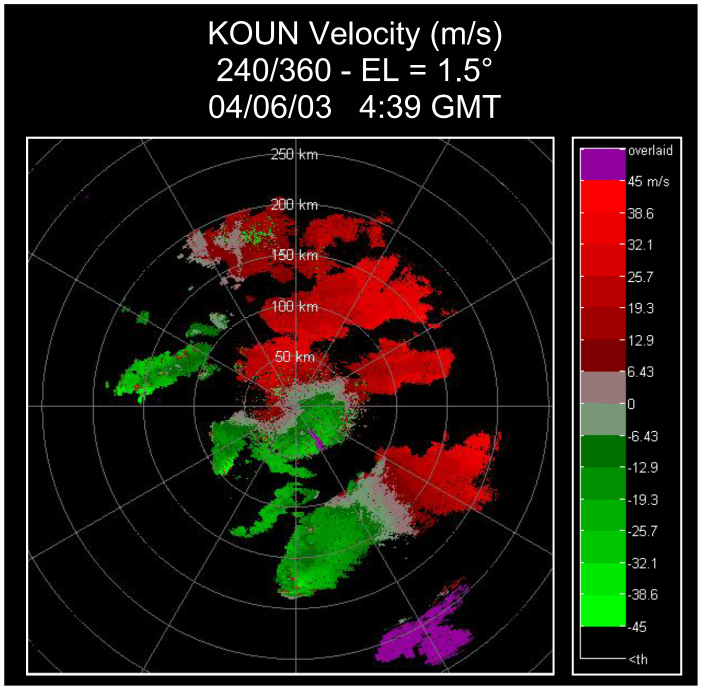

Fig. 4.5. KOUN Doppler velocity field obtained using the staggered PRT method. The set of PRTs for this scan is referred to as "long PRTs" and these correspond to T_1 = 1.6 ms (r_{a1} = 240 km) and T_2 = 2.4 ms (r_{a2} = 360 km).

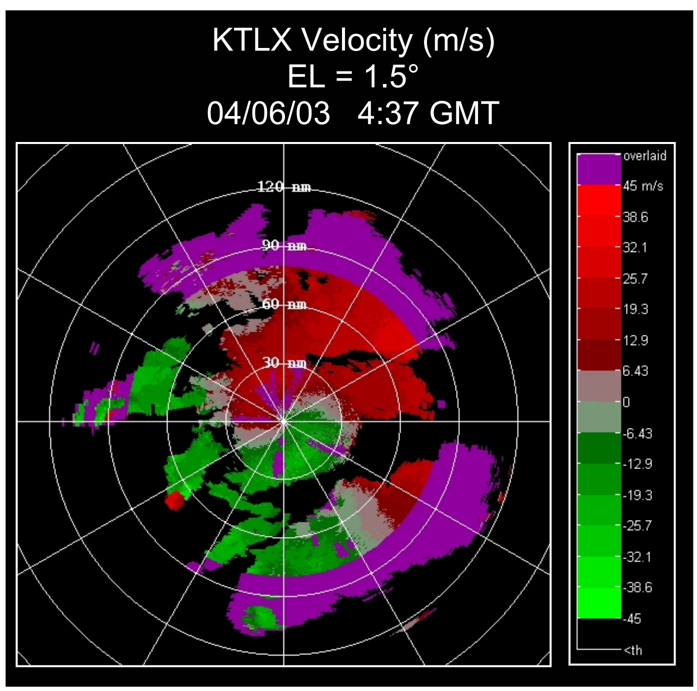

Fig. 4.6. KTLX Doppler velocity field obtained from legacy VCP 11 (2^{nd} half of a split cut)

5. Discussion

Phase coding and staggered PRT techniques have been applied to several events of time series data collected by the KOUN in Norman, OK. In reports 3 and 4 by Sachidananda et al. (1999, 2000), a volume coverage pattern (VCP) containing a combination of phase coding and staggered PRT methods was proposed. Since then, time series data of both staggered and phase coded returns from several events have been collected by the KOUN radar. All of the events have overlaid echoes in the short PRT mode, and most have overlaid echoes in the medium PRT mode as well. Because time separation between scans (with phase coded transmission and staggered PRT transmission) is small compared to changes due to storm evolution and translation, it is possible to make semi quantitative comparisons between the two methods. Qualitative examination of these data confirms that the VCP suggested by Sachidananda et al. (2000 and 2001) would be free of range overlaid echoes at higher elevations (staggered PRT), and would provide good clutter filtering and decrease areas of unrecoverable signals at low elevation (phase coding).

If it were not for ground clutter filtering, staggered PRT would have an advantage over phase coding because it can completely eliminate range overlay; but theory suggests that its ground clutter filter could have 10 dB smaller rejections than the filter on uniform pulse trains (Sachidananda et al. 1999, 2000). This, however, remains to be tested on real data. Another advantage of uniform pulse sequences is their suitability for spectral analysis, which in turn can improve data quality. Except at the highest elevations, overlaid echoes are unavoidable if the currently available PRTs on the WSR-88D are used for Doppler measurements. These PRTs have evolved from collective experience; further changes, such as increasing or decreasing the PRTs, are unlikely to reduce the occurrence of range and velocity ambiguities. Thus, one can argue that while spectral analysis (on uniformly spaced sequences) could improve quality of some data, there would be areas with overlaid echoes. This is in contrast to staggered PRT, which is inferior for spectral analysis but can provide data completely free of overlaid echoes. With staggered PRTs, the unambiguous range for reflectivity fields is larger than for velocity fields. Therefore, it is possible to satisfy the WSR-88D specs on the range for velocity measurements (currently 230 km which will shortly be increased to cover the whole second trip) and have no overlaid echoes in the reflectivity fields!

5.1. VCP recommendations

The recommendation by Sachidananda et al. (2001) is still a robust frame on which subsequent improvements could build. As a possible first step NCAR-NSSL's interim report (2003) suggests a modified VCP 11 which contains phase coding alone (Table 5.1).

It is our opinion that staggered PRT could be implemented at the higher elevations with less effort than would take to implement the phase coding. This is because the SZ-1 phase code (proposed for higher elevations) is sufficiently different from the SZ-2, especially in censoring. The caveat behind such reasoning is to implement the staggered PRT version described herein. Such version is much less complicated than the advanced version proposed in our previous reports (Sachidananda et al. 1999, 2000). Main simplifications are in the ground clutter filter (a removal of DC power from autocovariances at zero lag), in using only the existing PRTs of the legacy system, and in giving up the one overlay recovery. Each of these relaxations is briefly explained next.

Scan				Surveillance		Doppler PRF No.				
Elevation (deg)	AZ rate (deg/sec)	Period (sec)	WF Type	PRF No.	No. pulses	4 No. pulses	5 No. pulses	6 No. pulses	7 No. pulses	8 No. pulses
0.5	18.675	19.38	CS	1	17	-	-	-	-	-
0.5	19.224	18.83	CDP	-	-	44	<u>52</u>	56	61	66
1.45	19.844	18.24	CS	1	16	-	-	-	-	-
1.45	19.225	18.83	CDP	-	-	44	<u>52</u>	56	61	66
2.4	16.116	22.46	CDP	-	-	51	<u>60</u>	63	66	68
3.35	17.893	20.23	CDP	-	-	47	<u>55</u>	58	62	67
4.3	17.898	20.23	CDP	-	-	47	<u>55</u>	58	62	67
5.35	17.459	20.73	CDP	-	-	48	<u>57</u>	60	64	70
6.2	17.466	20.73	CDP	-	-	48	<u>57</u>	60	64	70
7.5	25.168	14.38	CDP	-	-	34	41	<u>43</u>	46	50
8.7	25.398	14.25	CDP	-	-	33	41	43	<u>46</u>	50
10.0	25.421	14.24	CDP	-	-	33	41	43	<u>46</u>	50
12.0	25.464	14.22	CDP	-	-	33	41	43	<u>46</u>	50
14.0	25.515	14.19	CDP	-	-	33	41	43	<u>46</u>	50
16.7	25.596	14.14	CDP	-	-	33	41	43	<u>46</u>	50
19.5	25.696	14.09	CD	-	-	33	41	43	<u>46</u>	50

Table 5.1. Modified WSR-88D volume coverage pattern vcp-11 to include phase coding. Default Doppler PRF numbers (used in non-phase-coded vcp-11) are underscored and highlighted. CS: contiguous surveillance, CDP: contiguous Doppler with phase coding. CD: contiguous Doppler without phase coding.

Recall (Sachidananda et al. 1999) that the most effective ground clutter filter we have developed thus far requires an integer stagger ratio $k = m/n$, where m and n are small (less than 10). Our recommendation is $k = 3/2$, which requires a change in one of the PRTs because there are no two existing PRTs on the WSR-88D with such stagger ratio. Nevertheless, use of simple DC removal eliminates this stringent requirement. We submit that such simple clutter filter would be quite adequate at higher elevations. Because one overlay recovery is complicated and benefits are marginal, a better strategy might be to avoid it altogether by increasing the two PRTs. Otherwise, censoring can be used, and as demonstrated herein, it is quite effective.

Incorporation of staggered PRT at higher elevations would require some adjustments of the current velocity dealiasing scheme done in the RPG. That is, the effective unambiguous velocities would increase and so would the discontinuity threshold for assigning proper alias interval to velocity estimates.

5.2. Compatibility with future improvements

One of the improvements that would alter the signal processing is oversampling of echo signals and whitening in range. Oversampled signals are available in the RVP8 processor and might be used exactly as in the legacy system to produce oversampled covariances. If these covariances are averaged in range (over the pulse duration) the variance of estimates could decrease by about a factor of two (Torres and Zrnic 2003, Ivic et al. 2003). Such processing is completely compatible with either staggered PRT or phase coding. If spectral processing is the choice, then spectra of oversampled signals would be averaged.

Similarly, if signals are whitened in range to further decrease errors in estimates (or speed volume coverage) the two R/V mitigation methods remain compatible in principle, but there are differences in the expected outcome. Explanation follows.

The staggered PRT (described herein) is completely compatible with fast volume updates because it is not drastically affected by the number of pulse pairs per dwell time which at high volume update speeds would be small. Spectral clutter filter in the more sophisticated staggered PRT might be adversely affected by such fast speeds. This issue requires further study, a heuristic explanation of the effect on phase coding follows.

Phase coding relies on Fourier transforms; at short dwell times such transforms have poor frequency (velocity) resolution. It is possible to extend the dwell time by applying time windows and hope that effective taper will create an effective beamwidth (Doviak and Zrnic 1993, Fig. 7.25) of about 1°. This might work up to a point. For example take 5 rpm rotation, 1 ms PRT, and 64 time samples; during this dwell time the antenna moves 1.92 deg. The effective beamwidth for this case would be about 2.25^o (Fig 7.25 in Doviak and Zrnic 1993). It is conceivable that this effective beamwidth could be reduced to 1^o by windowing the time series data, and then the resultant azimuth resolution would equal the presently practiced norm. Nonetheless, NWS plans to increase the effective resolution to about 0.5 deg. At the rotation speeds of 5 rpm the way to get such resolution is to reduce the number of samples to 32 and apply the window. We expect some degradation in performance but have not tested the phase coding scheme on such short time series.

Another issue applicable if both methods process oversampled time series and average the intermediate results in range is how to treat "partial" contamination of signals in range. By partial we mean contamination over part of the resolution volume (i.e., few oversampled signals are contaminated while the rest are not). Obviously, the easiest solution is to do nothing and after averaging in range, censor such data. A better alternative is to eliminate the contaminated parts (range gates) and process the remaining ones. This, however, entails prohibitive computations and hence is deferred for future studies.

5.3. Issues for future studies

Verification of errors in staggered PRT by comparisons with theoretical predictions (Sachidananda et al. 1999, 2000) should be done. This can be achieved via statistical analysis of errors for a fixed antenna pointing; such data are available. Analysis of spatial averages over small azimuth-range cells could also produce statistically meaningful results. Although qualitative (visual) results presented herein are very appealing, a full confidence in the method will be achieved if the errors can be explained with physical principles. Further, there might be unusual circumstances where the method fails; it is important to uncover these, understand the cause, and devise censoring schemes to prevent contamination of the moment fields.

Very important is to test the sophisticated ground clutter filter (Sachidananda et al. 1999) for two reasons. One is to demonstrate that it is superior to the current filter (on the WSR-88D at higher elevations), and two is to see how much worse that filter is (from the WSR-88D recursive filter) at lowest elevations. If the sophisticated ground clutter filter is satisfactory say at 1.5 deg then staggered PRT could replace phase coding at that elevation; further the same might hold (for some radar locations) at 0.5 deg.

Another, albeit trivial, improvement of the staggered PRT is to extend the "unambiguous" range for reflectivity measurement to twice the short unambiguous range, r_{a1}. If this extension is satisfactory it would be worthwhile to consider such staggered PRT in lieu of the surveillance scan at the lowest two elevations. Mean velocities thus obtained would compliment the velocities from the Doppler scan especially in regions of strong echo overlay where phase coded data are unreliable.

Also left for further investigation is the interplay between extended unambiguous velocity, dealiasing error, and stagger ratio so that optimum parameters could evolve. Quantitative comparison between staggered PRT and phase coding should be made. Challenge is to make fair comparison because the two methods inherently yield different effective unambiguous range and velocity.

Remaining significant issues of the phase coding are ground clutter filtering and censoring in the SZ-1 algorithm. Recursive, or infinite-impulse-response (IIR), and finite-impulse-response (FIR) filters have been applied to the time series data. It has been demonstrated in the NCAR-NSSL Interim Report (2003) that the recursive filter creates bias in mean velocity estimates. This bias could be eliminated by correcting the phase shifts introduced by the filter. Overall more effective filtering might be possible with a FIR filter. Spectral filters are a subset of FIR filters and might not offer as much flexibility in the choice of parameters (notch width, attenuation etc.) as do the other FIR filters. Examination of more sophisticated filters is in order; obvious candidates are regression filters (Torres 1998) and optimum filters (Urkowitz 1998). Optimum choice of thresholds for censoring should be established and quantitatively tested on time series data. Because spectrum width from long PRT (surveillance scan) is a key censoring parameter it is important to determine bias caused by small number of samples, and underestimation at large spectrum widths due to self-aliasing. Staggered PRT technique is also prone to similar biases if $1/T_1$ and $1/T_2$ are not significantly larger than the Doppler spectrum width (in Hz).

Last, Sigmet has implemented a version of the SZ-1 algorithm and has given the code to NWS. We suggest detailed description of that implementation be made and compared with Sachidananda et al. (1998, also NCAR-NSSL Interim Report 2003). It may be possible to draw from the best of both, or perhaps minor changes in the Sigmet algorithm might be all that is needed. If so, that would be an expedient and efficient way to proceed.

6. References

Cho, J. Y. N., 2003: Evaluation of TDWR range-velocity ambiguity mitigation techniques. LL ATC-310, MIT Lincoln Laboratory, Lexington, Mass., 47 pp.

Doviak, R. J. and D. S. Zrnic, 1993: *Doppler radar and weather observations.* Academic Press, New York, 562p.

Frush, C., 1997: NEXRAD range-velocity: Exploring selected mitigation techniques, Second year report, WSR-88D Operational Support Facility, NCAR, Norman, OK, 88 pp.

Ivic, I., D. S. Zrnic, and S. Torres, 2003: Whitening in range to improve weather radar spectral moment estimates. Part II: Experimental evaluation. *J. Atmos. Oceanic Technol.*, 20, 1433-1448.

NCAR-NSSL Interim Report, 2003: NEXRAD Range-Velocity Ambiguity Mitigation SZ(8/64) Phase Coding Algorithm Recommendations.

Passarelli, R. E., Jr., P. Romanik, S. G. Geotis, and A. D. Siggia, 1981: Ground clutter rejection in the frequency domain. Preprints, *20th Conf. on Radar Meteorology,* Boston, MA, Amer. Meteor. Soc., 295–300.

Sachidananda, M. and D. Zrnic, 2002: An improved clutter filtering and spectral moment estimation algorithm for staggered PRT sequences. *J. Atmos. Oceanic Technol.*, 19, 2009-2019.

Sachidananda, M. and D. Zrnic, 2003: Unambiguous range extension by overlay resolution in staggered PRT technique. *J. Atmos. Oceanic Technol.*, 20, 673-684.

Sachidananda, M., 1998: Signal design and processing techniques for WSR-88D ambiguity resolution, Part 2, NOAA/NSSL Report, 105 pp.

Sachidananda, M., 1999: Signal design and processing techniques for WSR-88D ambiguity resolution, Part 3, NOAA/NSSL Report, 81 pp.

Sachidananda, M., 2000: Signal design and processing techniques for WSR-88D ambiguity resolution, Part 4, NOAA/NSSL Report, 99 pp.

Sachidananda, M., 2001: Signal design and processing techniques for WSR-88D ambiguity resolution, Part 5, NOAA/NSSL Report, 75 pp.

Sachidananda, M., 2002: Signal design and processing techniques for WSR-88D ambiguity resolution, Part 6, NOAA/NSSL Report, 57 pp.

Sirmans, D., 1992: Clutter filtering in the WSR-88D. NWS/OSF Internal Rep., 125 pp. [Available from National Weather Service Radar Operations Center, 1200 Weistheimer Dr., Norman, OK 73069.]

Sirmans, D., D. Zrnic, and B. Bumgarner, 1976: Extension of maximum unambiguous Doppler velocity by use of two sampling rates. Preprints *17th Conf. on Radar Meteorology*, Seattle, WA, Amer. Meteor. Soc., pp. 23-28.

Torres, S., 1998: Ground Clutter Canceling with a Regression Filter, NOAA/NSSL Report, 37 pp.

Torres, S. and A. Zahrai, 2002: Migration of WSR-88D signal processing functionality to open systems. Preprints *18th International Conf. on IIPS*, Orlando, FL, Amer. Meteor. Soc., paper 5.11.

Torres, S., and D. Zrnić, 2003: Whitening in range to improve weather radar spectral moment estimates. Part I: Formulation and simulation. *J. Atmos. Oceanic Technol.*, 20, 1433-1448.

Urkowitz, H., and H. S. Owen, 1998: A matrix clutter processor for agile beam radars. Preprints *IEEE 1998 National Radar Conf.*, Dallas, TX, Institute of Electrical and Electronics Engineers, 153-158.

Zrnic, D. and R. Cook, 2002: Evaluation of techniques to mitigate range and velocity ambiguities on the WSR-88D. Preprints *18th International Conf. on IIPS*, Orlando, FL, Amer. Meteor. Soc., paper 5.13.

Zrnic, D., and P. Mahapatra, 1985: Two methods of ambiguity resolution in pulse Doppler weather radars. *IEEE Trans. Aerosp. Electron. Syst.*, 21, 470-483.

LIST OF NSSL REPORTS FOCUSED ON POSSIBLE UPGRADES TO THE WSR-88D RADARS

Schuur, T., P. Heinselman, and K. Scharfenberg, 2003: Overview of the Joint Polarization Experiment (JPOLE), NOAA/NSSL Report, 38 pp.

Ryzhkov, A, 2003: Rainfall Measurements with the Polarimetric WSR-88D Radar, NOAA/NSSL Report, 99 pp.

Schuur, T., A. Ryzhkov, and P. Heinselman, 2003: Observations and Classification of echoes with the Polarimetric WSR-88D radar, NOAA/NSSL Report, 45 pp.

Melnikov, V. M, D. S. Zrnic, R. J. Doviak, and J. K. Carter, 2003: Calibration and Performance Analysis of NSSL's Polarimetric WSR-88D, NOAA/NSSL Report, 77 pp.

NCAR-NSSL Interim Report, 2003: NEXRAD Range-Velocity Ambiguity Mitigation SZ(8/64) Phase Coding Algorithm Recommendations.

Sachidananda, M., 2002: Signal Design and Processing Techniques for WSR-88D Ambiguity Resolution, NOAA/NSSL Report, Part 6, 57 pp.

Doviak, R. J., J. Carter, V. Melnikov, and D.S. Zrnic, 2002: Modifications to the Research WSR-88D to obtain Polarimetric Data, NOAA/NSSL Report, 49 pp.

Fang, M., and R. J. Doviak, 2001: Spectrum width statistics of various weather phenomena, NOAA/NSSL Report, 62 pp.

Sachidananda, M., 2001**:** Signal Design and Processing Techniques for WSR-88D Ambiguity Resolution, NOAA/NSSL Report, Part 5, 75 pp.

Sachidananda, M., 2000**:** Signal Design and Processing Techniques for WSR-88D Ambiguity Resolution, NOAA/NSSL Report, Part 4, 99 pp.

Sachidananda, M., 1999**:** Signal Design and Processing Techniques for WSR-88D Ambiguity Resolution, NOAA/NSSL Report, Part 3, 81 pp.

Sachidananda, M., 1998**:** Signal Design and Processing Techniques for WSR-88D Ambiguity Resolution, NOAA/NSSL Report, Part 2, 105 pp.

Torres, S., 1998: Ground Clutter Canceling with a Regression Filter, NOAA/NSSL Report, 37 pp.

Doviak, R. J. and D. S. Zrnic, 1998**:** WSR-88D Radar for Research and Enhancement of Operations: Polarimetric Upgrades to Improve Rainfall Measurements, NOAA/NSSL Report, 110 pp.

Sachidananda, M., 1997: Signal Design and Processing Techniques for WSR-88D Ambiguity Resolution, NOAA/NSSL Report, Part 1, 100 pp.

Sirmans, D., D. S. Zrnic, and M. Sachidananda, 1986: Doppler radar dual polarization considerations for NEXRAD, NOAA/NSSL Report, Part I, 109 pp.

Sirmans, D., D. S. Zrnic, and N. Balakrishnan, 1986: Doppler radar dual polarization considerations for NEXRAD, NOAA/NSSL Report, Part II, 70 pp.

APPENDIX

Algorithm Enunciation Language (AEL)

SZ-2 Algorithm

Prepared for:

The National Weather Service / WSR-88D Radar Operations Center
Norman, Oklahoma

Prepared by:

The National Severe Storms Laboratory
Norman, Oklahoma

2003

SZ-2

ALGORITHM DESCRIPTION

[036/01]

1.0 PROLOGUE

1.1 FUNCTIONAL DESCRIPTION

The purpose of the SZ-2 algorithm is to process signals that are phase coded with the SZ(8/64) code from data collected by the WSR-88D radar. This algorithm is used in the RADAR DATA ACQUISITION (RDA) unit.

A scan with phase-coded transmission follows a long-PRT surveillance scan. Powers and spectrum widths from the surveillance scan are stored and used in the phase-coded scan.

Several variables are fixed during the transmission phase of the WSR-88D radar and are used in the SZ-2 algorithm:

ATMOS= Atmospheric attenuation constant, depending on the antenna elevation angle (in dB/km).

DELTA_T= Range-time sampling period, real variable (in s). DELTA_T = 1.57×10^{-6} s in the legacy WSR-88D.

LAMBDA= Radar wavelength (in m).

NCELLS= Number of cells for TS, integer variable denoting the number of range cells in a sweep for pulse spacing TS.

NCELLS = TS / DELTA_T

NCELLS_L= Number of cells for TL, integer variable denoting the number of range cells in a sweep for pulse spacing TL.

NCELLS_L = TL / DELTA_T

NP_SZ= Phase-coded sweep count, integer variable denoting the number of pulses in each radial.

SYSCAL= System calibration constant (unitless).

TL= Pulse Repetition Time (PRT) of the long-PRT data, real variable (in s).

TS= Pulse Repetition Time (PRT), real variable (in s).

V_NYQ= Nyquist velocity for pulse spacing TS (in m/s).

V_NYQ = LAMBDA / (4xTS)

V_NYQ_L= Nyquist velocity for pulse spacing TL (in m/s).

V_NYQ = LAMBDA / (4xTL)

The following assumptions are made:

- The phases of the transmitted pulses are modulated with the SZ(8/64) switching code.
- The number of pulses transmitted in the dwell time is NP_SZ=64. Several options exist to handle fewer pulses within the dwell time and to feed the required 64 pulses to the SZ-2 algorithm.
- Ground clutter, if present, always occurs in the first trip range interval.
- The algorithm operates on one radial (NP_SZ range sweeps) of time-series data at a time.

1.2 SOURCE

The SZ-2 algorithm described herein has been implemented for offline processing of data acquired with NSSL’s Research RDA (KOUN radar).

REFERENCES

Sachidananda, M., and D. Zrnic, 1999: Systematic Phase Codes for Resolving Range Overlaid Signals in a Doppler Weather Radar. Journal of Atmospheric and Oceanic Technology, 16, 1351-1363.

Sachidananda, M., 1997-2002: Signal Design and Processing Techniques for WSR-88D Ambiguity Resolution. National Severe Storms Laboratory Report, Parts 1,2,3,4,5, and 6.

1.3 PROCESSING ENVIRONMENT

A long-PRT surveillance scan precedes the phase-coded scan. Powers and spectrum widths from the surveillance scan are stored and used by the SZ-2 algorithm. This algorithm requires also the phase coded data collected by the WSR-88D radar and the measured switching code which may differ from the theoretical SZ(8/64) phase code due to phase-shifter imperfections.

2.0 INPUTS

2.1 IDENTIFICATION

I_{nm} = In-phase component of the echo signal at range cell n for pulse m (unitless). It can take values in the interval [-841.40;840.98].

Q_{nm} = Quadrature-phase component of the echo signal at range cell n for pulse m (unitless). It can take values in the interval [-841.40;840.98].

P_L_n = Ground clutter filtered signal power at range cell n for the long_PRT scan (unitless).

$WIDTH\_L_n$ = Ground clutter filtered spectrum width from the long-PRT scan at range cell n (in m/s).

PSI_m = Measured SZ(8/64) switching code for pulse m (in radians).

2.2 ACQUISITION

I_{nm} and Q_{nm} values are acquired from the output of the WSR-88D radar receiver and are already AGC (Automatic Gain Control) corrected data without interference. P_L_n and $WIDTH\_L_n$ correspond to the surveillance-scan radial that is the closest in azimuth to the phase-coded radial to be processed.

3.0 PROCEDURES

3.1 ALGORITHM

```
BEGIN ALGORITHM (STAGGERED PRT)

1.0 DO FOR ALL (RADIALS)
    1.1  COMPUTE (RECOVERABLE TRIPS)
    1.2  COMPUTE (FIRST TRIP COHERED TIME SERIES)
    1.3  COMPUTE (GROUND CLUTTER FILTERED FIRST TRIP COHERED TIME
         SERIES)
    1.4  COMPUTE (GROUND CLUTTER FILTERED AND UNFILTERED POWERS)
    1.5  COMPUTE (STRONGEST TRIP COHERED TIME SERIES)
    1.6  COMPUTE (STRONGEST TRIP COHERED AUTOCORRELATIONS)
    1.7  COMPUTE (STRONG/WEAK TRIPS)
    1.8  COMPUTE (CLUTTER TO SIGNAL RATIO)
    1.9  COMPUTE (STRONG TRIP VELOCITY)
    1.10 COMPUTE (NOTCH FILTER CENTER VELOCITY)
    1.11 COMPUTE (WINDOWED STRONG TRIP COHERED TIME SERIES)
    1.12 COMPUTE (STRONG TRIP COHERED DISCRETE FOURIER TRANSFORM)
    1.13 COMPUTE (NOTCHED STRONG TRIP COHERED DISCRETE FOURIER
         TRANSFORM)
    1.14 COMPUTE (NOTCHED STRONG TRIP COHERED INVERSE DISCRETE
         FOURIER TRANSFORM)
    1.15 COMPUTE (WEAK TRIP COHERED TIME SERIES)
    1.16 COMPUTE (WEAK TRIP COHERED POWER)
    1.17 COMPUTE (POWER ADJUSTMENTS)
    1.18 COMPUTE (WEAK TRIP COHERED AUTOCORRELATIONS)
    1.19 COMPUTE (WEAK TRIP VELOCITY)
    1.20 COMPUTE (UNFOLDED POWERS AND VELOCITIES)
    1.21 COMPUTE (RETURN TYPE)
    1.22 COMPUTE (REFLECTIVITY)
    1.23 COMPUTE (CLIPPED REFLECTIVITY)
    1.24 COMPUTE (SCALED REFLECTIVITY)
    1.25 COMPUTE (CLIPPED VELOCITY)
    1.26 COMPUTE (SCALED VELOCITY)
    1.27 COMPUTE (CLIPPED SPECTRUM WIDTH)
    1.28 COMPUTE (SCALED SPECTRUM WIDTH)
    END DO

END ALGORITHM (STAGGERED PRT)
```

3.2 COMPUTATION

3.2.1 NOTATION

BYPASS= Clutter filter bypass map for the corresponding antenna azimuth and elevation positions. $BYPASS_n$ = 0 if clutter filtering must be applied at range cell n and 1 otherwise.

C_I = Intercept censoring parameter (in m/s). In general this would be a function of the spectrum width of the weak echo.

C_S = Slope censoring parameter (in dB/(m/s)). In general this would be a function of the spectrum width of the weak echo.

C_T = Threshold censoring parameter (in dB). In general this would be a function of the spectrum width of the weak echo.

CSR_n = Clutter-to-signal ratio at range cell n (unitless).

$ECHO_n$ = Combined echo power at range cell n (in dB).

$FREQ\_0_n$ = Integer denoting the processing notch filter center at range cell n.

$FREQ\_1_n$ = Integer denoting the processing notch filter first cut off frequency at range cell n.

$FREQ\_2_n$ = Integer denoting the processing notch filter second cut off frequency at range cell n.

$I\_TRIP\_1_{nm}$ = Unfiltered first trip cohered in-phase component of the echo signal at range cell n for pulse m (unitless).

$I\_TRIP\_1F_{nm}$ = Filtered first trip cohered in-phase component of the echo signal at range cell n for pulse m (unitless).

$I\_TRIP\_1FB_{nm}$ = Filtered and bypassed first trip cohered in-phase component of the echo signal at range cell n for pulse m (unitless).

$I\_TRIP\_A_{nm}$ = Trip A cohered in-phase component of the echo signal at range cell n for pulse m (unitless).

$I\_TRIP\_B_{nm}$ = Trip B cohered in-phase component of the echo signal at range cell n for pulse m (unitless).

$I\_TRIP\_S_{nm}$ = Strong Trip cohered in-phase component of the echo signal at range cell n for pulse m (unitless).

$I\_TRIP\_SN_{nm}$ = Strong Trip cohered and notched in-phase component of the echo signal at range cell n for pulse m (unitless).

$I\_TRIP\_SW_{nm}$ = Strong Trip cohered and windowed in-phase component of the echo signal at range cell n for pulse m (unitless).

$I\_TRIP\_W_{nm}$ = Weak Trip cohered in-phase component of the echo signal at range cell n for pulse m (unitless).

K_R = Power ratio threshold for recovery of weak trip signal (unitless). In general this would be a function of the spectrum widths of the strong and weak echoes.

K_S= Signal-to-noise ratio threshold for recovery of strong trip signals (unitless).

K_W= Signal-to-noise ratio threshold for recovery of weak trip signals (unitless).

NOISE= Receiver noise power level, scaled as a function of the antenna elevation angle (unitless).

NOISE_LIKE= Return type denoting that the cell in question must be declared noise-like for the purposes of reflectivity, velocity and spectrum width estimations.

NW_n = Integer denoting the processing notch filter notch width at range cell n.

OVERLAID_LIKE= Return type denoting that the cell in question must be declared overlaid for the purposes of reflectivity, velocity and spectrum width estimations.

P_n = Normalized estimated range-unfolded signal power at range cell n (unitless).

P_F_n = Normalized filtered signal power at range cell n (unitless).

P_S_n = Normalized strong trip adjusted signal power at range cell n (unitless).

P_SW_n = Normalized strong trip signal power corrected for window losses at range cell n (unitless).

P_U_n = Normalized unfiltered signal power at range cell n (unitless).

P_W_n = Normalized weak trip signal power at range cell n (unitless).

P_WN_n = Normalized weak trip signal power corrected for window and notch filter losses at range cell n (unitless).

P_WW_n = Normalized weak trip signal power corrected for window losses at range cell n (unitless).

PHI_A_m = Modulation code for trip A with respect to the first trip for pulse m (in radians).

PHI_B_m = Modulation code for trip B with respect to the first trip for pulse m (in radians).

PHI_WS_m = Modulation code for the weak trip with respect to the strong trip for pulse m (in radians).

PP_A_n = Normalized pulse-pair sum accumulation at range cell n for trip A (unitless).

PP_B_n = Normalized pulse-pair sum accumulation at range cell n for trip B (unitless).

PP_S_n = Normalized pulse-pair sum accumulation at range cell n for the strong trip (unitless).

PP_W_n = Normalized pulse-pair sum accumulation at range cell n for the weak trip after notching (unitless).

$Q\_TRIP\_1_{nm}$ = Unfiltered first trip cohered quadrature-phase component of the echo signal at range cell n for pulse m (unitless).

$Q\_TRIP\_1F_{nm}$ = Filtered first trip cohered quadrature-phase component of the echo signal at range cell n for pulse m (unitless).

$Q\_TRIP\_1FB_{nm}$ = Filtered and bypassed first trip cohered quadrature-phase component of the echo signal at range cell n for pulse m (unitless).

$Q\_TRIP\_A_{nm}$ = Trip A cohered quadrature-phase component of the echo signal at range cell n for pulse m (unitless).

$Q\_TRIP\_B_{nm}$ = Trip B cohered quadrature-phase component of the echo signal at range cell n for pulse m (unitless).

$Q\_TRIP\_S_{nm}$ = Strong Trip cohered quadrature-phase component of the echo signal at range cell n for pulse m (unitless).

$Q\_TRIP\_SN_{nm}$ = Strong Trip cohered and notched quadrature-phase component of the echo signal at range cell n for pulse m (unitless).

$Q\_TRIP\_SW_{nm}$ = Strong Trip cohered and windowed quadrature-phase component of the echo signal at range cell n for pulse m (unitless).

$Q\_TRIP\_W_{nm}$ = Weak Trip cohered quadrature-phase component of the echo signal at range cell n for pulse m (unitless).

$REFL_n$ = Estimated reflectivity at range cell n (in dBZ).

$REFL\_C_n$ = Estimated reflectivity after clipping at range cell n (in dBZ).

$REFL\_S_n$ = Estimated reflectivity after scaling at range cell n (in scaled dBZ units).

RT_n = Return type for range cell n. It could be SIGNAL_LIKE, OVERLAID_LIKE, or NOISE_LIKE.

S_S_{nk} = k-th spectral coefficient of the strong trip cohered and windowed time-series data at range cell n (unitless).

S_SN_{nk} = k-th spectral coefficient of the strong trip cohered windowed and notched time-series data at range cell n (unitless).

SIGNAL_LIKE= Return type denoting that the cell in question must be declared signal-like for the purposes of reflectivity, velocity and spectrum width estimations.

T_CSR= Clutter-to-signal ratio threshold used to determine the presence of clutter (unitless).

T_POWER= Power threshold used to determine the minimum allowable power level that a range cell must have to declare a valid signal for velocity estimation at this range cell (in dB).

TA_n = Integer denoting the trip number of the signal with strongest power at range cell n.

TB_n = Integer denoting the trip number of the signal with second strongest power at range cell n.

TS_n = Integer denoting the trip number of the strong trip signal at range cell n.

TW_n = Integer denoting the trip number of the weak trip signal at range cell n.

V_PNF_n = Processing notch filter center at range cell n (in m/s).

V_S_n = Strong trip estimated Doppler velocity at range cell n (in m/s).

V_W_n = Weak trip estimated Doppler velocity at range cell n (in m/s).

VEL_n = Estimated range-unfolded Doppler velocity at range cell n (in m/s).

VEL_C_n = Estimated Doppler velocity after clipping at range cell n (in m/s).

VEL_S_n = Estimated Doppler velocity after scaling at range cell n (in scaled m/s units).

WCF= Window correction factor (unitless). For the Von Hann window, WCF= 2.6257.

$WIDTH_n$ = Estimated spectrum width at range cell n (in m/s).

$WIDTH\_C_n$ = Estimated spectrum width after clipping at range cell n (in m/s).

$WIDTH\_S_n$ = Estimated spectrum width after scaling at range cell n (in scaled m/s units).

3.2.2 SYMBOLIC FORMULAS

Ln3 COMPUTE (RECOVERABLE TRIPS)

DO (n) FROM NCELLS_L TO 4(NCELLS)-1 BY 1
  $P\_L_n=0$
END DO
DO (n) FROM 0 TO NCELLS-1 BY 1
  Sort
  $\left\{P\_L_n,\ P\_L_{n+NCELLS},\ P\_L_{n+2(NCELLS)},\ P\_L_{n+3(NCELLS)}\right\}$ in descending order to get P1, P2, P3, and P4, and their corresponding trip numbers T1, T2, T3, and T4.
  $TA_n=0$
  $TB_n=0$
  IF ((P1>T_POWER) AND (P1>(P2+P3+P4+NOISE)K_S))
    THEN
      $TA_n=T1$
      IF $WIDTH\_L_{n+(T2-1)NCELLS}<5$ m/s
        THEN
          C_T=35 dB
          C_I=4.5 m/s
          C_S=-20/3 dB/(m/s)
        ELSE
          C_T=30 dB
          C_I=3.5 m/s
          C_S=-20/3 dB/(m/s)
      END IF
      IF $WIDTH\_L_{n+(T1-1)NCELLS}<C\_I$
        THEN
          $K\_R=10\text{^}\left(C\_T/10\right)$
        ELSE
      $K\_R=10\text{^}\left(\left(C\_T+C\_S\left(WIDTH\_L_{n+(T1-1)NCELLS}-C\_I\right)\right)/10\right)$
      END IF
      IF ((P2>T_POWER) AND (P2>(P3+P4+NOISE)K_W) AND (P1/P2<K_R))
        THEN
          $TB_n=T2$
        ELSE

```
                $TB_n=0$
            END IF
        ELSE
            $TA_n=0$
    END IF
END DO
```

where
n is the range cell.

Ln4 COMPUTE (FIRST TRIP COHERED TIME SERIES)

DO (n) FROM 0 TO NCELLS-1 BY 1
    DO (m) FROM 0 TO NP_SZ-1 BY 1

$$I\_TRIP\_1_{nm}=I_{nm}.\cos\left(PSI_m\right)+Q_{nm}.\sin\left(PSI_m\right)$$

$$Q\_TRIP\_1_{nm}=Q_{nm}.\cos\left(PSI_m\right)-I_{nm}.\sin\left(PSI_m\right)$$

    END DO
END DO

where
n is the range cell,
and m is the pulse number.

Ln5 COMPUTE (GROUND CLUTTER FILTERED FIRST TRIP COHERED TIME SERIES)

DO (n) FROM 0 TO NCELLS-1 BY 1
    Filter time series data $I\_TRIP\_1_{nm}$ and $Q\_TRIP\_1_{nm}$ using the map-based 5-pole elliptic ground clutter filter as in the legacy RDA to get $I\_TRIP\_1F_{nm}$ and $Q\_TRIP\_1F_{nm}$.
    IF ($BYPASS_n=1$)
        THEN
            $I\_TRIP\_1FB_{nm}=I\_TRIP\_1_{nm}$
            $Q\_TRIP\_1FB_{nm}=Q\_TRIP\_1_{nm}$
        ELSE
            $I\_TRIP\_1FB_{nm}=I\_TRIP\_1F_{nm}$
            $Q\_TRIP\_1FB_{nm}=Q\_TRIP\_1F_{nm}$
    END IF
END DO

where
n is the range cell.

Ln7 COMPUTE (GROUND CLUTTER FILTERED AND UNFILTERED POWERS)

DO (n) FROM 0 TO NCELLS-1 BY 1

$$P\_U_n=\left(1/NP\_SZ\right)\sum_{m=0}^{NP\_SZ-1}\left(I\_TRIP\_1_{nm}{}^2+Q\_TRIP\_1_{nm}{}^2\right)$$

$$P\_F_n=\left(1/NP\_SZ\right)\sum_{m=0}^{NP\_SZ-1}\left(I\_TRIP\_1FB_{nm}{}^2+Q\_TRIP\_1FB_{nm}{}^2\right)$$

END DO

where
n is the range cell.

Ln8 <u>COMPUTE</u> (STRONGEST TRIP COHERED TIME SERIES)

<u>DO</u> (n) <u>FROM</u> 0 <u>TO</u> NCELLS-1 <u>BY</u> 1
<u>IF</u> ($TA_n = 0$)
<u>THEN</u>
<u>DO</u> (m) <u>FROM</u> 0 <u>TO</u> NP_SZ-1 <u>BY</u> 1
$I\_TRIP\_A_{nm} = 0$
$Q\_TRIP\_A_{nm} = 0$
<u>END DO</u>
<u>ELSE</u>
<u>DO</u> (m) <u>FROM</u> 0 <u>TO</u> NP_SZ-1 <u>BY</u> 1
$PHI\_A_m = PSI_{mod(m - TA_n + 1, NP\_SZ)} - PSI_m$
$I\_TRIP\_A_{nm} = I\_TRIP\_1F_{nm}.\cos\left(PHI\_A_m\right) + Q\_TRIP\_1F_{nm}.\sin\left(PHI\_A_m\right)$
$Q\_TRIP\_A_{nm} = Q\_TRIP\_1F_{nm}.\cos\left(PHI\_A_m\right) - I\_TRIP\_1F_{nm}.\sin\left(PHI\_A_m\right)$
<u>END DO</u>
<u>END IF</u>
<u>IF</u> ($TB_n = 0$)
<u>THEN</u>
<u>DO</u> (m) <u>FROM</u> 0 <u>TO</u> NP_SZ-1 <u>BY</u> 1
$I\_TRIP\_B_{nm} = 0$
$Q\_TRIP\_B_{nm} = 0$
<u>END DO</u>
<u>ELSE</u>
<u>DO</u> (m) <u>FROM</u> 0 <u>TO</u> NP_SZ-1 <u>BY</u> 1
$PHI\_B_m = PSI_{mod(m - TB_n + 1, NP\_SZ)} - PSI_m$
$I\_TRIP\_B_{nm} = I\_TRIP\_1F_{nm}.\cos\left(PHI\_B_m\right) + Q\_TRIP\_1F_{nm}.\sin\left(PHI\_B_m\right)$
$Q\_TRIP\_B_{nm} = Q\_TRIP\_1F_{nm}.\cos\left(PHI\_B_m\right) - I\_TRIP\_1F_{nm}.\sin\left(PHI\_B_m\right)$
<u>END DO</u>
<u>END IF</u>
<u>END DO</u>

where
mod(x,NP_SZ) indicates “x modulo NP_SZ”, which is the remainder obtained after dividing x by NP_SZ,
cos(x) is the cosine function,
sin(x) is the sine function,
n is the range cell,
and m is the pulse number.

Ln9 COMPUTE (STRONGEST TRIP COHERED AUTOCORRELATIONS)

DO (n) FROM 0 TO NCELLS-1 BY 1

$$PP\_A_n real=(1/(NP\_SZ-1)) \sum_{m=0}^{NP\_SZ-2} (I\_TRIP\_A_{nm} . I\_TRIP\_A_{n\ m+1} + Q\_TRIP\_A_{nm} . Q\_TRIP\_A_{n\ m+1})$$

$$PP\_A_n imag=(1/(NP\_SZ-1)) \sum_{m=0}^{NP\_SZ-2} (I\_TRIP\_A_{nm} . Q\_TRIP\_A_{n\ m+1} - I\_TRIP\_A_{n\ m+1} . Q\_TRIP\_A_{nm})$$

$$PP\_B_n real=(1/(NP\_SZ-1)) \sum_{m=0}^{NP\_SZ-2} (I\_TRIP\_B_{nm} . I\_TRIP\_B_{n\ m+1} + Q\_TRIP\_B_{nm} . Q\_TRIP\_B_{n\ m+1})$$

$$PP\_B_n imag=(1/(NP\_SZ-1)) \sum_{m=0}^{NP\_SZ-2} (I\_TRIP\_B_{nm} . Q\_TRIP\_B_{n\ m+1} - I\_TRIP\_B_{n\ m+1} . Q\_TRIP\_B_{nm})$$

END DO

where
n is the range cell.

Ln10 COMPUTE (STRONG/WEAK TRIPS)

DO (n) FROM 0 TO NCELLS-1 BY 1
    IF (TA_n=0)
        THEN
            TS_n=0
            TW_n=0
            PP_S_n=0
            DO (m) FROM 0 TO NP_SZ-1 BY 1
                $I\_TRIP\_S_{nm}$=0
                $Q\_TRIP\_S_{nm}$=0
            END DO
    END IF
    IF (TB_n=0)
        THEN
            TS_n=TA_n
            TW_n=0
            PP_S_n=PP_A_n
            DO (m) FROM 0 TO NP_SZ-1 BY 1
                $I\_TRIP\_S_{nm}$=$I\_TRIP\_A_{nm}$
                $Q\_TRIP\_S_{nm}$=$Q\_TRIP\_A_{nm}$
            END DO
    END IF
    IF (($TA_n \neq 0$) AND ($TB_n \neq 0$))
        THEN

```
            IF (|PP_A_{n}|>|PP_B_{n}|)
               THEN
                  TS_{n}=TA_{n}
                  TW_{n}=TB_{n}
                  PP_S_{n}=PP_A_{n}
                  DO (m) FROM 0 TO NP_SZ-1 BY 1
                     I_TRIP_S_{nm}=I_TRIP_A_{nm}
                     Q_TRIP_S_{nm}=Q_TRIP_A_{nm}
                  END DO
               ELSE
                  TS_{n}=TB_{n}
                  TW_{n}=TA_{n}
                  PP_S_{n}=PP_B_{n}
                  DO (m) FROM 0 TO NP_SZ-1 BY 1
                     I_TRIP_S_{nm}=I_TRIP_B_{nm}
                     Q_TRIP_S_{nm}=Q_TRIP_B_{nm}
                  END DO
            END IF
      END IF
   END DO
```

where

$|PP\_A_n|=\sqrt{PP\_A_n real^2+PP\_A_n imag^2}$ is the complex modulus of PP_A_n,

$|PP\_B_n|=\sqrt{PP\_B_n real^2+PP\_B_n imag^2}$ is the complex modulus of PP_B_n,

n is the range cell,
and m is the pulse number.

Ln11 COMPUTE (GROUND CLUTTER TO SIGNAL RATIO)

```
DO (n) FROM 0 TO NCELLS-1 BY 1
   CSR_{n}=(P_U_{n}-P_F_{n})/P_F_{n}
END DO
```

where
n is the range cell.

Ln12 COMPUTE (STRONG TRIP VELOCITY)

```
DO (n) FROM 0 TO NCELLS-1 BY 1
   V_S_{n}=-(V_NYQ/PI)arg(PP_S_{n})
END DO
```

where
PI is the constant pi=3.14159…,

$arg(PP\_S_n)=tan^{-1}(PP\_S_n imag/PP\_S_n real)$ is the phase angle of PP_S_n, and n is the range cell.

Ln13 COMPUTE (NOTCH FILTER CENTER VELOCITY)

DO (n) FROM 0 TO NCELLS-1 BY 1
  IF ((CSR_n>T_CSR) AND (TS_n=1))
    THEN
      $V\_PNF_n = V\_S_n/2$
    ELSE
      $V\_PNF_n = V\_S_n$
  END IF
END DO

where
  n is the range cell.

Ln14 COMPUTE (WINDOWED STRONG TRIP COHERED TIME SERIES)

DO (n) FROM 0 TO NCELLS-1 BY 1
  DO (m) FROM 0 TO NP_SZ-1 BY 1
    $I\_TRIP\_SW_{nm} = I\_TRIP\_S_{nm} . h_m$
    $Q\_TRIP\_SW_{nm} = Q\_TRIP\_S_{nm} . h_m$
  END DO
END DO

where
  h_m=(1/2)(1-cos(2PI(m+1)/(NP_SZ+1))) is the Von Hann window without the zeros at either end,
  cos(x) is the cosine function,
  PI is the constant pi=3.14159…,
  n is the range cell,
  and m is the pulse number.

Ln15 COMPUTE (STRONG TRIP COHERED DISCRETE FOURIER TRANSFORM)

DO (n) FROM 0 TO NCELLS-1 BY 1
  DO (k) FROM 0 TO NP_SZ-1 BY 1

$$S\_S_{nk} = \sum_{m=0}^{NP\_SZ-1} (I\_TRIP\_SW_{nm} + jQ\_TRIP\_SW_{nm})\exp(-j2PImk/MP\_SZ)$$

  END DO
END DO

where
  exp(x) is the exponential function,
  j is the imaginary unit $\sqrt{-1}$,
  PI is the constant pi=3.14159…,
  n is the range cell,
  and k is the spectral coefficient.

Ln16 COMPUTE (NOTCHED STRONG TRIP COHERED DISCRETE FOURIER TRANSFORM)

DO (n) FROM 0 TO NCELLS-1 BY 1
  IF ($V\_PNF_n \leq 0$)
    THEN
      $FREQ\_0_n$=round(-(NP_SZ/2V_NYQ)V_PNF_n)
    ELSE

```
            FREQ_0n=round(NP_SZ-(NP_SZ/2V_NYQ)V_PNFn)
        END IF
        IF (((TSn=1) AND (TWn=3)) OR ((TSn=2) AND (TWn=4)) OR
           ((TSn=3) AND (TWn=1)) OR ((TSn=4) AND (TWn=2)))
            THEN
                NWn=NP_SZ/2
            ELSE
                NWn=3NP_SZ/4
        END IF
        IF (FREQ_0n-floor((NWn-1)/2)≥0)
            THEN
                FREQ_1n=FREQ_0n-floor((NWn-1)/2)
            ELSE
                FREQ_1n=FREQ_0n+NP_SZ-floor((NWn-1)/2)
        END IF
        IF (FREQ_0n+ceil((NWn-1)/2)<NP_SZ)
            THEN
                FREQ_2n=FREQ_0n+ceil((NWn-1)/2)
            ELSE
                FREQ_2n=FREQ_0n-NP_SZ+ceil((NWn-1)/2)
        END IF
        DO (k) FROM 0 TO NP_SZ-1 BY 1
            IF (FREQ_2n<FREQ_1n)
                THEN
                    IF ((k>FREQ_2n) AND (k<FREQ_1n))
                        THEN
                            S_SNnk=S_Snk
                        ELSE
                            S_SNnk=0
                    END IF
                ELSE
                    IF (((k≥0) AND (k<FREQ_1n)) OR ((k>FREQ_2n)
                        AND (k<NP_SZ)))
                        THEN
                            S_SNnk=S_Snk
                        ELSE
                            S_SNnk=0
                    END IF
            END IF
        END DO
    END DO
```

where
    round(x) is the nearest integer to x,
    floor(x) is the nearest integer to x that is smaller than x,
    ceil(x) is the nearest integer to x that is larger than x,
    n is the range cell,
    and k is the spectral coefficient.

Ln18 COMPUTE (NOTCHED STRONG TRIP COHERED INVERSE DISCRETE FOURIER TRANSFORM)

DO (n) FROM 0 TO NCELLS-1 BY 1
    DO (m) FROM 0 TO NP_SZ-1 BY 1

$$I\_TRIP\_SW_{nm}=(1/NP\_SZ)\sum_{k=0}^{NP\_SZ-1}(S\_S_{nk}real.cos(2PImk/MP\_SZ)-S\_S_{nk}imag.sin(2PImk/MP\_SZ))$$

$$Q\_TRIP\_SW_{nm}=(1/NP\_SZ)\sum_{k=0}^{NP\_SZ-1}(S\_S_{nk}imag.cos(2PImk/MP\_SZ)+S\_S_{nk}real.sin(2PImk/MP\_SZ))$$

    END DO
END DO

where
    cos(x) is the cosine function,
    sin(x) is the sine function,
    PI is the constant pi=3.14159…,
    n is the range cell,
    and m is the pulse number.

Ln20 COMPUTE (WEAK TRIP COHERED TIME SERIES)

DO (n) FROM 0 TO NCELLS-1 BY 1
    DO (m) FROM 0 TO NP_SZ-1 BY 1

$$PHI\_WS_{m}=PSI_{mod(m-TW_{n}+1,NP\_SZ)}-PSI_{mod(m-TS_{n}+1,NP\_SZ)}$$

$$I\_TRIP\_W_{nm}=I\_TRIP\_SN_{nm}.cos\left(PHI\_WS_{m}\right)+Q\_TRIP\_SN_{nm}.sin\left(PHI\_WS_{m}\right)$$

$$Q\_TRIP\_W_{nm}=Q\_TRIP\_SN_{nm}.cos\left(PHI\_WS_{m}\right)-I\_TRIP\_SN_{nm}.sin\left(PHI\_WS_{m}\right)$$

    END DO
END DO

where
    mod(x,NP_SZ) indicates “x modulo NP_SZ”, which is the remainder obtained after dividing x by NP_SZ,
    cos(x) is the cosine function,
    sin(x) is the sine function,
    n is the range cell,
    and m is the pulse number.

Ln21 COMPUTE (WEAK TRIP COHERED POWER)

DO (n) FROM 0 TO NCELLS-1 BY 1

$$P\_W_{n}=\left(1/NP\_SZ\right)\sum_{m=0}^{NP\_SZ-1}(I\_TRIP\_W_{nm}^{2}+Q\_TRIP\_W_{nm}^{2})$$

END DO

where
    n is the range cell.

Ln22 COMPUTE (POWER ADJUSTMENTS)

DO (n) FROM 0 TO NCELLS-1 BY 1
  $P\_SW_n = P\_F_n . WCF$
  $P\_WW_n = P\_W_n . WCF$
  $P\_WN_n = (NP\_SZ/(NP\_SZ - NW_n)) . P\_WW_n$
  IF ($P\_SW_n - P\_WN_n > 0$)
    THEN
      $P\_S_n = P\_SW_n - P\_WN_n$
    ELSE
      $P\_S_n = 0$
  END IF
END DO

where
  n is the range cell.

Ln23 COMPUTE (WEAK TRIP COHERED AUTOCORRELATIONS)

DO (n) FROM 0 TO NCELLS-1 BY 1

$$PP\_W_n real = (1/(NP\_SZ-1)) \sum_{m=0}^{NP\_SZ-2} (I\_TRIP\_W_{nm} . I\_TRIP\_W_{n\ m+1} + Q\_TRIP\_W_{nm} . Q\_TRIP\_W_{n\ m+1})$$

$$PP\_W_n imag = (1/(NP\_SZ-1)) \sum_{m=0}^{NP\_SZ-2} (I\_TRIP\_W_{nm} . Q\_TRIP\_W_{n\ m+1} - I\_TRIP\_W_{n\ m+1} . Q\_TRIP\_W_{nm})$$

END DO

where
  n is the range cell.

Ln24 COMPUTE (WEAK TRIP VELOCITY)

DO (n) FROM 0 TO NCELLS-1 BY 1
  $V\_W_n = -(V\_NYQ/PI) arg(PP\_W_n)$
END DO

where
  PI is the constant pi=3.14159…,
  $arg(PP\_W_n) = tan^{-1}(PP\_W_n imag / PP\_W_n real)$ is the phase angle of PP_W_n,
  and n is the range cell.

Ln25 COMPUTE (UNFOLDED POWERS AND VELOCITIES)

DO (n) FROM 0 TO NCELLS_L-1 BY 1
  $P_n = 0$
  $VEL_n = 0$
END DO

DO (n) FROM 0 TO NCELLS-1 BY 1

```
    IF (TS_n ≠ 0)
        THEN
            P_{n+(TS_n-1)NCELLS} = P_S_n
            VEL_{n+(TS_n-1)NCELLS} = V_S_n
    END IF
    IF (TW_n ≠ 0)
        THEN
            P_{n+(TW_n-1)NCELLS} = P_WN_n
            VEL_{n+(TW_n-1)NCELLS} = V_W_n
    END IF

END DO

where
    n is the range cell.
```

Ln26 COMPUTE (RETURN TYPE)

```
DO (n) FROM 0 TO NCELLS_L-1 BY 1
    IF ((P_L_n < T_POWER) OR ((P_n < T_POWER) AND (P_n > 0)))
        THEN
            RT_n = NOISE_LIKE
        ELSE
            RT_n = OVERLAID_LIKE
    END IF
END DO
DO (n) FROM 0 TO NCELLS-1 BY 1
    IF ((TS_n ≠ 0) AND (RT_{n+(TS_n-1)NCELLS} ≠ NOISE_LIKE))
        THEN
            RT_{n+(TS_n-1)NCELLS} = SIGNAL_LIKE
    END IF
    IF ((TW_n ≠ 0) AND (RT_{n+(TW_n-1)NCELLS} ≠ NOISE_LIKE))
        THEN
            RT_{n+(TW_n-1)NCELLS} = SIGNAL_LIKE
    END IF
END DO

where
    n is the range cell.
```

Ln27 COMPUTE (REFLECTIVITY)

```
DO (n) FROM 0 TO NCELLS_L/4-1 BY 1
```

$$ECHO_n = 10.LOG10\left((1/4)\sum_{k=0}^{3} P_{4n+k} - NOISE\right)$$

$$REFL_n = ECHO_n + SYSCAL + n.ATMOS + 20.LOG10(n)$$

```
END DO
```

```
        where
            LOG10(x) is the base-10 logarithm function,
            and n is the range cell.

Ln28    COMPUTE (CLIPPED REFLECTIVITY)

        DO (n) FROM 0 TO NCELLS_L/4-1 BY 1
            IF (REFL_n > 94.5 dBZ)
                THEN
                    REFL_C_n = 94.5 dBZ
            END IF

            IF ((REFL_n ≥ -32 dBZ) AND (REFL_n ≤ 94.5 dBZ))
                THEN
                    REFL_C_n = REFL_n
            END IF
            IF (REFL_n < -32 dBZ)
                THEN
                    REFL_C_n = -32 dBZ
            END IF
        END DO

        where
            n is the range cell.

Ln29    COMPUTE (SCALED REFLECTIVITY)

        DO (n) FROM 0 TO NCELLS_L/4-1 BY 1
            IF (RT_n=NOISE_LIKE)
                THEN
                    REFL_S_n = 0
            END IF
            IF (RT_n=OVERLAID_LIKE)
                THEN
                    REFL_S_n=1
            END IF
            IF (RT_n=SIGNAL_LIKE)
                THEN
                    REFL_S_n=round(2(REFL_C_n)+66)
            END IF
        END DO

        where
            round(x) is the nearest integer to x,
            and n is the range cell.

Ln30    COMPUTE (CLIPPED VELOCITY)

        DO (n) FROM 0 TO NCELLS_L-1 BY 1
            IF (VEL_n > 63 m/s)
                THEN
                    VEL_C_n = 63 m/s
            END IF
```

```
    IF ((VEL_n ≥ -63.5 m/s) AND (VEL_n ≤ 63 m/s))
        THEN
            VEL_C_n = VEL_n
    END IF
    IF (VEL_n < -63.5 m/s)
        THEN
            VEL_C_n = -63.5 m/s
    END IF
END DO
```

where
n is the range cell.

Ln31 COMPUTE (SCALED VELOCITY)

```
DO (n) FROM 0 TO NCELLS_L/4-1 BY 1
    IF (RT_n=NOISE_LIKE)
        THEN
            VEL_S_n=0
    END IF
    IF (RT_n=OVERLAID_LIKE)
        THEN
            VEL_S_n=1
    END IF
    IF (RT_n=SIGNAL_LIKE)
        THEN
            VEL_S_n=round(2(VEL_C_n)+129)
    END IF
END DO
```

where
round(x) is the nearest integer to x,
and n is the range cell.

Ln32 COMPUTE (CLIPPED SPECTRUM WIDTH)

```
DO (n) FROM 0 TO NCELLS_L-1 BY 1
    IF (WIDTH_L_n>V_NYQ_L/sqrt(3))
        THEN
            WIDTH_C_n=V_NYQ_L/sqrt(3)
    END IF
    IF (WIDTH_L_n<0 m/s)
        THEN
            WIDTH_C_n=0
    END IF
    IF ((WIDTH_L_n ≥0 m/s) AND (WIDTH_L_n<V_NYQ_L/sqrt(3)))
        THEN
            WIDTH_C_n=WIDTH_L_n
    END IF
END DO
```

where
sqrt(x) is the square root function,

and n is the range cell.

Ln33 COMPUTE (SCALED SPECTRUM WIDTH)

```
DO (n) FROM 0 TO NCELLS_L/4-1 BY 1
    IF ( RT_n =NOISE_LIKE )
        THEN
            WIDTH_S_n = 0
        ELSE
            WIDTH_S_n =round(2(WIDTH_C_n)+129)
    END IF
END DO
```

where
round(x) is the nearest integer to x,
and n is the range cell.

4.0 OUTPUTS

4.1 IDENTIFICATION

The SZ_2 algorithm outputs a reflectivity estimate, a Doppler velocity estimate, and a spectrum width estimate for each range cell in every radial in the scan.

4.2 DISTRIBUTION

These values can be sent directly to the RADAR PRODUCT GENERATION (RPG) unit or to an output device for display.

5.0 INFERENCES

5.1 LIMITATIONS

This algorithm assumes a Gaussian power spectral density for the weather signals.

5.2 FUTURE DEVELOPMENTS

To be determined.